Characterization of ADP dependent glucokinase in the embryonic development of zebrafish

Heidelberg University

presented by

M.Sc. Bei-Tzu Wang

January 2018

Dissertation

submitted to the

Combined Faculties for the Natural Sciences and for Mathematics

of the Ruperto-Carola University of Heidelberg, Germany

for the degree of

Doctor of Natural Sciences

presented by

Master of Science (M.Sc.) Bei-Tzu Wang

Born in Taichung City, Taiwan

Oral-examination: 22.01.2018

Characterization of ADP dependent glucokinase in the embryonic development of zebrafish

Referees: Prof. Dr. Andreas Draguhn
PD. Dr. Sven Sauer

SUMMARY

We aimed to characterize the function of ADP-dependent glucokinase (adpgk), a novel glucokinase in the embryonic development of zebrafish. Our study is the first study reporting the importance of adpgk in fine-tuning glucose metabolism during the early developmental process.

Knockdown of adpgk in zebrafish embryos significantly induced *hexokinase1* expression and increased the glucose consumption, indicated by decreased free glucose and increased glucose-6-phosphate levels. The adpgk knockdown embryos underwent an adaptive glucose metabolism with activated pentose phosphate pathway, exhibiting a reduction in one-carbon metabolism and hexosamine biosynthesis pathway. The dysregulated N-glycans synthesis further caused malfunctioning of proteins in the developmental signaling pathways which led to deformed convergent extension during the embryonic development of zebrafish. In concert with the altered glucose homeostasis, the adpgk knockdown embryonic cells endure an acid-base imbalance and compromised anti-oxidant systems. Furthermore, the metabolic disturbance induced the activation of cell cycle checkpoints, indicated by increased *cdkn1a* and *gadd45aa* expression and apoptosis, which in turn, exacerbated the deformed embryonic body patterning.

Overall, adpgk seems to act as a key regulator of glucose metabolism in the cell and thereby plays an important role in the embryonic development of zebrafish

ZUSAMMENFASSUNG

In dieser Arbeit wird die Funktion der ADP-abhängigen Glucokinase (adpgk) charakterisiert. Hierbei handelt es sich um eine neue Glucokinase in der Embryonalentwicklung des Zebrafisch. Wir demonstrieren erstmals die Notwendigkeit der adpgk in der Einstellung des Glukosemetabolismus während der frühen Entwicklungsprozesse.

Der adpgk Knock-down in Zebrafischembryonen führte zu einer signifikanten Induktion der *hexokinase1* Expression und einem Anstieg des Glukoseverbrauchs, was anhand der reduzierten Menge an freier Glukose und einem Anstieg des Glucose-6-Phosphat Levels nachgewiesen werden konnte. In den Embryonen erfolgte schließlich eine Anpassung des Glukosemetabolismus an die reduzierte Expression von *adpgk* und zwar durch Aktivierung des Pentosephosphatwegs. Nachgewiesen wurde dies durch Reduktion des C1-Stoffwechsels und des Hexosaminbiosynthesewegs. Weiterhin resultierte eine durch den Knock-down fehlregulierte N-Glykansynthese in defekten Proteinen, welche an Signalwegen, notwendig für die Embryonalentwicklung, beteiligt sind. Dies beeinträchtigte schließlich die konvergente Extension während der Entwicklung des Zebrafischs. Neben dem veränderten Glukosegleichgewicht zeigten die Zellen der adpgk Knock-down Embryonen zusätzlich ein Säure-Base Ungleichgewicht sowie ein geschädigtes antioxidatives System. Hinzu kommt, dass durch die metabolische Störung die Zellzyklus-Checkpoints aktiviert wurden. Dies wurde durch erhöhte Expression von *cdkn1a* und *gadd45aa* sowie einem Anstieg der Apoptose nachgewiesen, welche wiederum die deformierte Musterung des Embryonalkörpers verschlimmerten.

Zusammenfassend lässt sich sagen, dass adpgk als Schlüsselenzym in der Regulation des Glukosemetabolismus der Zelle fungiert und damit eine wichtige Rolle in der Embryonalentwicklung des Zebrafisch spielt.

ABBREVIATIONS

ADP	Adenosine diphosphate
Adpgk	ADP dependent glucokinase
AMP	Adenosine monophosphate
ATP	Adenosine triphosphate
Bbc3, puma	Bcl2 binding component 3
Bmp	Bone morphogenic proteins
Ca9	Carbonic anhydrase9
Cas9	CRISPR-associated nuclease 9
CDK	Cyclin-dependenet kinases
Cdkn1a; p21	Cyclin-dependent kinase inhibitor 1A
CO	Control
ConA	Concanavalin A
CRISPR	Clustered Regularly Interspaced Short Palindromic Repeats
Dsh	Dishevelled
ER	Endoplasmic reticulum
FBP	Fructose-1,6-bisphosphate
FGF	fibroblast growth factor
Fz	Frizzled
G6P	Glucose-6-phosphate
G6PD	Glucose-6-phsophate dehydrogenase
Gadd45aa	Growth arrest and DNA-damage-inducible, alpha, a
GAP	Glyceraldehyde-3-phosphate
Gata1	GATA Binding Protein 1
GFAT	Glutamine:fructose-6-phosphate amidotransferase
GFP	Green fluorescence
GSH	Reduced glutathione
GSSG	Oxidized glutathione
HDR	homology-directed repair
Hh	Hedgehog
HIF-1	hypoxia-inducible factor 1
Hk1	Hexokinase 1

Hk4	Hexokinase 4
Hpf	Hour post fertilization
Id1	Inhibitor of dna binding1
KD	Knockdown
Kdrl	Vascular endothelial growth factor receptor kdr-like
LC-MS/MS	Liquid chromatography tandem mass spectrometry
LDH	Lactate dehydrogenase
MMP	Matrix metalloproteinase
MO	Morpholino
MTA	Methylthioadenosine
Myc	Myelocytomatosis oncogene
Myl7	Myosin light chain 7
NADH	Nicotinamide adenine dinucleotide
NADPH	Nicotinamide adenine dinucleotide phosphate
NF-κB	Nuclear factor-κB
NHEJ	non-homologous end joining
Nqo1	NAD(P)H dehydrogenase, quinone 1
OGA	O-GlcNAcase
O-GlcNAc	O-linked N-acetylglucosamine
OGT	O-GlcNAc transferase
OXPHOS	Oxidative phosphorylation
PAM	Protospacer adjacent motif
PCP	Planar cell polarity
PEP	Phosphoenolpyruvate
PH_e	Extracellular pH
pH_i	Intracellular pH
PMA	Phorbol 12-myristate 13-acetate
PPP	Pentose phosphate pathway
PYR	Pyruvate
Rb	Retinoblastoma
ROS	Reactive oxygen species
Ru5P	Ribulose-5-phosphate
Runx1	Runt-related transcription factor

SAH	S-adenosylhomocysteine
SAM	S-adenosylmethionine
sgRNA	short guide RNA
Slc2a1a	Glucose transporter
SNA	Sambucus Nigra Lectin
TCA cycle	Tricarboxylic acid cycle
TGF-β	transforming growth factor β
TIGAR	TP53-inducible glycolysis and apoptosis regulator
TUNEL	Terminal deoxynucleotidyl transferase dUTP nick end labeling
Txnrd1	Thioredoxin reductase
UDP-GlcNAc	Uridine diphosphate-N-acetylglucosamine
UPLC	Ultra performance liquic chromatography
WGA	Wheat Germ Agglutinin
Wnt	Wingless
WT	Wild type

CONTENT

1. INTRODUCTION

2. AIM

3 MATERIALS

4. METHODS

5. RESULTS

6. DISCUSSION

7. CONCLUSION

8. REFERENCES

1. INTRODUCTION

1.1 Glucose metabolism

Glucose metabolism is essential in all living organisms. Hexokinases/glucokinases convert glucose to glucose-6-phosphate as the first glycolytic step [1] (Figure1.1). Through glycolysis, pyruvate is generated and further converted to acetyl-CoA. Acetyl-CoA participates in the tricarboxylic acid (TCA) cycle, which generates and provides precursors for the downstream amino acids and fatty acids synthesis [2, 3]. The reduced form of nicotinamide adenine dinucleotide (NADH) is the by-product in the TCA cycle and it subsequently enters the mitochondrial respirator chain for oxidative phosphorylation (OXPHOS); thereby, generating energy. [4] Pyruvate can also be converted to lactate and generate a small amount of energy in the process called fermentation (anaerobic glycolysis). High proliferative cells such as embryonic cells and tumors cells, albeit in the presence of oxygen, undergo aerobic glycolysis for generating lactate and energy, which is recognized as the Warburg effect. [5, 6] Warburg effect is originally described by Otto Warburg and the colleagues in the 1920s from the observation of increased glucose consumption in the cancer cells. [5] The increased glucose uptake and lactate production become the feature of the Warburg effect [4, 7, 8].

1.2 Pentose phosphate pathway

In addition to glycolysis, glucose metabolism also includes the pentose phosphate pathway (PPP), serine biosynthesis pathway, hexosamine biosynthesis pathway, and glucogenesis. [4, 9] During PPP, glucose-6-phosphate is converted to ribulose-5-phosphate with the production of reduced nicotinamide adenine dinucleotide phosphate (NADPH). NADPH is an important molecule of anti-oxidative defense by reducing oxidized glutathione (GSSG) to reduced glutathione (GSH) via glutathione reductase. This process detoxifies hydrogen peroxide to water and protects cells against reactive oxygen species (ROS)-induced damage. Furthermore, ribulose-5-phosphate is converted to ribose-5-phosphate, which provides the precursors for ribonucleotides synthesis (DNA and RNA). Ribose-5-phosphate undergoes transaldolation and transketolation, and generates fructose-6-phosphate, erythrose-4-phosphate, and glyceraldehyde-3-phosphate. [9, 10] The products of PPP contribute to amino acid synthesis, and refuel glycolysis and hexosamine biosynthesis pathway. [4, 9-11]

Glucose
↓ HK

Glycogen ← ← Glucose-1-P ← Glucose-6-P ⟶ Fatty Acids synthesis

GFAT

Fructose-6-P   Ribulose-5-P

Glucosamine-6-P   Ribose-5-P

↓   Glyceraldehyde-3-P

UDP-GlcNAc   ↓   Amino acid synthesis

Glycosylation   3-Phosphoglycerte ⟶ Serine ⟶ One-Carbon metabolism

Pyruvate ⟶ TCA cycle ⟶ OXPHOS

Lactate   Nucleotide synthesis
Fatty acids synthesis
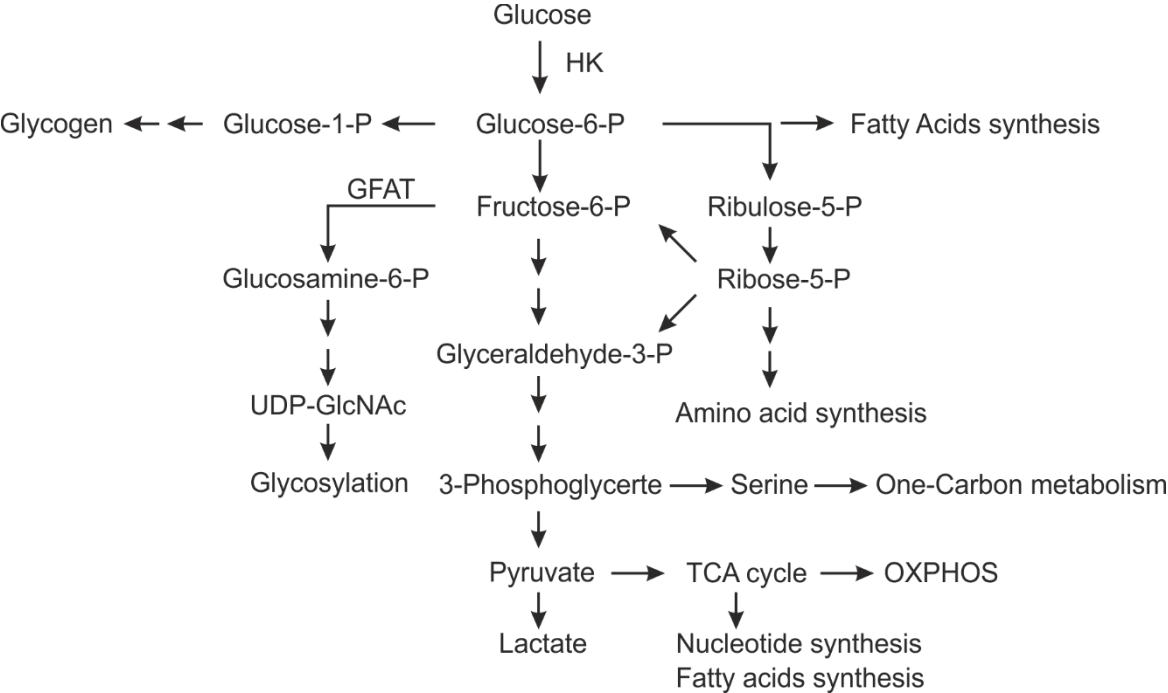
Figure 1.1 Overview of the glucose metabolism. Glucose metabolism provides precursors for the synthesis of glycans, amino acids, nucleotides, fatty acids and glycogen.

Hexokinase (HK); phosphate (P); glutamine:fructose-6-phosphate amidotransferase (GFAT); tricarboxylic acid (TCA); uridine diphosphate-N-acetylglucosamine (UDP-GlcNAc); oxidative phosphorylation (OXPHOS)

1.3 Serine biosynthesis pathway

Glucose metabolism provides precursors for serine biosynthesis pathway (Figure 1.2). [12] Under the catalysis of phosphoglycerate dehydrogenase, phosphoserine aminotransferase and phosphoserine phosphatase, 3-phosphoglycerate is converted to serine. In addition, it plays a role in nucleotide synthesis and methylation. During the conversion between serine to glycine, serine denotes one-carbon unit to tetrahydrofolate cycle, which couples with methionine cycle in one-carbon metabolism. [13, 14] Serine derived one-carbon units are then utilized for synthesizing adenosine, guanosine and thymidylate. During methionine cycle, S-adenosylmethionine (SAM) is produced. Through methyltransferase enzymes, SAM donates the methyl group for DNA, RNA, proteins and lipids methylation, and produces S-adenosylhomocysteine (SAH). SAH is subsequently converted to homocysteine which can be used for cysteine and glutathione synthesis. In addition to being the methyl group donor, SAM also participates in the polyamine biosynthetic pathway with the generation of by-product, methylthioadenosine (MTA). [12, 15]
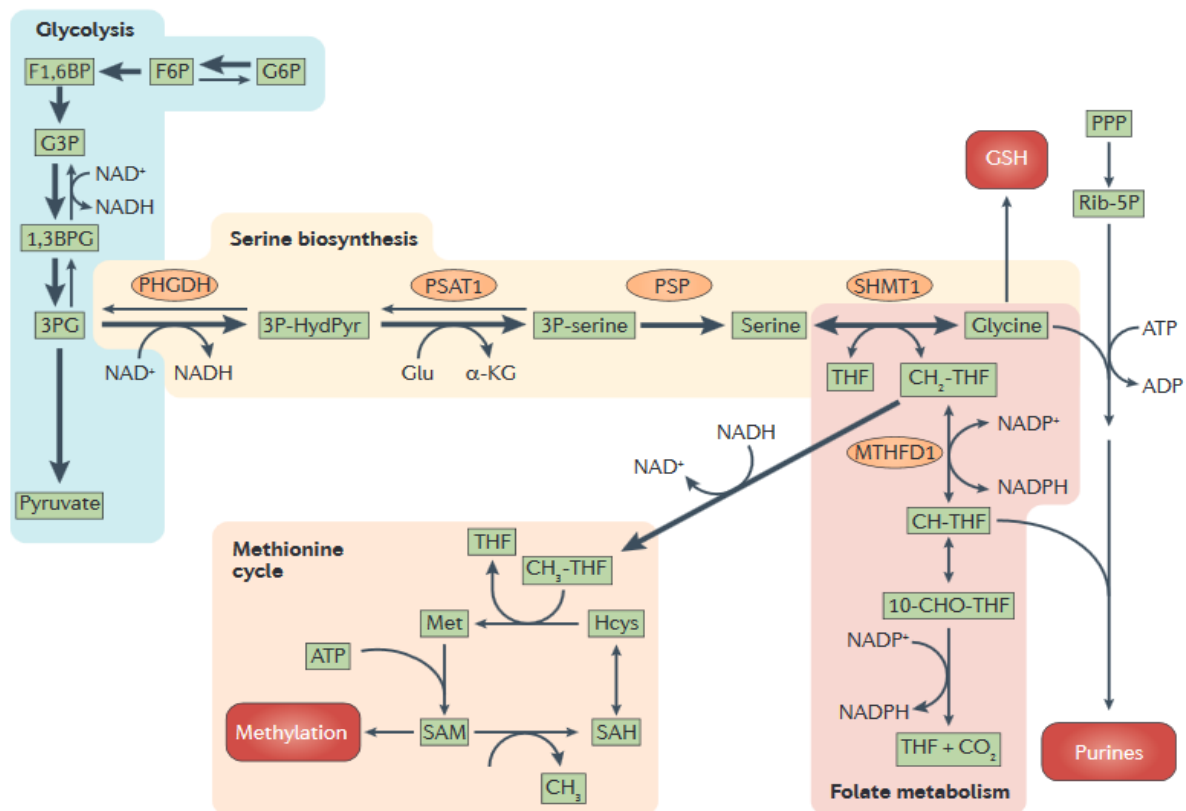
Figure 1.2 Scheme of serine biosynthesis and one-carbon metabolism pathway Glycolysis provides resource (3-phosphoglycerate) for serine biosynthesis. The conversion of serine to glycine refuels the one-carbon metabolism, the coupling of tetrahydrofolate and methionine cycles. The Figure is from Hay, N. Nat Rev Cancer 2016 16: (10) 635-649 [4]

1.4 Hexosamine biosynthesis pathway

Hexosamine biosynthesis pathway regulates posttranslational protein modification by generating uridine diphosphate-N-acetylglucosamine (UDP-GlcNAc). It starts with glucose-6-phosphate and fructose-6-phophate. The subsequent reactions utilize glutamine, acetyl-CoA and UDP for UDP-GlcNAc synthesis. UDP-GlcNAc acts as the fundamental building block for the biosynthesis of O-GlcNAcylation, N-linked glycosylation, and O-linked glycosylation. [4]

1.4.1 O-GlcNAcylation

O-GlcNAcylation is the attachment of O-linked N-acetylglucosamine (O-GlcNAc) moieties to serine and threonine residues of the proteins. The attachment and removal of O-GlcNAc to proteins is catalyzed by only a pair of enzymes, O-GlcNAc transferase (OGT) and O-GlcNAcase (OGA), respectively. The nucleocytoplasmic and short isoforms of OGT are present in the nucleus and cytoplasm. Other isoforms include mitochondrial OGT and ER-expressed EGF domain specific OGT. UDP-GlcNAc is the product of glucose metabolism; thus, O-GlcNAcylation is very sensitive to nutrient and stress stimuli. [16-18] OGT can be recruited by specific adaptor proteins to O-GlcNAcylate peroxisome proliferator-activated receptors co-activator 1α (PCG1α) and pyruvate kinase isoform 2 (PKM2); thereby, regulating gluconeogenesis and glycolysis to maintain glucose homeostasis. [19, 20] In addition, nuclear OGT can directly regulate the activation and repression of gene transcription by targeting to RNA polymerase II [21, 22] and transcription factors including nuclear factor-κB (NF-κB) and specificity protein 1 (Sp1) [23-26], and influences epigenetic regulation by targeting to histone-modifying enzymes. [27-32] Alteration of O-GlcNAcylation can increase or decrease phosphorylation.[33] Moreover, O-GlcNAcylation and phosphorylation show mutual exclusivity from each other when acting on the same site of the proteins such as RNA polymerase II [21, 34] and myelocytomatosis oncogene (c-Myc).[35]. Overall, O-GlcNAcylation is a highly dynamic protein modification. [17, 36]

1.4.2 N-linked glycosylation

Asparagine (N)-linked glycosylation is the covalent attachment of an oligosaccharide (glycan) to the nitrogen atom of asparagine residues in the polypeptide chains. This protein modification system is present in all domains of life including Bacteria, Archaea and Eukarya. [37] More than half of the eukaryotic proteins have been predicted to be glycoproteins and 90% of them most likely carry N-linked glycans. [38] Proteins with N-linked glycosylation serve diverse functions. The N-linked glycosylation modification is important in enhancing the protein solubility, stabilizing the proteins against proteolysis and degradation, facilitating the orientation of the proteins to the membrane and mediating immune responses. [39] The biosynthetic pathway of N-glycans (Figure 1.3) is initiated at the cytosolic side of the endoplasmic reticulum (ER) membrane. It starts with the binding of nucleotide-activated sugar donor (UDP-GlcNAc) to the lipid anchor, dolichylprophosphate, which generates dolichol pyrophosphate *N*-acetylglucosamine (Dol-P-P-GlcNAc). With a series of different specific glycosyl transferase, UDP-GlcNAc and guanosine diphosphate-mannose (GDP-Man) serve as the substrate for extending Dol-P-P-GlcNAc to $Dol-P-P-GlcNAc_2Man_5$. This dolichol-linked oligosaccharide is then flipped to the luminal face of the ER membrane where dolichylphosphomannose and dolichylphosphoglucose are used as the substrate for synthesizing glucose$_3$-mannose$_9$-N-acetylglucosamine$_2$ $(Glc_3Man_9GlcNAc_2)$. Oligosaccharyltransferase then catalyses the *en bloc* transfer of $Glc_3Man_9GlcNAc_2$ to the nascent polypeptide chains containing the consensus sequence (N-X-S/T). [37, 40-42] Subsequently, the polypeptide-bound $Glc_3Man_9GlcNAc_2$ is trimmed and modified in the ER. Glucosidase I and II remove the outtermost α1–2-bound glucose and the inner α1–3 glucose, respectively. $Glc_1Man_9GlcNAc_2$ associates with lectin chaperones calnexin and calreticulin, recruiting the lectin-associated oxidoreductase ERp57 for folding polypeptides. [43, 44] After being released from calnexin/calreticulin/ERp57, glucosidase II removes another glucose residue $(Man_9GlcNAc_2)$ to prevent its re-association. [45] Before exiting the ER, an ER degradation-enhancing α-mannosidase I–like protein (EDEM) can recognize and target the misfolded glycoproteins for degradation. The trimming and modification of the glycans continue in the Golgi by N-acetylglucosaminyltransferases and mannosidases, which generates hybrid and complex N-glycans. Moreover, the hybrid and complex N-glycans become mature N-glycans by elongating the GlcNac branching and adding sugar to the core and the branch such as sialic acid, fucose and galactose. [37, 40] After the trimming, processing and modification in ER and Golgi, the N-linked glycoproteins were secreted. [39]
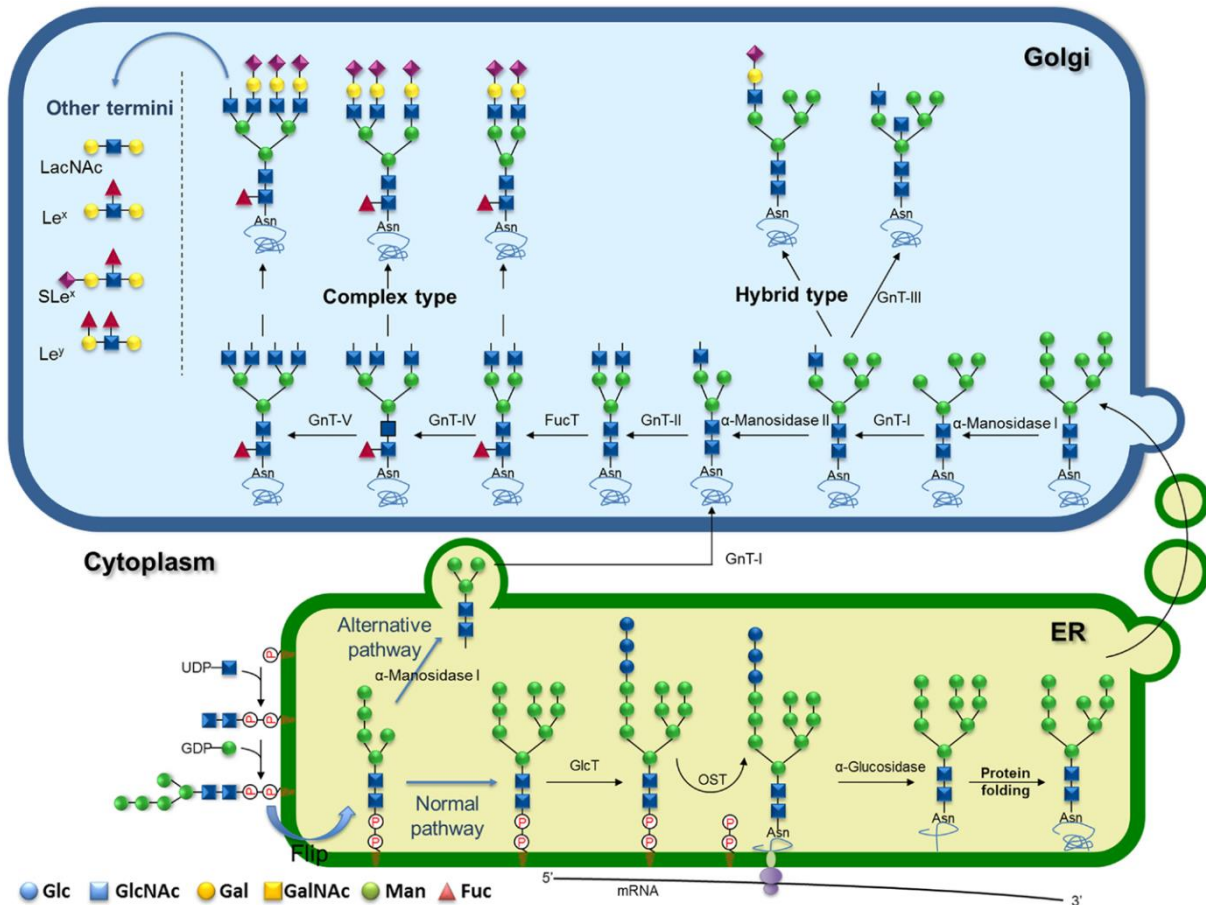
Figure 1.3 Schematic representation of biosynthesis of N-glycosylation. UDP-GlcNAc, the product of hexosamine biosynthesis pathway, binds to the lipid anchor of the ER membrane and acts as the building block of N-glycans. The glycans are further extended with mannose and trimmed in the ER. Subsequently, the high mannose glycas are extended with other sugars and modified in the Golgi; furthermore, forming the complex- and hybrid-type glycans.
The Figure is modified from Vasconcelos-dos-Santos, A. et al. Frontiers in Oncology, 2015. 5(138) [46]

1.5 ADP-dependent glucokinase (ADPGK)

ADP-dependent glucokinase (EC 2.7.1.147) utilizes ADP as the phosphoryl donor to catalyze the reaction of glucose to glucose-6-phosphate. It was first identified in Archaea involved in glucose breakdown in a modified Embden-Meyerhof glycolytic pathway. [47] Richter, S. et al. has determined the structure of mammalian ADPGK and identified its ribokinase-like tertiary fold, which is similar to archaeal orthologues. In contrast to archaeal adpgks that can utilize other nucleotide diphosphates as the phosphoryl donor, human ADPGK shows high specificity for ADP. [48] In addition, ADPGK has high substrate specificity for glucose and accepts no other sugars including 2-deoxyglucose as substrates. The activity of ADPGK is inhibited by high concentration of glucose and AMP, while hexokinase I to IV are inhibited by their product, glucose-6-phosphate. [49] Human ADPGK exhibits Km for glucose at 0.48 (±0.09) mm, and K_i for glucose and AMP inhibition at 2.9 (±0.6) mm and 0.5 (±0.07) mm, respectively. [48] ADPGK has bimodal optimal pH at around 5.75 to 6.5 and 8.75 to 9.0 [49], and the optimal temperature is at 42° [50].

Human ADPGK is located at chromosome 15 (15q24.1). It is localized in the ER and expressed in various normal and tumor tissues with high expression in the immune cells and bone marrow, and in leukemia. [51, 52] The precise function of eukaryotic ADPGK is still poorly understood. It has been shown that ADPGK is activated in the phorbol 12-myristate 13-acetate (PMA)-stimulated Jurkat cells. [50] The T cell receptor-triggered induction of ADPGK modulates the downstream oxidative signals and the NF-κB-dependent gene expression including IL-2 and IL-8. [50, 53, 54] In the PMA-stimulated T cells, the ADPGK-driven alteration of the glucose metabolism coincides with the deviation of glycolytic flux to the mitochondrial glycerol-3-phosphate dehydrogenase shuttle. [50] In addition, it has once been postulated that ADPGK has a role in anaerobic glycolysis by using ADP as the phosphate donor to save ATP in hypoxic cells. However, the results from ADPGK knockout lung cancer cell (H460) and colon cancer cells (HCT116) show that ADPGK is not activated by hypoxia-inducible factor 1 (HIF-1) and not regulated by hypoxia and anoxia. Interestingly, the genomics study identifies almost half of the top 150 genes related to ADPGK knockout encode proteins that can be glycosylated, suggesting ADPGK may play a role in glycosylation. [55] Given the high expression of ADPGK in high proliferative cells, we sought its functions in embryonic cells using the zebrafish model.

1.6 Zebrafish model

Zebrafish (Danio rerio) belong to the family of cyprinids (Cyprinidae) in the class of ray finned fish (Actinopterygii) and are originally from Indian rivers. This small aquatic vertebrate has become an excellent model organism for biomedical research especially in the field of developmental biology, metabolism, pharmacology and neuroscience. [56, 57] Zebrafish have average 4- to 5-year life span and remain sexually active almost all of this period. [58] A single female zebrafish can lay several hundred eggs per week and the development of the embryos is very rapid. The embryos take only 48 hours to develop through the stages of zygote, cleavage, blastula, gastrulation, segmentation, pharyngula to hatching when the primary organ synthesis is finished. [59] Unlike mammals, zebrafish develop ex utero and in transparent embryos, which enables easy visual observation for organ development and in vivo live-cell imaging, and easy accessibility for experimental manipulations such as gene or drug injection. Zebrafish possess 25 pair of chromosomes which contain 26,206 protein coding genes. The genetic homology of zebrafish is relatively high to humans with approximately 70% of zebrafish genes possessing at least one human orthologue and 82% of human genes related to diseases having zebrafish counterparts. [60, 61]

1.7 Zebrafish embryonic development

Upon fertilization, the non-yolky cytoplasm starts to stream to the animal pole and form the blastodisc. The segregation of the blastodisc from yolk vegetal cytoplasm continues during the cleavage stages. When cells have divided and reached the 512-cell stage (2.75 hpf), the embryos enter mid-blastula transition and the yolk syncytial layer forms. [59, 62] During mid-blastula transition, the developmental control is transferred from maternal to zygotic genes. [62] In the late blastula stage, epiboly starts and the cells intercalate radically to thin and spread the blastoderm over the yolk. During the gastrulation period, the collective cell involution, convergence and extension occur, leading to the formation of hypoblast, primary germ layers and embryonic axis. Convergence is the collective cell migration and intercalation from lateral and ventral area of the blastoderm to the dorsal side of the embryos; furthermore, forming the shield, a thickening region that is equivalent to the amphibian Spemann-Mangold organizer. [59, 62] Concomitantly, the converging and intercalated cells spread along the animal-ventral axis and form the anterior-posterior axis. [63] At the end of the gastrulation stage, the tail bud becomes prominent and the prechordal plate hypoblast accumulates to form a prominent bulge, known as polster. As the tail extends, the segmentation starts and the embryo length increases rapidly. Kupffer's vesicle forms at 5-somite stage which is the organizer for the establishment

of the left-right asymmetric patterning. Subsequently, through the pharyngula to hatching periods, the organs start forming and developing. [59, 62-64]

1.8 Early developmental signaling pathways

The coordination of the main signaling pathways Hedgehog (Hh), Wingless (Wnt), Notch, Transforming growth factor β (TGF-β), fibroblast growth factor (FGF) and Bone morphogenic proteins (bmp) signaling define cell fate and control embryonic morphogenesis. [62]

1.8.1 Dorsal-ventral axis control

During zebrafish embryonic development, the dorsal-ventral (back to belly) patterning is determined by the maternal factors such as β-catenin. (Figure 1.4) In the canonical wnt signaling pathway, the binding of Wnt to Frizzled (Fz) recruits lipoprotein receptor-related protein (LRP5/6), Dishevelled (Dsh) and axin, which prevents the degradation and promotes the translocation of β-catenin to the nuclei. [65, 66] β-catenin accumulates specifically in the dorsal region of the blastomeres and regulates the gene expression for inhibiting ventralizing factors and furthermore, inducing the mesoendodermal fate at the dorsal region. [62, 67, 68] In turns, the gradient of the Nodal and FGF-related signaling molecules is generated, which induces the patterning of mesoderm. [69, 70] During gastrulation, the embryonic shield becomes apparent in the dorsal mesoderm and generates organizer genes including chordin and noggin to inhibit Bmp signals, the ventral fate-determinator. Overall, the coordination of the Wnt, FGF Nodal, and Bmp signaling pathways determines proper development of dorsal-ventral axis. [71]
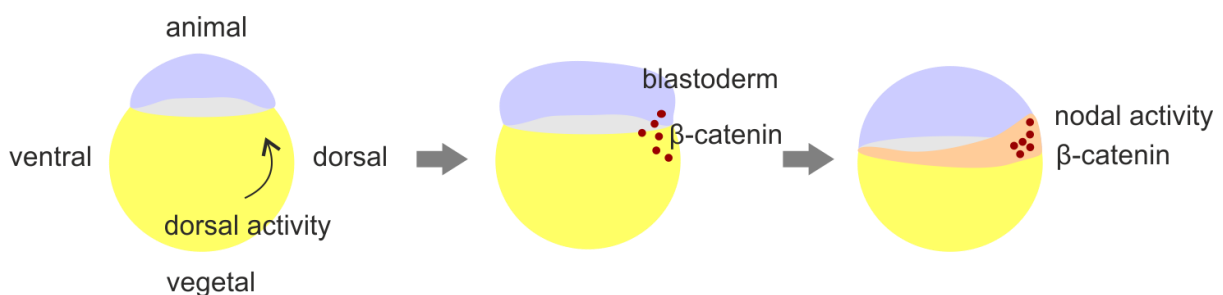
Figure 1.4 Scheme of the molecular regulation in the dorsal-ventral patterning. Nuclear β-catenin is specifically accumulated in the dorsal region of the blastomere, which inhibiting the ventralizing factor, generating the signaling gradients and promoting the mesoendodermal fate.

1.8.2 Convergent extension control

Convergent extension narrows the embryonic tissues mediolaterally and extends them anterioposteriorly. (Figure 1.5) Signaling pathways including β-catenin-Stat3-Liv1-Snail1, platelet-derived growth factor (PDGF)/phosphatidylinositol 3-kinase (PI3K), and noncononical wnt regulate the convergent and extension cell movement. [63, 72-74] The noncanonical wnt/planar cell polarity (PCP) signaling pathway (Figure 1.5) is β-catenin independent. [65] The binding of Wnt to Fz recruits Dsh, which activates the small GTPase family proteins. The small GTPase family proteins including Rac1 and Rho subsequently regulate the cytoskeleton modification during the cell movement. [75] Studies have shown that the molecules of noncanonical Wnt signaling including Wnt5 [76], Wnt11 [77], Fz2 [78] and Glypican4 [79] regulate convergent and extension. In addition, the ventral expression of Wnt/PCP components is regulated by bmp signals; therefore, the cross-talk between signaling pathways orchestrate the convergent extension and body patterning. [80]
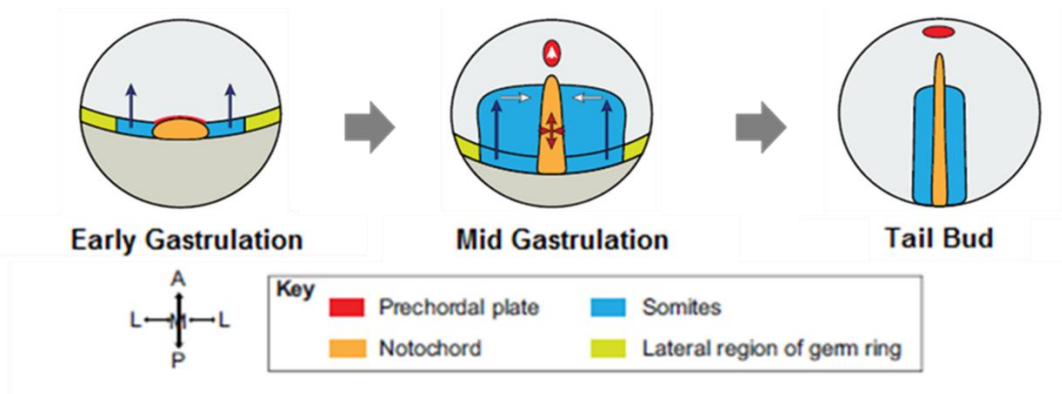
Figure 1.5 Scheme of convergent extension during zebrafish development. Convergent extension during gastrulation stage determines the embryonic body length. Convergent extension is the collective cell movement which narrows the embryonic tissues mediolaterally and extends them anterioposteriorly. The figure is modified from Tada, M., et al. Development 139, 3897-3904; 2012 [63]

1.8.3 Left-right asymmetry control

The determination of left-right asymmetry is another hallmark of the embryonic development. Under the regulation of Nodal, FGF, Wnt, Hh and Notch signaling, dorsal surface epithelial cells develop into dorsal forerunner cells. The dorsal forerunner cells migrate collectively and form the Kupffer's vesicle, a fluid-filled organ[64]. The counterclockwise fluid flow generated by motile cilia rotation in Kupffer's vesicle promotes the accumulation of the intracellular Ca^{2+} and determines the asymmetric expression of spaw on the left side of Kupffer's vesicle. Spaw initiates a genetic cascade that transfers the directional LR asymmetric information to lateral plate mesoderm and further to organ primordia. [64, 80-83]

1.9 Cell cycle

The coordination of cell migration, differentiation and proliferation during embryonic development is important. From many aspects, cell cycle is integrated in regulating these processes. During early zebrafish embryonic development, cells divide synchronously and the cell cycle oscillates rapidly between synthesis (S) and mitosis (M) phase without the intervention of Gap (G1 and G2) phase. [59]. After the midblastula transition (approximately 3 hour post fertilization), cells lose the division synchrony, and the cell cycle length increases with the intervention of G1 and G2 phase. [84, 85] Exposing zebrafish embryos to cell cycle inhibitors induces apoptosis, indicating zebrafish embryonic cells also possess cell cycle checkpoints. [86-89]

Cell cycle is regulated by cyclin-dependenet kinases (CDKs) and their cyclin partners (Figure 1.6). Upon receiving the signals from mitogenic factors such as epidermal growth factor, CDK4/6 forms a complex with cyclin D, which sequesters the CDK inhibitors including p21^{CIP1} (cdkn1a) and p27^{KIP1}, and phosphorylates retinoblastoma (Rb). [90, 91] The phosphorylated Rb1 enables E2F to activate the transcription of genes involved in G1-S phase cell cycle progression and DNA replications. E2F activates the transcription of cyclin E1 and E2. Cyclin E-CDK2 complexes further phosphorylate Rb; thus, creating a positive feedback-loop. In addition to cyclin-CDK complexes, other proteins such as polo-like kinase 1 and aurora kinases also control the cell cycle progression. [92] The entry of each cell-cycle phase is highly controlled at the cell-cycle checkpoints. It occurs at the late G1 phase and late G2 phase, which prevents the entry to S phase and M phase, respectively. DNA damage triggers cell cycle arrest via checkpoint kinase 1 and 2, and p53. [93, 94] The cell cycle checkpoints allow cells to enter to the next phase when it is assured that the previous phase has been successfully accomplished and the cell damage has been repaired. Cells failing to repair the damage undergo quiescence and/or cell death. [95]
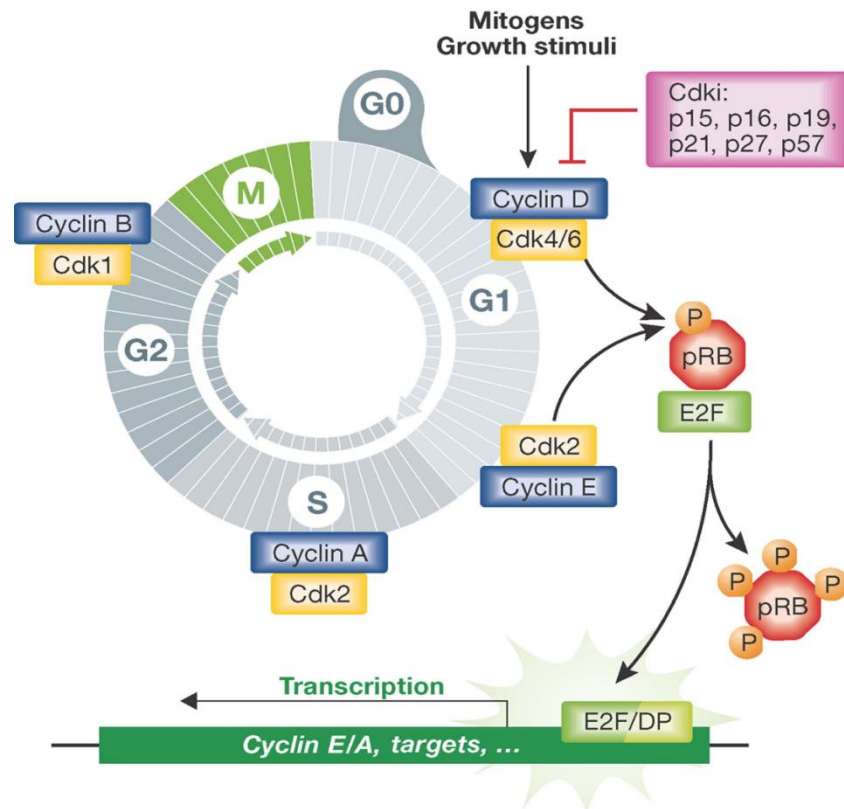
Figure 1.6 Molecular regulation of cell cycle. The cell cycle starts when receiving the signals from mitogens or growth factors. CDK4/6 subsequently forms a complex with cyclin D phosphorylates retinoblastoma (Rb), enabling E protein (E2F) to initiate the transcription of genes requiring for the cell cycle progression. The figure is modified from Aguilar, V., et al.EMBO Molecular Medicine (2010) 2, 338-348 [96]

1.10 Apoptosis

Apoptosis is a programmed cell death with the feature of cell shrinkage, blebbing, DNA fragmentation, chromatin condensation, and nuclear and cytoskeletal proteins decaying. [97] The central apoptotic pathways are highly conserved within vertebrates. Zebrafish possess all the core components of the intrinsic and extrinsic apoptosis pathways that are also functionally equivalent to mammals. [98-100] The apoptotic machinery is important in embryonic development for maintaining and shaping the morphogenesis. Dysregulation of apoptosis results in developmental abnormalities. [101] Caspase-dependent apoptosis is activated by two major signaling pathways, intrinsic and extrinsic pathways. (Figure 1.6) [102] Intrinsic signals such as DNA damage, hypoxia, ER stress and metabolic stress stimulate the activation of BCL-2 homology 3 (BH3)-only proteins, which up-regulate pro-apoptotic molecules including bax, bak, bcl2 binding component 3 (bbc3; puma), noxa and sequester anti-apoptotic molecules such as bcl2 and bcl2-xl. The activation of Bax and bak induces the mitochondrial outer membrane permeabilization, which causes the release of second mitochondria-derived activator of caspases (SMAC) and cytochrome c. The association of cytochrome c and

apoptotic protease activating factor 1 (APAF1) then activates caspase 9. Subsequently, caspase-9 activates the effector caspase-3 and -7 to execute apoptosis. [103-105] The extrinsic signaling pathways initiate apoptosis via transmembrane receptor-mediated interactions. The most characterized ligands and the death receptors are FasL/FasR and TNF-α/TNFR1. FasL/FasR recruits Fas-associated protein with a death domain (FADD). TNF-α/TNFR1 recruits TNF receptor 1-associated death domain protein (TRADD) with FADD and RIP. [97, 106, 107] Furthermore, FADD associates with procaspase 8, which can be further activated by death-inducing signaling complex (DISC). [108] Caspase 8 then activates caspase 3 to initiate apoptosis. Caspase 8 can also cleave BH3-interacting domain death agonist (BID). The truncated Bid translocates to the mitochondria and then promotes the release of cytochrome c; furthermore, triggering apoptosis. [97, 102, 109]

1.11 Techniques of establishing loss-of-function model in zebrafish

Creating loss-of-function model is essential in studying gene function. Several gene silencing and editing strategies are available for achieving this purpose in zebrafish.

1.11.1 Morpholinos

Antisense morpholinos (MOs) are the most commonly used gene knockdown tool in zebrafish. MO oligonucleotides are altered DNA analogs that possess methylenemorpholine rings linked through non-ionic phosphorodiamidate groups. The sequence of MO is usually around 25 base pair long and binds to the targeted nucleotide sequences by Watson-Crick base-pairing. MO interferes with proper protein synthesis either by blocking the splicing process of pre-mRNA or the translation. [57, 110] MO blocks pre-mRNA splicing by inhibiting the binding of splicing-directing small nuclear ribonucleoproteins (snRNP) complexes to the intron borders of the pre-mRNA, or by preventing the forming of the splice lariat structures. [111] The modified pre-mRNA splicing results in the synthesis of complete or partial intron inclusions or exon exclusions of mRNA. As for translation blocking morpholinos, it targets to the start codon or the 5'-untranslated region (UTR) of the mRNA and prevent the translation machinery from binding. [57, 110]

1.11.2 Clustered Regularly Interspaced Short Palindromic Repeats (CRISPR)

Genome editing technologies have been widely used for generating zebrafish mutants to study the function of genes. In addition to zinc finger nucleases (ZFNs) and transcription-activator-like effector nucleases (TALENs), Clustered Regularly Interspaced Short Palindromic Repeats (CRISPR) has become the most popular genome editing tool in recent years due to its flexibility and simplicity of the experimental setup. [112] CRISPR was originally discovered in bacteria where it functions as a type II adaptive immune defense system against foreign DNA elements such as phage infection. Re-infection creates the complementary mature CRISPR RNA (crRNA) and recruits CRISPR-associated nuclease (Cas) to form a double-strand cut at the targeted DNA sequence. [113, 114] The typical CRISPR/Cas9 technology requires a short guide RNA (sgRNA) and a Cas9. The sgRNA is designed to contain a 20-nucleotide sequence for targeting the genome of interest and a scaffold sequence for Cas9 binding. The targeting site in the genome of interest has to be at the upstream of a protospacer adjacent motif (PAM) sequence. When sgRNA and Cas9 targets to the PAM sequence, it activates the HNH and RuvC domains of Cas9 and creates the double-strand cleavage in the targeting sequence. Subsequently, the double strand break is repaired by either non-homologous end joining (NHEJ) or the homology-directed repair (HDR) pathway. [113, 115, 116] Using CRISPR/Cas9 system, NHEJ is the dominant repair pathway, an error-prone repair system which creates random insertions or deletions (Indels) of the sequence. Depending on the number of bases, indels generate premature stop codons or affect protein functions. [117-119]

2. AIM

ADPGK converts glucose to glucose-6-phosphate in the ER and it has been described so far that PMA stimulates ADPGK induction in T cells. The activation of ADPGK accompanies the alteration of ROS signaling and glucose metabolism in T cells. However, the function of adpgk is poorly understood.

Due to the strong expression of adpgk in high proliferative cells, we aimed to characterize its role in embryonic development using the zebrafish model. Overall, we hypothesized in this study that adpgk mediates glucose metabolism and regulates the developmental signaling pathways by controlling the posttranslational protein glycosylation modification during embryonic development in zebrafish.

For the purpose of investigation, we focused on the following perspectives in this study

1. Establishment of loss-of-function adpgk zebrafish model using CRISPR and morpholino including genotyping and phenotyping

2. RT-qPCR screening of the signal transduction pathways; including the developmental, oxidative and cell death signaling pathways.

3. Targeted metabolomics study including the LC-MS/MS method establishment for measuring the glucose intermediates and the quantification of the glucose intermediates, energy metabolites and the amino acids.

4. Glycomics study of the differential n-glycan patterning in adpgk knockout zebrafish embryos.

3. MATERIALS

3.1 Sequences of morpholinos and primers

3.1.1 Morpholinos

Name	Sequence
adpgk MO1	GTGTTCTCCAAGTTGCTCACCCCAC
adpgk MO2	CAGCACAGCCTTCCTCCACATGA
adpgk CO	GTATTATCCAAATTGCTAACCCAAC
p53 MO	GCGCCATTGCTTTGCAAGAATTG

3.1.2 Genotyping

Name		Sequence
MO1 #1	FW	CTCCACATACACACACTCTCTGC
	RE	CGTGCGATCCTCTGGAAAAC
MO1 #2	FW	GTGTCTGTCAGGTCCTCTGTGTG
	RE	TTGCAGTGGGGTGAGCAACTT

3.1.3 CRISPR

Name		Sequence
sgRNA #1	FW	ACAAGCGGTGTTGGCGCTGGGGAT
	RE	AAACATCCCCAGCGCCAACACCGC
sgRNA #2	FW	CACCCCGCCCACCCACACTGGAGG
	RE	AAACCCTCCAGTGTGGGTGGGCGG

3.1.4 Primer list_ adpgk mRNA for rescue

Name		Sequence
zebrafish adpgk	FW	GAGAGGGATCCCTCAACTTCTCCACATACA
rescue	RE	GAAGAGAATTCGGATGTTTCTTTTTATTTGAGTGA
human	FW	GAGAGATCGATGTAGCGCTTGTGTCG
adpgk rescue	RE	GAAGAGAATTCCCTGAAATGTAAATTGTTTTTAATATATTTAAGAG

16

3.1.5 Primer list_ In situ hybridization probe

Name		Sequence
adpgk	FW	CGCTGGGGATGGGTTATCTC
	RE	CCACAGCCTCTTTGAGTCGT
chordin	FW	CGCAAAGACACACACACT
	RE	TCTGAAGGGTTGCGTCTGAT
dlx3	FW	GTGTTACAGGCATCGTCCCA
	RE	CTGTGCTCTAGCGGAACCTC
hgg1	FW	AAGAGACCGCCTCTATGTTCG
	RE	TGACTGCTCAGAATCCAGCC
ntl	FW	AGACGAATGTTTCCCGTGCT
	RE	GAACCAGCCACCGAGTTGT
runx1	FW	TGGGACGCCAAATACGAACC
	RE	TGCTCATACGACCAGGATGG
wnt11	FW	CGTGGTGTATCTTGACCGTTG
	RE	CCTGTCTGCCAACAGCATTG

3.1.6 Primer list_qPCR

Name		Sequence
adpgk	FW	CGCTGGGGATGGGTTATCTC
	RE	GTAGCACCTCGTGGTCTCTG
adpgk	FW	TCA GAT AAG GAG GTT TTC CAG AGG AT
	RE	CGT TTC CGC CCA CAT AAA GC
axin2	FW	CAATGGACGAAAGGAAAGATCC
	RE	AGAAGTACGTGACTACCGTC
badb	FW	CAGCTCCTCCTGCTTTGTGG
	RE	CTTTTTACTCTCTTCATCTGCCCT
bbc3	FW	ACATCCCCTCACATGATGCC
	RE	TCTGTTCCTGAATTGTCCCTGAG
bcl2	FW	GGAAAATGGAGGTTGGGATGC
	RE	AAACGGGTGGAACACAGAGT
bcl2l	FW	GCAGATTGTGTTATGGGTATGAGC
	RE	TGTTGCTCGTTCTCCGATGT

ca9	FW	TCAAGGAATCTAGTGCTCATCCA
	RE	TGTGCTGTCGATACGTGTAA
cdkn1a	FW	GCAGAAGCTCAAAACATATTGTCAC
	RE	CGATGCGTCCTCCAGATCG
ef1a	FW	ACCGGCCATCTGATCTACAA
	RE	CAATGGTGATACCACGCTCA
gadd45aa	FW	GTCCCTCAATGTGGACCCTG
	RE	GTTGATGTCGTTCTCGCAGC
gli1	FW	CAGACGTCCTCTCGCCTTAC
	RE	AGTAGCGCTGTCCTTGCATT
hk1	FW	GGTGAATTGGACGAAGGGCTTTAA
	RE	CCTCTTGATCCCCTCTCTCAGAAG
hk4	FW	TGAACGACACAGTAGCCACC
	RE	GCCTGTACCTACTATCATGCCG
mycb	FW	CAGCGAATCCGATGACGAAGA
	RE	TCTCTTTTCCACCGTGACCA
nqo1	FW	AGAATCCCGAGCACTTTGTGT
	RE	CTTCTGCGATCAAGCTGAAAGAT
ptch1	FW	GCCGCATCCCAGGCCAACAT
	RE	CGTCTCGCGAAGCCCGTTGA
rab1ab	FW	GATTGACCGCTACGCCAGT
	RE	CAAATTCCTTTGCCGTTGTGTA
rb1	FW	GCCCCTAAACCCCTGAAGAG
	RE	CTCGCCACTGGATTTGCTTC
shha	FW	GGGAGCGGACAGGCTCAT
	RE	GCCAGTGGTTCATTACAGAGATGG
slc2a1a	FW	TAAACCGCTTTGGCAGGAGG
	RE	AGACCCACAATGAACCGTCC
stat1a	FW	TAGAAAGCCACGACTGGGAC
	RE	CTCCATCACGAAGCGACTGT
txnrd1	FW	GTGGCTTTCTGGCTGGTTTG
	RE	AGCTGCTCGATCTTAGTGGG

3.2 Antibodies

Name	Company
anti-ADPGK	Sigma-Aldrich, St. Louis, U.S.A.
anti-Calreticulin	Abcam, Cambridge, UK
Anti-Digoxigenin-AP, Fab fragments	Roche, Basel, Switzerland
anti-GFAT1	Santa Cruz Biotechnology, Dallas, U.S.A.
anti-Rac1/2/3	Cell signaling Technology, Danvers, U.S.A.
anti-β-actin	Santa Cruz Biotechnology, Dallas, U.S.A.
Chicken Anti-Mouse IgG H&L (HRP)	Abcam, Cambridge, UK
Chicken Anti-Rabbit IgG H&L (HRP)	Abcam, Cambridge, UK
ConA	Vector Laboratories, Burlingham, USA.
SNA	Vector Laboratories, Burlingham, USA.
Streptavidin-HRP anti-biotin IgG	Vector Laboratories, Burlingham, USA.
WGA	Vector Laboratories, Burlingham, USA.

3.3 Chemicals

Name	Company
2-mercaptoethanol	Merck, Darmstadt, Germany
2-propanol	Carl Roth, Karlsruhe, Germany
6-aminocaproic acid	Sigma-Aldrich, St. Louis, U.S.A.
Acetic acid	Carl Roth, Karlsruhe, Germany
Acetone	Sigma-Aldrich, St. Louis, U.S.A.
Agarose	Carl Roth, Karlsruhe, Germany
Amino persulfate (APS)	Sigma-Aldrich, St. Louis, U.S.A.
Ammonium bicarbonate	Sigma-Aldrich, St. Louis, U.S.A.
Ampicilin	PanReac AppliChem, Darmstadt, Germany
Bacteriological agar	Sigma-Aldrich, St. Louis, U.S.A.
Bovine serum albumin (BSA)	Santa Cruz Biotechnology, Dallas, U.S.A.
Bromophenoblue	Merck, Darmstadt, Germany
C_3-lactate	Sigma-Aldrich, St. Louis, U.S.A.
Calcium chloride (CaCl)	Sigma-Aldrich, St. Louis, U.S.A.

MATERIALS

Citric acid monohydrate	Carl Roth, Karlsruhe, Germany
Diethyl pyrocarbonate (DEPC)	Sigma-Aldrich, St. Louis, U.S.A.
Dipotassium phosphate (K_2HPO_4)	Sigma-Aldrich, St. Louis, U.S.A.
Dithiothreitol (DTT)	Merck, Darmstadt, Germany
Ethanol	Carl Roth, Karlsruhe, Germany
Ethylenediaminetetraacetic acid disodium salt dihydrate (EDTA)	Carl Roth, Karlsruhe, Germany
Formaldehyde	Sigma-Aldrich, St. Louis, U.S.A.
Formamide	Sigma-Aldrich, St. Louis, U.S.A.
Fructose-1,6-bisphosphate (FBP)	Sigma-Aldrich, St. Louis, U.S.A.
Glucose-6-phosphate (G6P)	Sigma-Aldrich, St. Louis, U.S.A.
Glyceraldehyde-3-phosphate (GAP)	Sigma-Aldrich, St. Louis, U.S.A.
Glycerol	Sigma-Aldrich, St. Louis, U.S.A.
Glycine	Sigma-Aldrich, St. Louis, U.S.A.
Perchloric acid ($HClO_4$)	Sigma-Aldrich, St. Louis, U.S.A.
Hydrogen chloride	Sigma-Aldrich, St. Louis, U.S.A.
Iodoacetamide (IAA)	Sigma-Aldrich, St. Louis, U.S.A.
Lithium chloride (LiCl)	Applichem, Darmstadt , Germany
Magnesium chloride 6-hydrate (MgCl)	PanReac AppliChem, Gatersleben, Germany
Methanol	Carl Roth, Karlsruhe, Germany
Milk powder	Carl Roth, Karlsruhe, Germany
Monopotassium phosphate (KH_2PO_4)	Sigma-Aldrich, St. Louis, U.S.A.
N,N,N′,N′-Tetramethylethylenediamine (TEMED)	Sigma-Aldrich, St. Louis, U.S.A.
Nicotinamide adenine dinucleotide (NADH)	Sigma-Aldrich, St. Louis, U.S.A.
Paraformaldehyde (PFA)	Merck, Darmstadt, Germany
Phosphoenolpyruvate (PEP)	Sigma-Aldrich, St. Louis, U.S.A.
Potassium bicarbonate ($KHCO_3$)	Sigma-Aldrich, St. Louis, U.S.A.
Potassium chloride (KCl)	Carl Roth, Karlsruhe, Germany
Potassium hydroxide (KOH)	Sigma-Aldrich, St. Louis, U.S.A.
Potassium phosphate (K3PO4)	Sigma-Aldrich, St. Louis, U.S.A.
Proteinase inhibitor	Roche, Basel, Switzerland
Proteinase K	Carl Roth, Karlsruhe, Germany

Pyruvate (PYR)	Sigma-Aldrich, St. Louis, U.S.A.
Ribonucleic acid from torula yeast, type IV RNA	Sigma-Aldrich, St. Louis, U.S.A.
Ribulose-5-phosphate (Ru5P)	Sigma-Aldrich, St. Louis, U.S.A.
Sodium bicarbonate (NaHCO$_3$)	PanReac AppliChem, Gatersleben, Germany
Sodium carbonate anhydrous (Na$_2$CO$_3$)	Carl Roth, Karlsruhe, Germany
Sodium chloride (NaCl)	Carl Roth, Karlsruhe, Germany
Sodium deoxycholate	Sigma-Aldrich, St. Louis, U.S.A.
Sodium dodecyl sulfate (SDS) pellet	SERVA, Heidelberg, Germany
Sodium hydroxide	Carl Roth, Karlsruhe, Germany
Sulfosalicylic acid	Sigma-Aldrich, St. Louis, U.S.A.
Tributylamine	Sigma-Aldrich, St. Louis, U.S.A.
Tris base	Carl Roth, Karlsruhe, Germany
Triton X-100	Carl Roth, Karlsruhe, Germany
Trypton	Carl Roth, Karlsruhe, Germany
Tween 20	Carl Roth, Karlsruhe, Germany
Urea	Sigma-Aldrich, St. Louis, U.S.A.
Yeast extract	Sigma-Aldrich, St. Louis, U.S.A.

MATERIALS

3.4 Reagents

Name	Company
40% acrylamide and bis-acrylamide solution	Bio-Rad, Hercules, U.S.A.
Acridine orange	Sigma-Aldrich, St. Louis, U.S.A.
BamHI restriction enzyme	Thermo Fisher Scientific, Waltham, U.S.A.
BbsI restriction enzyme	Thermo Fisher Scientific, Waltham, U.S.A.
Bsu15I restriction enzyme	Thermo Fisher Scientific, Waltham, U.S.A.
Digoxigenin-RNA labeling mix	Roche, Basel, Switzerland
DNase I, RNase free	Thermo Fisher Scientific, Waltham, U.S.A.
EcoRI restriction enzyme	Thermo Fisher Scientific, Waltham, U.S.A.
GeneRuler 1 kb DNA Ladder	Thermo Fisher Scientific, Waltham, U.S.A
GeneRuler 100 bp DNA Ladder	Thermo Fisher Scientific, Waltham, U.S.A
Latate dehydrogenase (LDH)	Sigma-Aldrich, St. Louis, U.S.A.
Lowry assay	Bio-Rad, Hercules, U.S.A.
MyTaq HS red mix	Bioline, London, UK
NBT/BCIP Stock Solution	Roche, Basel, Switzerland
Not I restriction enzyme	Thermo Fisher Scientific, Waltham, U.S.A.
PageRuler prestained protein ladder	New England BioLabs, Ipswich, U.S.A.
Phusion PCR	New England BioLabs, Ipswich, U.S.A.
PNGaseF	New England BioLabs, Ipswich, U.S.A.
Q5® High-Fidelity DNA polymerase	New England BioLabs, Ipswich, U.S.A.
RNase inhibitor	Roche, Basel, Switzerland
S.O.C. medium	New England BioLabs, Ipswich, U.S.A.
SensiFAST™ SYBR®	Bioline, London, UK
SP6 or T7 polymerase	Roche, Basel, Switzerland
SSC buffer 20x concentrate	Sigma-Aldrich, St. Louis, U.S.A.
SuperSignal™ West Pico chemiluminescent Substrate	Thermo Fisher Scientific, Waltham, U.S.A.
T4 ligase	New England BioLabs, Ipswich, U.S.A.
T4 polynucleotide kinase	New England BioLabs, Ipswich, U.S.A
Trizol reagent	Thermo Fisher Scientific, Waltham, U.S.A.
XbaI restriction enzyme	Thermo Fisher Scientific, Waltham, U.S.A.

3.5 Kits

Name	Company
GeneJET plasmid miniprep kit	Thermo Fisher Scientific, Waltham, U.S.A.
GenElute(TM) gel extraction kit	Sigma-Aldrich, St. Louis, U.S.A.
Glucose colorimetric kit	Cayman, Ellsworth, U.S.A.
HiSpeed plasmid midi kit	Qiagen, Hilden, Germany
Maxima first strand cDNA synthesis kit for RT-qPCR	Thermo Fisher Scientific, Waltham, U.S.A.
MEGAscript ® T7 in vitro transcription kit	Thermo Fisher Scientific, Waltham, U.S.A.
mMESSAGE mMACHINE® T3 in vitro transcription kit	Thermo Fisher Scientific, Waltham, U.S.A.
NEB 5-α competent E.coli	New England BioLabs, Ipswich, U.S.A.
Signal transduction PathwayFinder PCR array	Qiagen, Hilden, Germany
Topo TA cloning kit dual promotor	Invitrogen/Thermo Fisher Scientific, Waltham, U.S.A.
TUNEL assay	Roche, Basel, Switzerland

MATERIALS

3.6 Machines and Devices

Name	Sequence
Acquity BEH C18 column 150 mm × 2.1 mm, 1.7 µm	Waters, Milford, Massachusetts, U.S.A
Autoclave	Systec, Linden, Germany
Biochrom 30+ cation exchange chromatography	Biochrom, Cambridge, UK
Blotting semidry system	PeqLab, Erlangen, Germany
C1000 Touch Thermo Cycler	Bio-Rad,Hercules, U.S.A.
Centrifuge Heraeus instrument	Heraeus, Hanau, Germany
CFX Connect Real Time System	Bio-Rad, Hercules, U.S.A.
Electrophoresis chamber	Bio-Rad, Hercules, U.S.A.
FemtoJet micro-injector	Eppendorf, Hamburg, Germany
Fluoresence microscope	Olympus U-RFL-T, Tokyo, Japan
Fusion-SL Advance 4.2 MP	Peqlab, Erlangen, Germany
Herathermo incubator	Thermo Fisher Scientific, Waltham, U.S.A.
LC-FLR-QTOF-MS	Waters, Milford, Massachusetts, U.S.A.
Microloader 20 µL	Eppendorf, Hamburg, Germany
Micromass Quattro Ultima LC-MS/MS	Waters, Milford, Massachusetts, U.S.A
Microscope	Olympus SZX16, Tokyo, Japan
Microwave	Sharp, Osaka, Japan
NanoDrop LiTe spectrophotometer	Thermo Fisher Scientific, Waltham, U.S.A.
Olympus AU400	Beckman Coulter, Brea, U.S.A.
Phenomenex Synergi™ 4 µm Hydro-RP 80 Å, 150 × 2 mm	Phenomenex, Torrance, U.S.A.
pH-Meter	WTW, Weilheim , Germany
SDS PAGE electrophoresis system	Bio-Rad, Hercules, U.S.A.
Sonicator	Branson, Dietzenbach, Germany
Spectamax Plus 384	Molecular Devices, Sunnyvale, U.S.A.
Ultracentrifuge Typ Optima TLX	Beckman Coulter, Brea, U.S.A.
UV-Handlampe VL-4.LC	Vilber, Eberhardzell, Germany
UV-Transilluminator CN-TFX	Vilber, Eberhardzell, Germany
Waters BEH Glycan amide column 150 ×1.0 mm ID, 1.7 µm	Waters, Milford, Massachusetts, U.S.A

| Weighing machine PH204L | Mettler Toledo, Greifensee, Switzerland |
| Weighing machine XP56 | Mettler Toledo, Greifensee, Switzerland |

3.7 Disposables

Name	Company
0.45 µm nitrocellulose membrane	Neolab, Heidelberg, Germany
10cm dish	Sarstedt, Nümbrecht,Germany
Amicon Ultra-0.5 mL centrifugal 10 kDa filter	Merck, Darmstadt, Germany
Hard-Shell® 96-well PCR Plates, thin wall	Bio-Rad, Hercules, U.S.A
Microseal® 'B' PCR plate sealing film	Bio-Rad, Hercules, U.S.A
PCR tube (0.2 ml)	Sarstedt, Nümbrecht,Germany
Thin wall capillary, 1.0 mm	World Precision Instruments, Berlin, Germany

4. METHODS

4.1 Zebrafish husbandry

Wild-type AB (Danio rerio), and transgenic zebrafish Tg (myl7:GFP) and Tg (kdrl:GFP, gata1:dsRed) were maintained at 28.5°C on a 14-hour light/10-hour dark cycle. Embryos collected from natural mating were cultured in embryo E3 medium (150 mM NaCl, 0.5 mM KCl, 1.0 mM CaCl$_2$, 0.37 mM, KH$_2$PO$_4$, 0.05 mM Na$_2$HPO$_4$, 2.0 mM MgSO$_4$, 0.71 mM NaHCO$_3$ in deionized water, pH 7.4) and staged according to Kimmel et al. (Kimmel et al., 1995). The animals were held in accordance with the regulations of the University Heidelberg and the Regierungspräsidium Karlsruhe.

4.2 Generation of the CRISPR-based adpgk mutants

4.2.1 Cloning of the guide RNAs

Two guide RNAs targeting different regions of adpgk were designed from DKFZ E-CRISPR (*www.e-crisp.org*). The targeting sequences were GCGGTGTTGGCGCTGGGGAT and CCGCCCACCCACACTGGAGG. Firstly, the oligos (sgRNA sequences) were annealed and phosphorylated using *T4 Polynucleotide Kinase*. The annealing was carried out at the thermocycler with 37 °C for 30 minutes and 95 °C for 5 minutes with the ramp of 5 °C/minutes down to 25 °C. The annealed oligos were then ligated with the BbsI digested and purified px330 plasmid with the concentration ratio of 1:3 using T4 DNA Ligase (New England BioLabs, Ipswich, U.S.A.) for overnight incubation. The ligate was cloned and transformed into NEB 5-α competent E.coli. Briefly, the ligated oligo-px330 plasmid was added to the NEB 5-α competent E.coli cells and mixed by gently flicking. After 30 minutes of incubation on ice, the heat shock reaction was carried out at 42 °C for exactly 30 seconds. Subsequently, the competent E.coli were incubated on ice for 5 minutes, diluted by S.O.C. medium and incubated at 37°C for 1 hour shaking at 300 rpm. One hundred microliter of the diluted cells were spread on a LB agar plate (1.5 % bacterial agar, 1 % tryptone, 0.5 % yeast extract, and 1 % NaCl in sterilized water) with 100 µg/ml ampicillin. After the overnight incubation at 37°C, colonies were picked and cultured in the LB broth (1 % tryptone, 0.5 % yeast extract, and 1 % NaCl in sterilized water) for mini plasmid (GeneJET Plasmid Miniprep Kit) preparation. The extracted DNA plasmid was then sent out for sequencing (Seqlab, Göttingen, Germany). The plasmid with the correct oligo sequence was amplified by midi plasmid culture and further purified.

4.2.2 Guide RNAs and Cas9 mRNA synthesis

The oligo-px330 plasmid was fused with T7 promoter using Phusion PCR. The T7-oligo-px330 plasmid was used as the template for guide RNAs synthesis using MEGAscript ® T7 in vitro Transcription Kit. The plasmid of zebrafish Cas9, pT3TS-nCas9n, was linearized by Xbal restriction enzyme and transcribed to Cas9 RNA using *mMESSAGE* mMACHINE® T3 in vitro Transcription Kit following the manufacture's instruction. Briefly, the plasmid template was mixed with reaction buffer, enzyme mix and NTP mix and incubated at 37°C overnight.

The synthetic sgRNAs and Cas 9 RNA were purified using lithium chloride precipitation. To be short, the RNA probe was mixed with DEPC-water and 7.5 M lithium chloride followed by incubating at -20 °C for at least 30 minutes. After centrifuging at 13000 rpm for 15 minutes and washing with 70 % methanol, the RNA pellet was dissolved in DEPC-water.

4.2.3 Microinjection of the guide RNA and Cas9

The concentration was determined by NanoDrop LiTe Spectrophotometer. Two guide RNAs and Cas9 were then mixed at the final concentration of 200 ng/dL and 300 ng/dL, respectively. Two nl of the mixture of guide RNAs and Cas9 was injected into the embryos at one cell stage using FemtoJet micro-injector.

4.2.4 Genotyping of the CRISPR mutants

The genotyping was performed in 24 hour post fertilization (hpf) embryos or adult zebrafish. The genomic DNA was extracted from the embryos or clipped fin. Briefly, the embryos or fin were dissolved in 75 µl Buffer A (25 mM NaOH, 0.2 mM Na_2EDTA) at 95 °C for 15 minutes and mixed with 75 µl Buffer B (40 mM HCl). The genomic DNA was amplified with adpgk primers by PCR. The PCR product was then purified and cloned into the Topoisomerase I-activated pCR™II-TOPO® vector following by transformation into NEB 5-α competent E.coli. The plasmids were further amplified by mini culture. The purified plasmid was sent out for sequencing.

METHODS

4.3 Establishment of the Morpholino-based knockdown model

4.3.1 Morpholinos

In the morphlino based adpgk knockdown (KD) model, we used three morpholinos: two morpholinos (MO) targeting adpgk and one control morpholino, which were custom-synthesized by Gene Tools (Philomath, U.S.A.). The splice blocking morpholino targeting the junction of exon 2 and intron 2 (MO1 for KD1): GTGTTCTCCAAGTTGCTCACCCCAC. The translation blocking morpholino targeting at the start codon (MO2 for KD2): CAGCACAGCCTTCCTCCACATGA. The control morpholino (CO) was the mismatch of splice blocking morpholino: GTATTATCCAAATTGCTAACCCAAC. The morpholinos were first reconstituted in sterilized water to make the stock solution of 300 mM. Besides the study of concentration dependency, the injection concentration was 300 µM for MO1, 250 µM for MO2 and 300 µM for CO.

In addition, we also used p53 MO in our apoptosis study. p53 MO (GCGCCATTGCTTTGCAAGAATTG) was also synthesized by Gene Tools (Philomath, U.S.A.). We injected 300 µM of p53 MO in together with 300 µM of MO1 into the embryos.

4.3.2 Adpgk rescue mRNA generation

The zebrafish or human cDNA was synthesized (the detailed procedures were indicated as below) and used as template for zebrafish or human adpgk amplification by PCR. The PCR was performed using Q5® High-Fidelity DNA Polymerase with an annealing temperature at 60 °C. Briefly, the primers were designed with the overhang sequence containing BamHI and EcoRI restriction sites in zebrafish adpgk primers, and Bsu15I and EcoR1 in human adpgk primers. After amplification, the PCR products were loaded on a 1 % agarose gel for electrophoresis. Subsequently, we cut out the bands of adpgk and performed gel elutions using GenElute(TM) Gel Extraction Kit. The purified zebrafish and human adpgk was digested with BamHI and EcoRI, and with Bsu15I and EcoRI, respectively. Accordingly, the PCS2+ vector plasmids were also digested with the same restriction enzymes as for zebrafish and human adpgk cloning. The linearized zebrafish and human adpgk were ligated separately with the linearized PCS+ vector with the concentration ratio of 1:3 using T4 DNA Ligase and incubated on ice overnight. The ligate was transformed into NEB 5-α competent E.coli. The plasmid was purified from mini bacterial culture, sequenced and after further inoculation for midi culture again purified. Afterwards, the plasmid was digested with NotI restriction enzyme and used as the template for mRNA synthesis using MEGAscript ® T7 in vitro Transcription Kit. In short, the plasmid template was mixed with reaction buffer, enzyme mix and NTP mix and incubated at 37ºC overnight. Subsequently, the synthetic RNA was purified by lithium chloride solution and dissolved in DEPC-water.

4.3.3 Dishevelled rescue mRNA generation

Plasmids containing Dishevelled, Dishevelled_ΔC and Dishevelled_ΔN came from Dr. Matthias Carl. The plasmids were transformed into NEB 5-α competent E.coli. After mini plasmid purification, sequencing and midi purification, the plasmids were digested with NotI restriction enzyme and used as template for in vitro transcription. The template was mixed with Sp6 polymerase, reaction buffer, and NTP mix and incubated at 37 $^{\circ}$C overnight. Subsequently, the synthetic RNA was purified by lithium chloride solution and dissolved in DEPC-water.

4.3.4 Microinjection of the rescue experiment

The concentration of the mRNAs was determined by NanoDrop LiTe Spectrophotometer. The rescue mRNA was diluted with sterilized water and mixed with the morpholinos. The injection concentration used is mentioned in the results. Two nanoliter of the mixture was injected into embryos at one cell stage.

4.4 RNA extraction and cDNA synthesis

The embryos were collected and homogenized by mixing them with 1 ml Trizol followed by an incubation for 5 minutes at room temperature. The homogenate was subsequently mixed with 200 μl chloroform and incubated for 2 minutes. After centrifuging at 7500 ×g for 15 minutes at 4 $^{\circ}$C, the upper aqueous phase was taken and gently mixed with 500 μl isopropanol. The mixture was incubated at -80 $^{\circ}$C for 30 minutes and subsequently centrifuged at 7500 ×g for 10 minutes at 4 $^{\circ}$C to pellet the RNA. The supernatant was discarded and the RNA pellet was washed twice with 500 μl ice-cold ethanol. After centrifugation at 7500 ×g for 10 minutes at 4 $^{\circ}$C, the RNA pellet was dried at room temperature and dissolved with DEPC-H$_2$O. The RNA was stored at -80 $^{\circ}$C.

Prior to cDNA synthesis, RNA was treated with DNase I, RNase free, to remove the residual DNA. The cDNA synthesis was carried out using Maxima First Strand cDNA Synthesis Kit for RT-qPCR. Briefly, 1000 ng of RNA template were mixed with the reaction buffer and enzyme mix. The mixture was incubated for 10 minutes at 25 $^{\circ}$C followed by 15 minutes at 65 $^{\circ}$C. The reaction was terminated by heat inactivation at 85 $^{\circ}$C for 5 minutes. The cDNA was stored at -80 $^{\circ}$C.

4.5 Real time-quantitive PCR (RT-qPCR)

The gene expression was measured using RT-qPCR. The synthesized cDNA was used as template and mixed with the master mix containing SensiFAST™ SYBR®, H_2O and primers of the targeted gene, in the 96-well. For the broad pathway screening, the signal transduction PathwayFinder PCR array (Qiagen, Hilden, Germany) was used. The plate was sealed with Microseal®membrane and centrifuged at 4000 ×g for 2 minutes at room temperature. RT-qPCR was carried out using CFX Connect Real Time System. Program used for targeted gene quantification was as followed.

95 °C 0:25

95 °C 0:03

60 °C 0:30 40 cycles

95 °C 0:15

Melt curve 65 °C to 95 °C, increment 0.5 °C 1:00

60 °C 0:15

Program used for signal transduction pathway array

95 °C 10:00

95 °C 0:15

60 °C 1:00 39 cycles, 1 °C ramp/sec

95 °C 0:10

Melt curve 65 °C to 95 °C, increment 0.5 °C 1:00

4.6 *In situ* hybridization

4.6.1 Cloning and generation of the *in situ* probe

Adpgk, wnt11, runx1, hgg1, dlx3, ntl, chordin and sox17 were amplified by PCR. The reaction was carried out using zebrafish cDNA as template adding the specific primers and MyTaq HS *Red Mix.* The PCR products were loaded onto a 1 % agarose gel. After gel electrophoresis, we cut out the bands of the targeted genes and performed gel elutions using GenElute(TM) Gel Extraction Kit. The purified genes were cloned into a Topoisomerase I-activated pCR™II-TOPO® vector using Topo TA Cloning Kit Dual Promotor following the manufacture's instruction. In short, the PCR product of the gene of interest was mixed with salt solution and vector. After incubating at room temperature for 5 minutes and on ice for 30 minutes, the ligate was transformed into NEB 5-α competent E.coli. Subsequently, the transformed competent E.coli were cultured, amplified and purified. The extracted DNA plasmid was then sent out for

sequencing (Seqlab, Göttingen, Germany). The plasmid with the correct target gene sequence was then amplified by midi plasmid preparation. The purified plasmid was digested with BamHI or NotI. The linearized plasmid was mixed with the transcription buffer, digoxigenin-RNA labeling mix (UTP), RNase inhibitor and SP6 or T7 polymerase for the in vitro transcription at 37 °C overnight. The synthetic RNA probe was purified using lithium chloride precipitation and dissolved in DEPC-water.

4.6.2 *In situ* hybridization staining

Zebrafish embryos were collected at the desired stages and fixed with 4 % cold paraformaldehyde (PFA) in PBS (0.8 % NaCl, 0.02 % KCl, 0.02 M PO$_4$, pH 7.4) at 4 °C overnight. After dechorionating, the embryos were hydrated by a serial incubation of 25 %, 50 % and 75 % methanol in PBST (PBS and 0.1 % Tween) and 100 % methanol for 5 minutes each, and subsequently stored at -20 °C at least overnight before use. The embryos were rehydrated in a serial incubation of 75 %, 50 % and 25 % methanol/PBST, and 100 % PBST for 5 minutes each, and digested with 10 ug/ml of Proteinase K in PBST. Following by washing three times with PBST, the embryos were re-fixed with 4% PFA for 20 minutes. The embryos were pre-hybridized in the hybridization buffer (50% formamide, 5× SSC, 50 µg/ml heparin, 500 µg/ml tRNA, 9 mM citric acid, 0.1 % Tween 20 in DEPC-H$_2$O) at 70 °C for 3 hours and subsequently hybridized with the in situ probe at 70 °C overnight.

The hybridized embryos were washed with 25 %, 50 %, 75 % 2× SSC in hybridization buffer and 100 % 2× SSC each for 10 minutes and following by 2 times 30 minutes wash with 0.2× SSC at 70 °C. The embryos were incubated with 25 %, 50 % and 75 % PBST in 0.2× SSC and 100 % PBST each for 5 minutes. After 4 hours of blocking (BSA 2 mg/ml and 2 % sheep serum in PBST), the embryos were incubated with anti-digoxigenin-AP, Fab fragments in blocking solution overnight at 4°C.

The embryos were washed with PBST 4 times for 25 minutes and with alkaline phosphatase (AP) buffer (100 mM Tris HCl, 50 mM MgCl$_2$, 100 mM NaCl and 0.1 % Tween in DEPC-H$_2$O, pH 9.5) 3 times for 5 minutes; and subsequently stained with NBT/BCIP in AP Buffer. After the staining, the embryos were washed with PBS and stored in 70 % glycerol at 4°C.

4.7 Deyolking

For western blot analysis, the embryos were deyolked. The embryos were mixed with 1 ml deyolking buffer (55 mM NaCl, 1.8 mM KCl and 1.25 mM $NaHCO_3$) by pipetting up and down several times until the yolk was dissolved. The embryos were centrifuged at 5000 rpm, 1 minute at 4 °C, and the supernatant was discarded. The pellets were washed twice with washing buffer (110 mM NaCl, 3.5 mM KCl, 2.7 mM $CaCl_2$, 10 mM Tris/HCl, pH 8.5) followed by centrifuging at 5000 ×g, 1 minute at 4 °C. The pellets were dissolved with RIPA buffer (5 mM Tris, 7.4 mM EDTA, 0.5 % NP40, 6 mM sodium deoxycholate, 0.05 % SDS and proteinase inhibitor, pH 7.5) and homogenated by sonication. After centrifuging at 13000 rpm for 20 minutes at 4 °C, the supernatant was collected for further measurements.

4.8 Protein measurement

The protein concentration of the zebrafish samples were determined by Lowry assay. Five microliter of sample and bovine serum albumin (BSA) standards (0.1, 0.2, 0.5, 0.8, 1, 1.6, 2 mg/mL of BSA) were pipetted in duplicate into a 96 well plate. Twenty-five microliter of Reagent A and 200 µl of reagent B were subsequently added into the 96 wells. After 15 minutes of mixing at room temperature, the absorbance at 750 nm was measured by a Spectamax Plus 384 spectrophotometer.

4.9 Western blot/lectin blot

Protein samples (20 µg) were mixed with 6× SDS loading dye (480 mM Tris/HCl, 12 % SDS, 45 % glycerol, 12 % β-mercaptoethanol, 0.06 % bromophenoblue, pH 6.8) and denatured at 95 °C for 5 minutes. The denatured samples were loaded into wells and separated by SDS gel electrophoresis (4 % stacking gel: 40 % acrylamide, 0.5 M Tris/HCl pH 6.8, 10 % SDS, 10 % APS, TEMED, H_2O; 10 % separating gel: 40 % acrylamide, 1.5 M Tris/HCl pH 8.8, 10 % SDS, 10 % APS, TEMED, H_2O) with 80 voltages for 30 minutes and then 130 voltages for 1 hour. Subsequently, the proteins were transferred to the 0.45 µm nitrocellulose membrane. The blotting was done using a semidry system (Anode Buffer: 75 mM Tris/HCl, 20 % methanol; Cathode Buffer: 25 mM Tris/HCl pH 9.0, 40 mM aminocapronic acid, 20 % methanol) with the current of 1 mA/cm^2 for 50 minutes. The western blot was blocked with 5 % non-fat milk in 0.1 % TBST followed by incubation with the primary anti-ADPGK (1:250 dilution), Rac1/2/3 (1:1000 dilution), GFAT1 (1:500) or β-actin (1:1000) antibody at 4 °C overnight. After washing with 0.1 % TBST 3 times for 10 minutes, the blot was incubated with secondary anti-rabbit (1:10000) or anti-mouse IgG (1:10000) antibody conjugated with Horseradish Peroxidase (HRP) at room

temperature for 1 hour.

The lectin blot was blocked with 0.5 % TBST followed by incubation with the biotinylated ConA, SNA, or WGA or lectins (1:1000) at 4 °C overnight. After washing with 0.1 % TBST 3 times for 10 minutes, the blot was incubated with the streptavidin-HRP anti-biotin IgG antibody (1:10000) at room temperature for 1 hour.

The signal was developed using SuperSignal West Pico Chemiluminesent Substrate and detected using Fusion-SL Advance 4.2 MP. If reprobing was needed, the blot was washed three times with 0.1 % TBST and incubated with 10 % acetic acid for 10 minutes. After completely removing the 10 % acetic acid by washing with 0.1% TBST, the blot was re-blocked with 5 % non-fat milk for 30 minutes and incubated with primary antibody at 4 °C overnight.

4.10 Acridine orange staining

The live imaging of Acridine orange staining was used to determine the dead cells. The embryos were stained with 5 µg/µl acridine orange in E3 medium for 30 minutes followed by three times washing with PBS. The staining was then observed under fluorescence microscope with excitation/emission at 502/525 nm for green and 460/650 nm for red fluorescence.

4.11 TUNEL assay

The apoptotic cells were detected by Terminal deoxynucleotidyl transferase dUTP nick end labeling (TUNEL) assay. Firstly, the embryos were fixed with 4 % PFA in PBS overnight. After the fixation, they were washed with PBS twice for 5 minutes and then dechorinated. The dehydration of the embryos was performed by incubating them in 50 % methanol in PBST for 5 minutes and 100 % methanol for 5 minutes. Subsequently, the embryos were stored at -20 °C for 12 hours or until use. The embryos were washed with acetone for 20 minutes followed by rehydration in a serial incubation of 75 % methanol, 50 % methanol, 25 % methanol and 100% PBST for 5 minutes. Next, they were permeabilized with proteinase K for 5 minutes and fixed with 4 % PFA for 20 minutes. The PBST wash, proteinase K permeabilization and fixation steps were repeated one more time. After washing out the 4 % PFA with PBST (PBS, 1 % Triton-X) 3 times for 20 minutes, the embryos were stained with the TUNEL assay reagent (1:9 enzyme solution: labeled solution) for 1 hour at dark at 37 °C. The stained embryos were washed with PBS twice for 5 minutes and stored in PBS until observation. The TUNEL staining was observed under a fluorescence microscope with FITC excitation/emission at 502/525 nm.

METHODS

4.12 Glucose measurement

The whole mount zebrafish glucose content was measured by a glucose colorimetric assay kit. Fifteen microliter of standard (0, 2.5, 5, 7.5, 10, 15, 20, 25 mg/dl) or zebrafish homogenate samples were mixed with 85 µl of diluted assay buffer in the 96 well plates. The reaction was initiated by adding 100 µl enzyme mixture to each wells. After 10 minutes incubation at 37 ᵒC, the absorbance at 500-520 nm was measured using spectrophotometer.

4.13 Lactate and pyruvate measurement

The level of lactate and pyruvate in zebrafish embryos was measured based on the enzymatic assay. Zebrafish embryos were collected and homogenated in water. Depends on the pH, lactate dehydrogenase (LDH) determines the reversible conversion between pyruvate and lactate. At pH 7 LDH catalyzes the conversion of pyruvate and NADH to lactate and NAD^+. At pH 9 LDH catalyzes the conversion of lactate and NAD^+ to pyruvate and NADH. For pyruvate measurement the zebrafish homogenate was mixed with reaction buffer 1 containing NADH, 1.5M Tris Base and 0.2 % $HClO_4$ and then with reaction buffer 2 containing LDH. For the lactate measurement zebrafish homogenate was mixed with NADH, glycine buffer and LDH. The reaction and measurements were performed on the Olympus AU400.

4.14 Adenosine and GSH/GSSH measurements

Thirty embryos were homogenated in water and snap-frozen in liquid N_2. The embryo homogenates were stored at -80 ᵒC until measurement. The measurement including ATP, ADP, AMP, NADH, NAD, NADPH, SAM, SAH, MTA as well as GSH and GSSG was done in cooperation with the Metabolomics Core Facility of Heidelberg University. The following information regarding the detailed procedure of the measurement was provided by Dr. Gernot Poschet. "Metabolites were extracted from 30 zebrafish embryos with 0.3 ml of 0.1 M HCl in an ultrasonic ice-bath for 10 min. The resulting homogenates were centrifuged twice for 10 min at 4 °C and 16400 ×g to remove cell debris. AMP, ADP and ATP were derivatized with chloroacetaldehyde as described in Bürstenbinder et al. [120] and separated by reversed phase chromatography on an Acquity BEH C18 150 mm × 2.1 mm, 1.7 µm column connected to an Acquity H-class UPLC system. Prior separation, the column was heated to 42°C and equilibrated with 5 column volumes of buffer A (5.7 mM TBAS, 30.5 mM KH_2PO_4 pH 5.8) at a flow rate of 0.45 ml min^{-1}. Separation of adenosine derivates was achieved by increasing the concentration of buffer B (2/3 acetonitrile in 1/3 buffer A) in buffer A as follows: 1 min 1 % B, 1.6 min 2 % B, 3 min 4.5 % B, 3.7 min 11 % B, 10min 50 % B, and return to 1 % B in 2 min.

The separated derivates were detected by fluorescence (Acquity FLR detector, Waters, excitation: 280 nm, emission: 410 nm, gain: 100) and quantified using ultrapure standards. Data acquisition and processing was performed with the Empower3 software suite."

4.15 Glucose intermediates_LC-MS/MS measurement

Zebrafish glucose-6-phosphate (G6P), fructose-1,6-bisphosphate (FBP), glyceraldehyde-3-phosphate (GAP), phosphoenolpyruvate (PEP), pyruvate (PYR), and ribulose-5-phosphate (Ru5P) were measured by liquid chromatography tandem mass spectrometry (LC-MS/MS). Zebrafish embryos were homogenated in water and snap-frozen in liquid N_2. One hundred microliter of G6P, FBP, GAP, PEP, PYR and Ru5P standard (0, 0.1, 0.25, 0.5, 1, 2, 5, 10 µM) and zebrafish homogenate were mixed with 400 µl methanol containing internal standard (C_3-lactate) for de-proteinization. After centrifuging at 13000 rpm for 5 minutes at 4 ℃, the supernatant was dried under N_2. The samples were re-dissolved in H_2O and filtered through 10 kDa filter (Amicon Ultra-0.5 mL Centrifugal Filters, Merck, Darmstadt, Germany). The filtrates were collected and then injected into a Micromass Quattro Ultima (LC-MS/MS). The liquid chromatography separation was carried out by a Phenomenex Synergi™ 4 µm Hydro-RP 80 Å, 150 × 2 mm column with the mobile phase of 10 mM tributylamine (pH 4.95) and methanol.

4.16 Amino acid measurement

Thirty embryos were homogenated in water and snap-frozen in liquid N_2. The samples were then deproteinized with 20 % sulfosalicylic acid. After centrifuging, the supernatant was collected and injected into a Biochrom 30+ cation exchange chromatography.

4.17 Glycan measurement

Two hundred zebrafish embryos were homogenated in UA buffer (8 M urea in Tris-HCl, pH 8.5) and sonicated for three cycles (15 seconds on, 15 seconds off) on ice. After centrifuging at 16000 ×g for 10 minutes at 4 °C, the supernatant was collected for protein measurement. The aliquots of 2 mg of protein were transferred onto a 10 kDa MWCO filter (Amicon Ultra-0.5 mL Centrifugal Filters) followed by centrifuging at 14000 ×g for 20 minutes. The concentrated samples were mixed with Dithiothreitol (DTT) in UA buffer (final concentration of 10 mM), vortexed and incubated at room temperature for 30 minutes. Afterwards, the samples were centrifuged and mixed with iodoacetamide in UA buffer at a final concentration of 50 mM. After vortexing and incubation at room temperature for 30 minutes in the dark, the samples were centrifuged at least three times to exchange the buffer to 50 mM ammonium bicarbonate (ABC buffer, pH ~7.8). Two microliter of PNGaseF was added per filter and incubated at 37 °C overnight. The samples were centrifuged at 4 °C for 10 minutes and the filtrates were collected and dried using lyophilisation. The samples were sent out to National Institute for Bioprocessing Research and Training (NIBRT) in Ireland for glycan measurement.

The glycans were first separated based on the degree of sialylation by weak Anion Exchange analysis/separation. The liquid chromatography was carried out using BioSuiteDEAE Anion-exchange column, 1000 Å 10 µm, 7.5 mm x 75 mm (Waters; Milford, Massachusetts, U.S.A.) with 20 % AcCN (mobile phase A) and 100 mM Ammonium Acetate, 20 % AcCN pH 7.0 (mobile phase B). The fractions were collected and digested at 37 °C overnight with panels of exoglycosidase using 50 mM ammounium acetate pH 5.5 for glycan structure study. The exoglycosidase included α(2-3,6,8,9)-Sialidase, α(1-3,4)-Fucosidase, α(1-2,3,4,6)-Fucosidase, α(1-3,4,6)-Galactosidase, β(1-4)-Galactosidase, β(1-3,4)-Galactosidase and β-N-acetylhexosaminidase. The glycans were separated and detected by a Waters Acquity UPLC system equipped with an online fluorescence detector and Quadrupole Time-of-Flight-mass spectrometry (LC-FLR-QToF-MS) with a 150 ×1.0 mm ID, 1.7 µm Waters BEH Glycan amide column. The glycan measurement and the data analysis were performed by Dr. Stefan Mittermayr and Dr. Sara Carillo in the NIBRT.

4.18 Statistics

The results were shown as mean $\pm$ standard deviation (SD). Unpaired t-test was performed using Prism 6.0 (GraphPad Software Inc., USA). A p value less than 0.05 was considered statistically significant. The n number shown in the embryonic phenotypes and staining (*in situ* hybridization) indicated the exact numbers of evaluated embryos. The studies of the genomics, glucose, lactate, and metabolomics were done using a pool of embryos and the n number represented the number of independent batches of pooled embryos collection.

5. RESULTS

5.1 Adpgk expression pattern

Zebrafish adpgk is located at chromosome 25 and the protein shares 64 % similarity with human ADPGK. To understand the function of adpgk in embryonic development, we firstly screened *adpgk* gene expression at different developmental stages using RT-qPCR. The embryos were collected from four independent batches during one cell, blastula, gastrulation, segmentation, pharyngula and hatching stages as shown in Figure 5.1A [59].

Our results showed that zebrafish embryos displayed the highest adpgk expression at one cell stage. Afterwards, the expression was decreased and remained very low through the whole developmental process till 96 hpf examined (Figure 5.1B). The early expression and its changes during the mid-blastula transition indicated adpgk functioned as a maternal gene. On the contrary, other well characterized hexokinases such as *hexokinase 1 (hk1)* was expressed in a very low level at one cell stage. After the mid-blastula stage, the embryos started expressing zygotic *hk1* and kept the expression in high levels through the rest of the developmental process (Figure 5.1C). According to the low expression of adpgk after the mid-blastula stage, we hypothesized a role of adpgk in fine-tuning glucose metabolism in the embryonic development.

Furthermore, we investigated the specific embryonic expression of adpgk by the *in situ* hybridization method. During the blastula stage, zebrafish embryos showed ubiquitous *adpgk* expression and during the gastrulation stage, embryos expressed *adpgk* at the dorsal side of the body. *Adpgk* was expressed highly in the notochord during the segmentation stage and afterwards, un-specifically in the whole body in the pharyngula stage (Figure 5.1D). Therefore, adpgk could play a role in the embryonic body patterning due to its dorsal and notochord expression in the embryos.
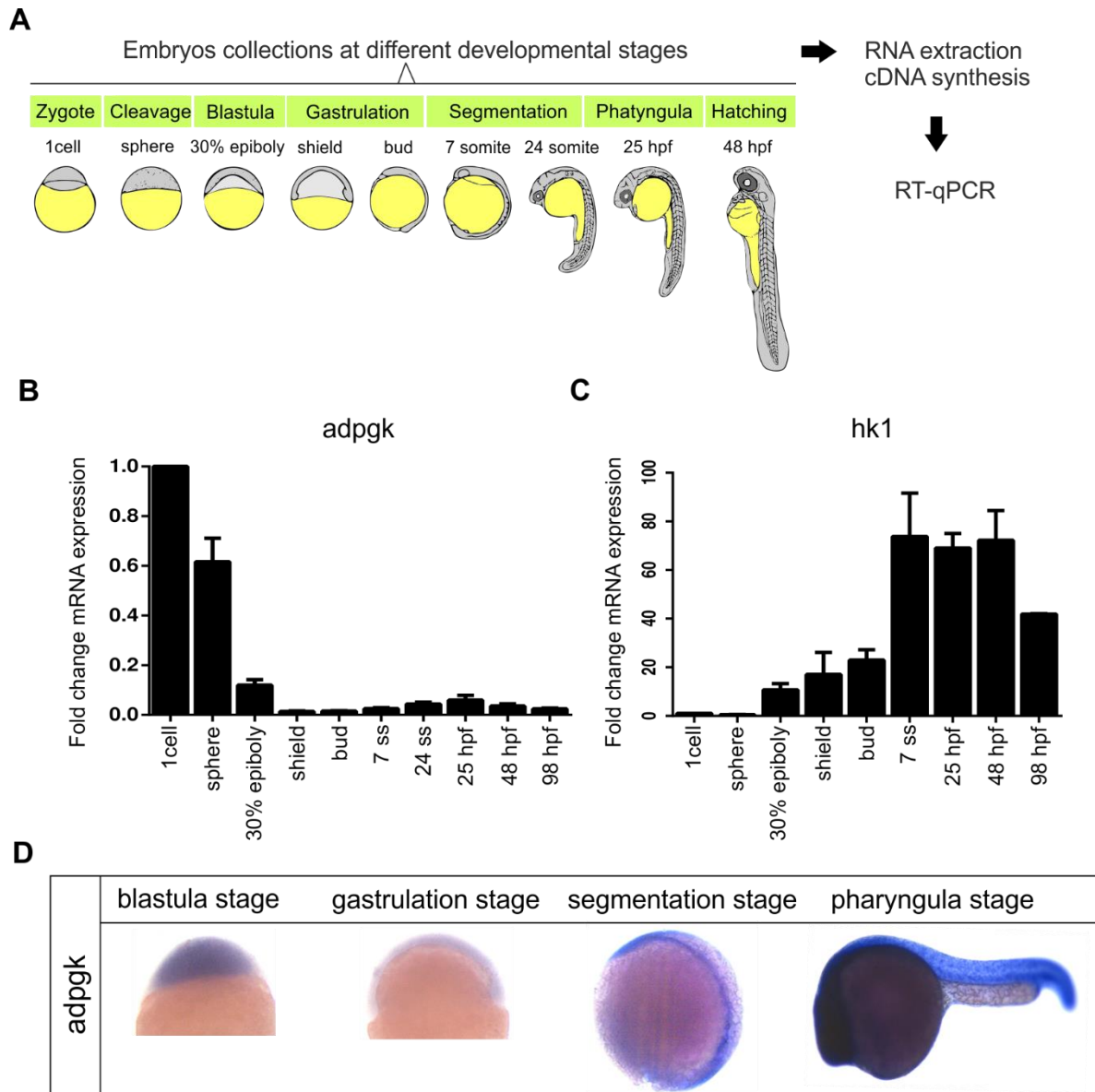
Figure 5.1 *Adpgk* is a maternal gene with high expression at one cell stage. (A) Zebrafish embryos were collected at one cell, blastula, gastrulation, segmentation, pharyngula and hatching stages [59] for the screening of *adpgk* expression using RT-qPCR. (B) The embryos showed the highest *adpgk* expression at one cell stage. The expression decreased after mid-blastula and remained low till 96 hpf tested (n=4). (C) *Hk1* was expressed very low at one cell stage and highly expressed after mid-blastula stage (n=4). (D) In the embryonic patterning, *adpgk* was expressed ubiquitously in the embryos during the blastula stage and was expressed at the dorsal side of the body during the gastrulation stage. During the segmentation stage, *adpgk* was expressed highly in the notochord; afterwards, un-specifically in the whole body in the pharyngula stage. The gene expression was measured from 4 independent batches of pooled embryos.

5.2 Establishment of loss-of-function adpgk zebrafish model

5.2.1 CRISPR-mediated adpgk mutants

To characterize the function of adpgk, we next aimed to establish the loss-of-function zebrafish models using the CRISPR/Cas9 system and the anti-sense morpholino knockdown.

In the CRISPR/Cas9 system, we designed and injected two sgRNAs together with Cas9 into the zebrafish embryos at one cell stage. After the embryos had grown, the fins of the adult zebrafish were then clipped for genotyping. Scheme of the experimental design was shown in Figure 5.2.1A.

Three founders out of ten zebrafish were identified and further out-crossed with the wild type zebrafish. At the crossed-out F1 generation, 6 different types of heterozygous mutations were identified among 120 zebrafish. However, due to the imbalanced numbers of male and female zebrafish carrying the same heterozygous mutations, we were only able to mate two pairs of CRISPR heterozygous-mutated zebrafish (deletion at 24914-24919 and deletion at 24916-24921) (Figure 5.2.1B). In the F2 generation, although we did not genotype the embryos, the surviving zebrafish did not show any prominent phenotypes. We postulated that the homozygous *adpgk* mutations could be lethal or the mutants showed false negative phenotype due to the compensatory effect [121]. Since the false negative phenotype has only been observed in CRISPR but not morpholino method [121]; plus, the mating, genotyping and raising of the CRISPR mutants are time-consuming processes, we decided to focus on using morpholino-mediated knockdown strategy to address the function of adpgk in this study.

A

sg1 sg2

exon2 — adpgk

sg1 target sequence: GCGGTGTTGGCGCTGGGGAT
sg2 target sequence: CCGCCCACCCACACTGGAGG

sg1

Cas9

sg2

genotyping_sequencing
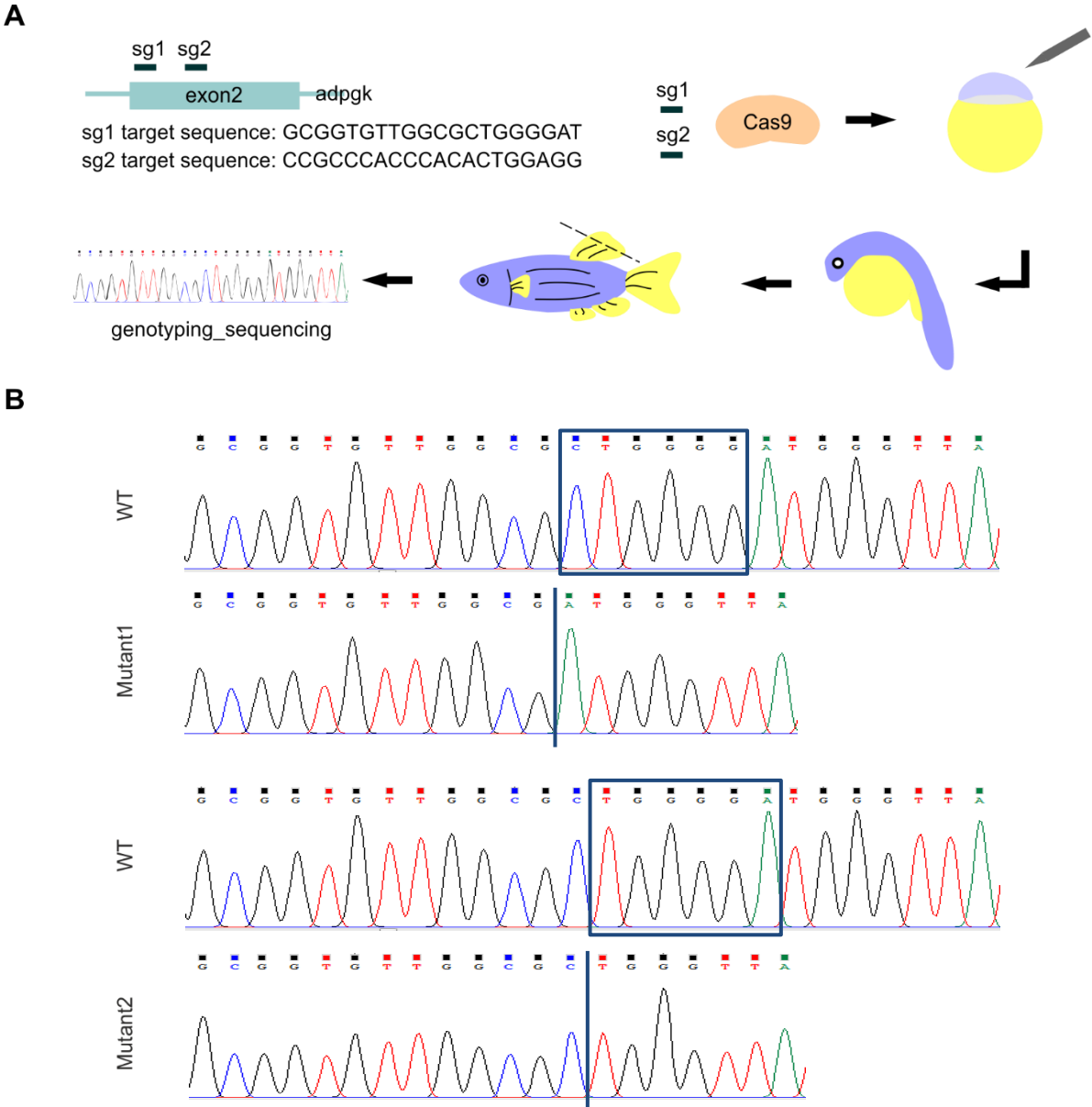
B

WT

Mutant1

WT

Mutant2

Figure 5.2.1 The establishment of CRISPR mediated loss of function zebrafish model. (A) Scheme of the experimental design. (B) The genotypes of the two CRISPR heterozygous mutants used for further mating.

5.2.2 Morpholinos-mediated adpgk knockdown

Antisense morpholinos are the most widely used gene knockdown (KD) tool in zebrafish model. Morpholinos can either block the splicing process of pre-mRNA or the translation by targeting the start codon to interfere the proper protein synthesis [122].

In the study, we used two morpholinos for the gene knockdown purpose, one splice-blocking targeting exon 2 (MO1 for KD1) and one translation-blocking (MO2 for KD2) morpholinos (Figure 5.2.2A). MO1 targeted the boundary of adpgk exon 2 and intron 2, and was predicted to create a 275-nucleotide-long exon excision. We designed the genotyping primers at the exon 1 and 3 with expected full size of 512 base pair (bp); if MO1 functioned well, it would create a truncated size of 237 bp adpgk. Our genotyping results from pooled embryos showed that both the wild type (WT) and MO1-injected group of embryos (KD1) had the 512-bp fragments. The KD1 embryos additionally showed a small fragment around the size of 200-300 bp, indicating the partial knockdown of *adpgk* in the KD1 embryos (Figure 5.2.2B). In addition, we designed primers targeting exon 2 and exon 3 junctions to further confirm the exon excision in the KD1 embryos. The RT-qPCR results showed a more than 2 hold change decrease of *adpgk* mRNA ($p<0.005$, n=6, compared to the WT) in the KD1 embryos (Figure 5.2.2C).

Furthermore, we studied the knockdown efficiency of the morpholino at the protein levels. Both MO1 and MO2-injected embryos had decreased adpgk protein at the injection concentration of 200 µM and 300 µM, compared to the WT or morpholino control-injected (CO) group (Figure 5.2.2D). Therefore, we showed the good adpgk knockdown efficiency in the KD1 and KD2 embryos on genomic and protein levels, and successfully established the morpholino-based adpgk loss-of-function zebrafish model in our study.

A

MO1 splice blocking

Exon1 (UTR) | Intron1 | Exon2 | Intron2 | Exon3 — adpgk

MO2 translation blocking

Exon1 (UTR) | Exon2 | Exon3 — adpgk

MO1 — KD1

MO2 — KD2

B

primer → ← primer

Exon1 (UTR) | Exon2 | Exon3 — WT

primer → ← primer

Exon1 (UTR) | Exon3 — KD1

WT KD1

500 bp
300 bp
200 bp

C

primer → ←

Exon1 (UTR) | Exon2 | Exon3 — WT

Exon1 (UTR) | Exon3 — KD1

adpgk

Fold change mRNA expression

■ WT
□ KD1

***

D

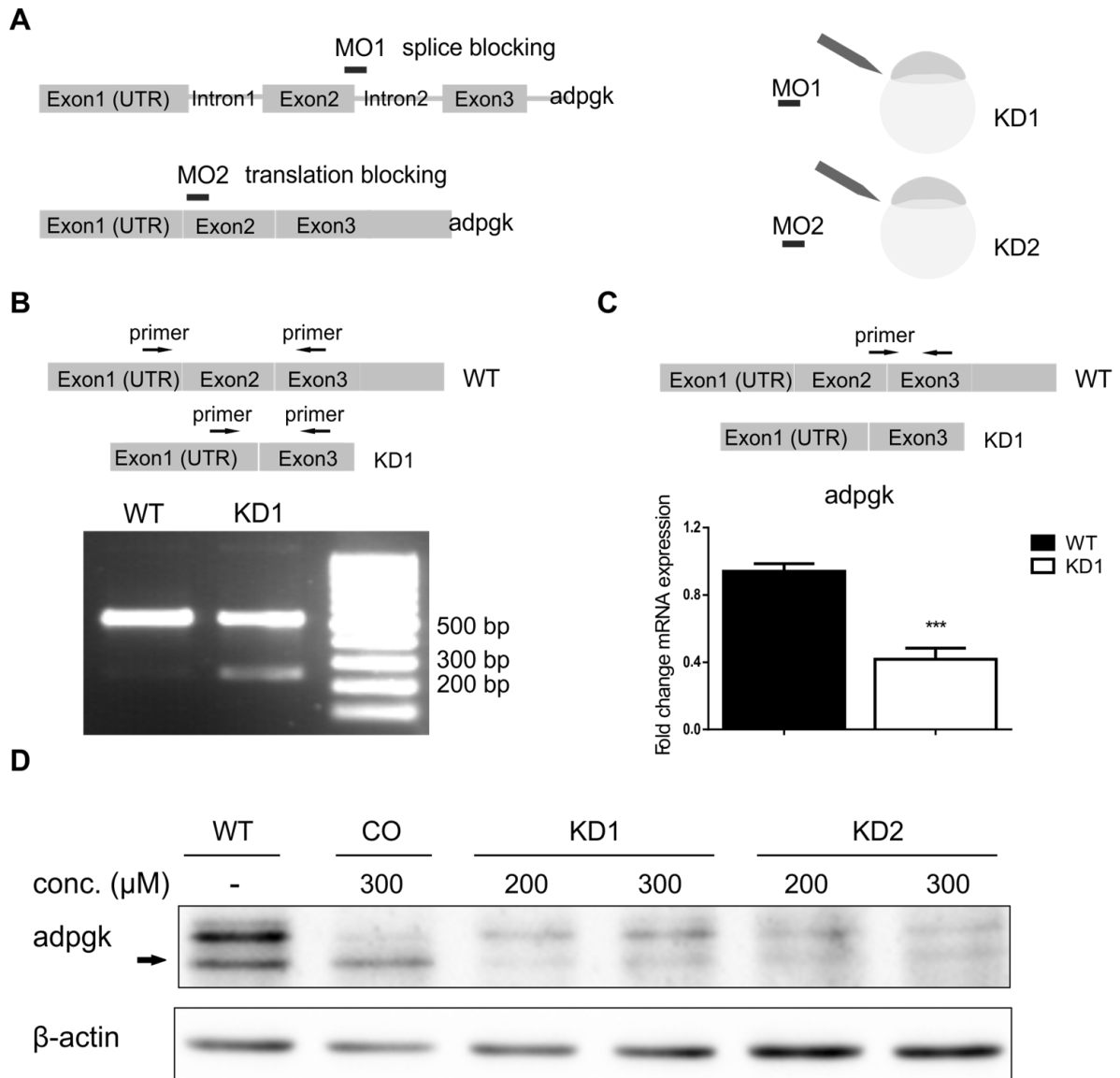|	WT	CO	KD1		KD2	
conc. (µM)	-	300	200	300	200	300

adpgk →

β-actin

Figure 5.2.2 Adpgk knockdown by morpholino based method. (A) The principles of the adpgk morpholinos used in the study. (B) The pooled of WT embryos showed a full size of 512 bp *adpgk* while the KD1 embryos had an additional 237-bp fragment (a truncated *adpgk)*. (C) For the quantitive *adpgk* mRNA measurement, the primers were designed at the exon 1 and 2 junction. The KD1 embryos showed significantly decreased *adpgk* expression ($p<0.005$; n=6), compared to the WT. (D) Both KD1 and KD2 embryos had significantly decreased adpgk protein (as indicated by the arrow) at the injection concentration of 200 µM and 300 µM, compared to the WT or CO group. The embryos for the measurement were collected from 6 independent batches. Unpaired *t*-test was performed with p value less than 0.05 considered as statistically significant.

5.3 Phenotypes of the adpgk knockdown embryos

5.3.1. Body and somite phenotypes

The short body axis

After establishing adpgk loss-of-function model, we examined the phenotype of the adpgk knockdown embryos. The KD1 embryos developed short body axis (Figure 5.3.1A and 5.3.1B). The lethality and severity of the phenotype was dependent on the concentration of injected morpholino. The lethality was 17 % (n=34), 38 % (n=50) and 43 % (n=17) at injection concentration of 150 μM, 250 μM and 300 μM, respectively (Figure 5.3.1C). At 150 μM, 9 % (n=34) of the KD1 embryos showed dorsalized body (severe) while 91 % of the KD1 embryos did not show prominent body phenotype. At 250 μM, 47 % (n=132) of the KD1 embryos showed short body axis (mild) and 17 % (n=132) of the embryos had the severe dorsalized body phenotype. When the injection concentration increased to 300 μM, the percentage of KD1 embryos showed severe phenotype increased to 38 % (n=108) while the mild short body phenotype decreased to 15 % (n=108). (Figure 5.3.1D) Based on the percentage of the phenotype and lethality, we selected and focused on injecting 300 μM of morpholino to the embryos in the following experiments.

Deformed somitogenesis

It has been shown that adpgk is expressed in the muscle and heart of the adult zebrafish [123]. Due to the dorsalized body phenotype, we wondered whether adpgk deficiency affected the somitogenesis of the embryos. Wnt11 is expressed in the embryonic myotome at 25 hpf [124]. The result from the *in situ* hybridization showed that the WT embryos had bilateral and uniformed wnt11 patterning while the KD1 embryos showed asymmetric and irregular *wnt11* staining. In accordance with the dorsalized body phenotype, the KD1 embryos also showed the deformed somiogenesis. (Figure 5.3.1E)

A

Lateral View

B

Dorsal View

C
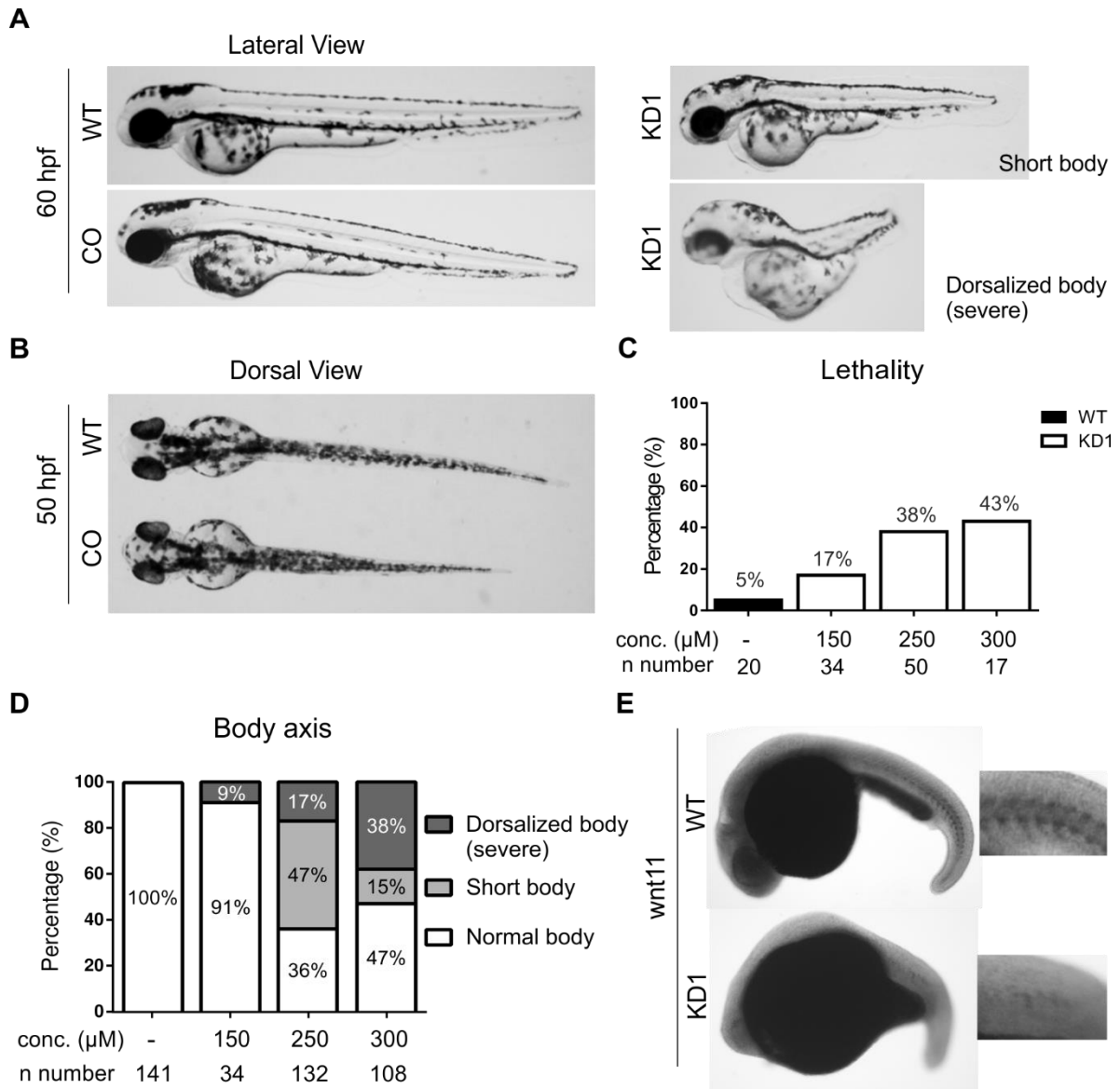
Lethality

D

Body axis

E

Figure 5.3.1 Short body axis and deformed somitogenesis in the adpgk knockdown embryos. (A-B) At 60 hpf, the lateral view and dorsal view of the embryos showed the shorter and/or dorsalized body in the KD1 embryos, compared to the CO and WT. (C) The lethality of the KD1 embryos was 17 % (n=34), 38 % (n=50) and 43 % (n=17) at the injection concentration of 150 μM, 250 μM and 300 μM, respectively. (D) The percentage of the KD1 embryos showing dorsalized (severe) phenotype increased from 9 % (n=34), 17 % (n=132) to 38 % (n=108) at the injection concentration of 150 μM, 250 μM and 300 μM, respectively. The mild phenotype decreased from 47 % (n=132) at the injection concentration of 250 μM to 15 % (n=108) at 300 μM. (E) The KD1 embryos showed deformed somitogenesis, indicated by the asymmetric and irregular *wnt 11* staining, compared to the WT.

5.3.2 Eye, cardiovascular system and hematopoiesis phenotypes

Deformed eye development

In addition to the short body and somitogenesis phenotypes, the KD1 embryos showed less pigmentation in the eyes, compared to the WT and CO. The eyes of the KD1 embryos were also not well separated to the lateral side. Overall, 37 % (n=54) of the KD1 embryos had an impaired eye development while none of the WT (n=106) and CO (n=66) embryos had the eye phenotypes (Figure 5.3.2A).

Heart malformation

Since adpgk is expressed in the heart of the adult zebrafish [123], we injected MO1 to the embryos of the transgenic zebrafish line Tg(*myl7*:GFP), labeling *myosin light chain 7 (myl7)* with green fluorescence (GFP) to observe the morphological change of the heart development. Thirty-seven percent of the KD1 embryos (n=91) exhibited the normal heart morphology while 4 % (n=91) showed the normal heart shape but reversed position of the atrium and ventricle (reversed heart looping). In addition, 18 % (n=91) of the KD1 embryos exhibited the correct heart looping but tubular heart shape while 41 % (n=91) of the embryos showed reversed heart looping and tubular heart shape. (Figure 5.3.2B).

Dysregulated vasculature and hematopoiesis

Human ADPGK is highly expressed in the immune cells [52]. Accordingly, to understand whether adpgk plays a role in hematopoietic cells, we knockdown adpgk in the Tg(*kdrl*:GFP, *gata1*:dsRed) and Tg(*pU.1*:dsRed) transgenic zebrafish lines. When *vascular endothelial growth factor receptor kdr-like (kdrl)* and *gata binding protein1 (gata1)* are expressed, the Tg(*kdrl*:GFP, *gata1*:dsRed) zebrafish has the highlighted vasculature in GFP and erythroid lineage cells in dsRed. Additionally, the Tg(*pU.1*:dsRed) zebrafish has the dsRed-labeled myeloid lineage cells when *pU.1* is expressed.

Eighty-seven percent of the Tg(*kdrl*:GFP, *gata1*:dsRed) KD1 embryos (n=23) developed irregular vasculature and reduced erythrocyte synthesis (Fig. 5.3.2C). The Tg(*pU.1*:dsRed) KD1 embryos showed reduced numbers of myeloid lineage cells, compared to the WT (Figure 5.3.2D). In addition, the KD1 embryos also showed reduced expression of primitive and definitive hematopoiesis marker, *runt-related transcription factor (runx1)* [125], suggesting the malformation of the myeloid development (Figure 5.3.2E).
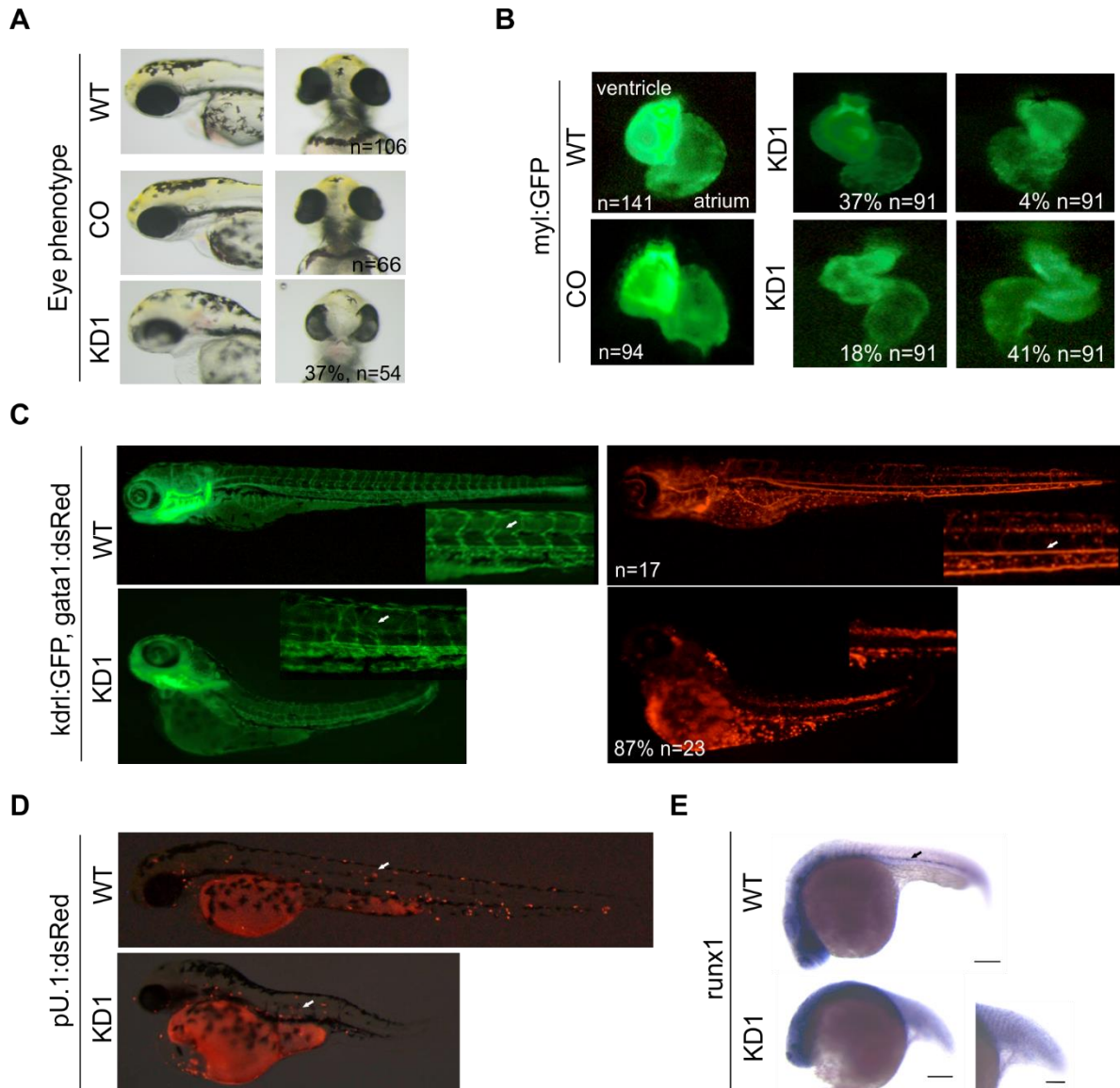
Figure 5.3.2 The malformation of eye, cardiovascular system and hematopoiesis in the KD1 embryos. (A) Thirty-seven percent (n=54) of the KD1 embryos had impaired eye development. (B) Thirty-seven percent of the KD1 embryos (n=91) exhibited the normal heart morphology while 4 % (n=91) of the embryos showed the normal heart shape but reversed heart looping. Eighteen percent of the KD1 embryos exhibited the correct heart looping but tubular heart shape while 41 % (n=91) of the embryos showed reversed heart looping and tubular heart shape. (C) Eighty-seven percent (n=23) of the Tg(*kdrl*:GFP, *gata1*:dsRed) KD1 embryos showed irregular vasculature and improper erythroid cell lineage development. (D) The Tg(*pU.1*:dsRed) KD1 embryos showed impaired development of the myeloid lineage cells. (E) The dysregulated definitive hematopoiesis indicated by the *in situ* hybridization of *runx1* staining in the KD1 embryos.

myl7: myosin light chain; kdrl: vascular endothelial growth factor receptor kdr-like; gata1: gata binding factor 1 (erythroid transcription factor); pU.1: Sp1 myeloid transcription factor; runx1: runt-related transcription factor.

5.4 Confirmation of the adpgk KD phenotype

There are debates of using morpholinos [126]; however, many studies highlight that morpholino based research is reliable when proper experimental design and control are used [122, 127]. Accordingly, we used three different strategies including overexpression experiments, rescue experiments and an additional morpholino (translation-blocking morpholino) to confirm the specificity of the KD1 phenotypes.

First of all, we performed the overexpression experiments since studies indicate that overexpression and knockdown of the gene of interest in zebrafish usually create the same phenotype [122]. We generated and injected zebrafish or human *adpgk* mRNA to overexpress *adpgk* in the WT embryos. WT embryos injected with high amounts of zebrafish (600 µM) (22 %, n=45) or human *adpgk* mRNA (700 µM) (40 %, n=67) showed a dorsalized body phenotype, which was highly similar to the KD1 embryos (Figure 5.4A).

Next, we used the "rescue" approach to confirm the specificity of the morpholinos (Figure 5.4B). We generated zebrafish *adpgk* mRNA and injected it with MO1 to the embryos to evaluate whether the phenotype could be rescued if there were proper *adpgk*. Our results showed that injecting 150 ng/dL of zebrafish *adpgk* mRNA to KD1 embryos partially rescued the short/dorsalized body axis. In the MO1-injected group, 64 % (n=47) percent of the KD1 embryos showed the short/dorsalized body phenotype. In the MO1 plus zebrafish *adpgk* mRNA injected-group, 59 % (n=76) of the KD1 embryos showed rescue effect (the percentage reduced to 41 % of the KD1 embryos showed the phnotype) (Figure 5.4C).

Last, we confirmed the results of the KD1 embryos using translation blocking morpholino. The KD2 embryos showed slightly short body and irregular somite (Figure 5.4D). However, the KD2 embryos did not show the phenotypes of the cardiovascular system and hematopoiesis, indicating these phenotypes might be secondary effect resulting from the severe dorsalized body development. Furthermore, we performed the rescue experiments in the KD2 embryos using human *ADPGK* mRNA since the mRNA sequence used for the rescue experiments cannot contain the morpholino target sequence. Our results showed that injecting 100 ng/dL of human *ADPGK* mRNA could also partially rescue the short body phenotype. In the MO2 injected group, 66 % (n=41) of the KD2 embryos showed the short body. In the group of MO2 co-injecting with human *ADPGK* mRNA, 60 % (n=45) of the embryos had the rescue effect (Figure 5.4D). To increase to rescue efficiency, we attempted to increase the concentration of the injected zebrafish or human *adpgk* mRNA. However, increasing the concentration could not reach the complete rescue but increase the lethality of the KD embryos (Table 5.1). It has been shown that rescue experiments seldom results in true wild type and it may only be partial

due to the injected mRNA expression is generally mosaic and/or the expressed protein may last not long enough [128-130].

Overall, the three different applied strategies suggested the good specificity of the dorsalized body phenotype in adpgk deficiency; therefore, we focused on investigating how adpgk deficiency led to the short body phenotype. It was also worth noting that morpholino control (CO) embryos did not show any phenotype. Thereby, we skip the CO injection for some experiments to save the injection time and increase the injection quality. We performed the following studies based on the splice blocking morpholino (for KD1) and used translation blocking morpholino (for KD2) for the confirmatory experiments.

Table 5.1 Summary of *adpgk* mRNA rescue_ correlation between the injected concentration and lethality

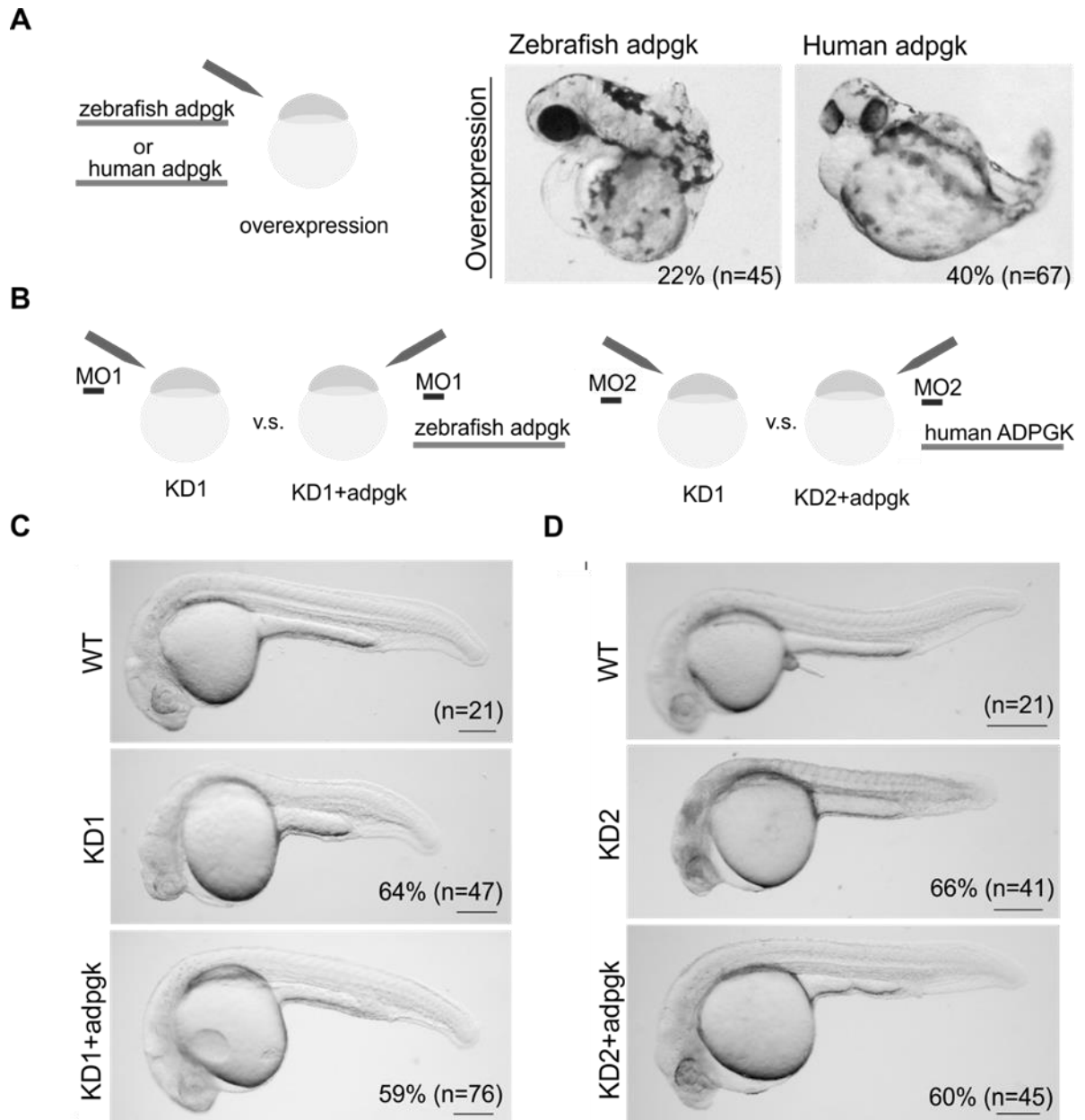| Genotype	Zebrafish *adpgk* mRNA (ng/µL)	Lethality (%)	n number
KD1	-	40	414
KD1	100	49	51
KD1	150	39	312
KD1	300	20	15
KD1	500	80	76
KD1	600	77	123
Genotype	Human *ADPGK* mRNA (ng/µL)	Lethality (%)	n number
KD2	-	42	418
KD2	100	43	359
KD2	200	29	72
KD2	300	77	52
KD2	500	70	50
KD2	700	65	79

Figure 5.4 Confirmation of the specificity of the short body phenotype in adpgk deficiency. (A) Twenty-two percent (n=45) of the embryos with zebrafish *adpgk* overexpression and 40 % (n=67) of the embryos with human *ADPGK* overexpression showed dorsalized body, which were highly similar to the KD1 embryos. (B) Scheme of the rescue experiments. (C) Co-injecting 150 ng/dL of the synthetic zebrafish *adpgk* mRNA with splice blocking morpholino to the embryos partially rescued the short/dorsalized body axis in the KD1 embryos. (D) The KD2 embryos showed short body and irregular somite. Co-injecting 100 ng/dL of the human *ADPGK* mRNA partially rescued the phenotype in the KD2 embryos.

5.5 Defected extension during gastrulation in embryos with adpgk deficiency

Embryonic body patterning is organized in the early developmental process. During the gastrulation stage, convergent extension determines the body length [131, 132]. To investigate whether the KD1 embryos showed defected convergent extension during the gastrulation, the prechordal plate, anterior edge of the neural plate and the developing notochord of the bud-stage-embryo (10 hpf) were stained by *in situ* hybridization using *hgg1*, *dlx3* and *ntl* probe, respectively. Compared to the WT, the KD1 embryos had defected extension (p<0.05, n=59), indicated by the shorter distance between prechordal plate and the developing notochord (Figure 5.5A).

Since convergent extension is the process of collective cell movement and small Rho-GTPases proteins-related signaling pathway mediates the cell migration and intercalation (Figure 5.5B) [133], we next measured the level of Rac1/2/3 to understand whether the cell migration was dysregulated. Compared to the WT, the KD1 and KD2 embryos at 22 hpf showed decreased Rac1/2/3 (p<0.05 in the KD1; p=0.0549 in the KD2, n=3), indicating the involvement of dysregulated Rho-GTPase-related signaling pathway in adpgk deficiency. (Fig 5.5C)

Rac1/2/3 is regulated by the wnt signaling and the wnt signaling pathways has been shown to be highly related to convergent extension [76, 77]. Accordingly, to investigate whether there were dysregulated wnt signals leading to the malformation of convergent extension, we attempted to rescue the phenotype with different synthetic *dishevelled (dsh)* mRNA, the key component of wnt signaling pathway including *dsh* (general *dsh*), *dsh_ΔC* (*dsh* with domain specifically activates canonical wnt) and *dsh_ΔN* (*dsh* with domain specifically activates noncanonical wnt) [134]. However, increasing *dsh* expression in the KD1 embryos could not rescue the short/dorsalized body phenotype. Table 5.2 showed that 70 % (n=46) of the KD1 embryos developed short/dorsalized body; however, when co-injecting MO1 with 200 ng/dL of *dsh*, *dsh_ΔC* or *dsh_ΔN* mRNA, 65 % (n=121), 58 % (n=24) or 69 % (n=32) of the embryos still exhibited the short/dorsalized body, respectively.

Overall, the insufficiency of the *dsh* mRNA rescue experiments suggested that wnt signals might not be the main factors causing the short body axis in adpgk deficiency or the effects were not on genomic levels.

Table 5.2 Summary of *dishevelled* mRNA rescue

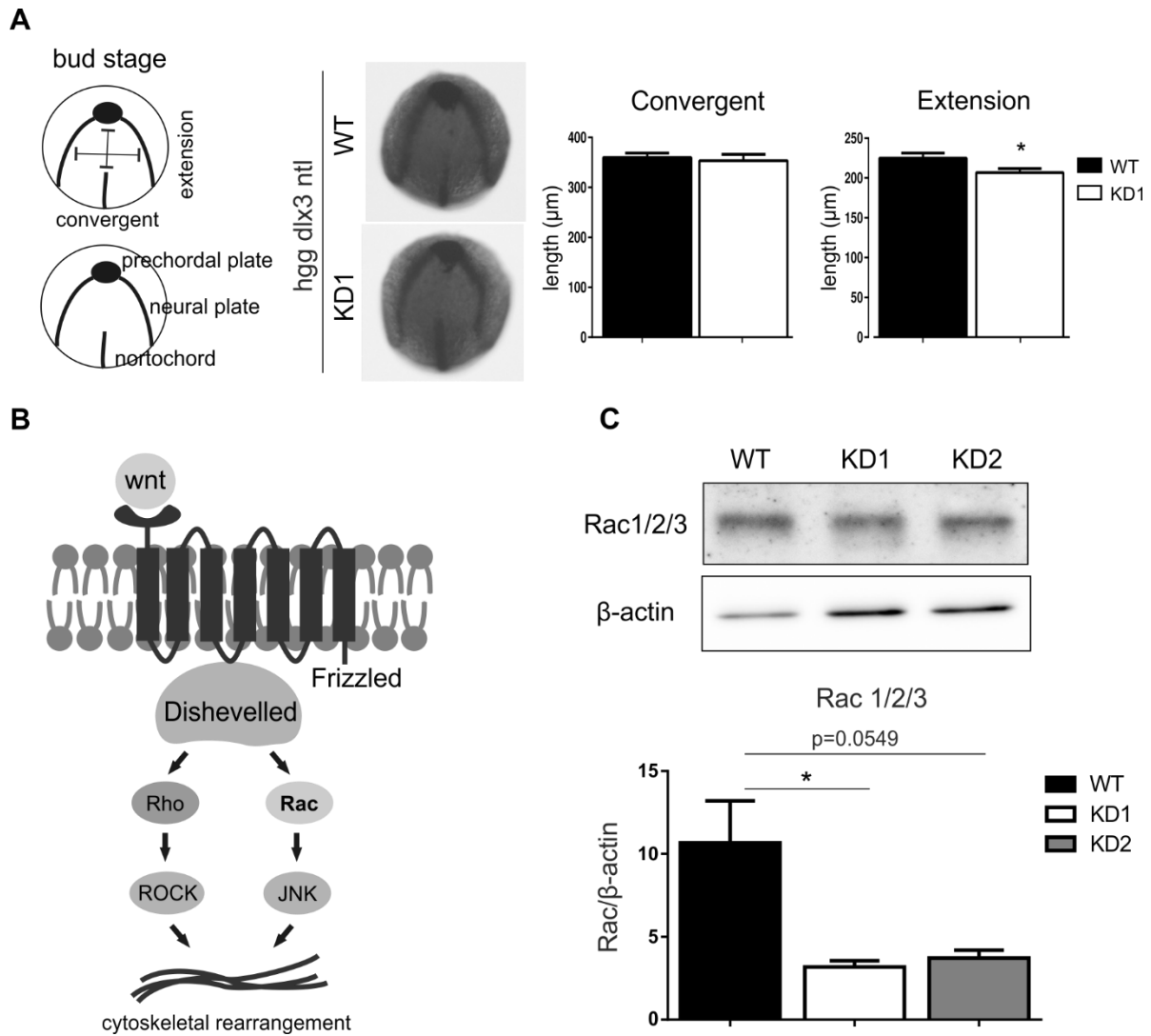| Genotype	mRNA injected	Conc.(ng/μL)	Phenotype (%)	n number
KD1	-	-	70%	46
KD1	*Dsh*	100	66%	83
KD1	*Dsh*	200	65%	121
WT	*Dsh*	200	0%	5
KD1	*Dsh_ΔC*	100	70%	89
KD1	*Dsh_ΔC*	200	58%	24
WT	*Dsh_ΔC*	200	0%	5
KD1	*Dsh_ΔN*	100	75%	52
KD1	*Dsh_ΔN*	200	69%	32
WT	*Dsh_ΔN*	200	13%	8

A

B

C

Figure 5.5 Defected extension during the gastrulation with reduced GTPase protein in adpgk deficiency. (A) The KD1 embryos had shorter extension, indicated by the short length between prechordal plate (*hgg1*) and nortochord (*ntl*) (p<0.05 n=59 embryos), compared to the WT. (B) Scheme of the GTPase proteins-related signaling pathway. (C) Compared to the WT, KD1 (p<0.05, n=3) and KD2 embryos (p=0.0549, n=3) showed decreased Rac1/2/3 protein level. The n number shown in the *in situ* hybridization indicated the exact numbers of evaluated embryos. The levels of Rac1/2/3 were measured from three independent batches of pooled embryos. Unpaired *t*-test was performed with p value less than 0.05 considered as statistically significant.

5.6 Unchanged gene expression of the developmental signaling pathways in embryos with adpgk deficiency

In addition to wnt, hedgehog (hh) signaling pathway regulates the ciliogenesis and determines the body patterning. In hh signaling pathway, the binding of shh to its receptor, patch1 (protein patched homolog 1) activates the downstream transcription factor, gli1 (glioma-associated oncogene homolog); furthermore, gli1 targets to the genes involving in regulating cell proliferation, apoptosis and angiogenesis [135]. Interestingly, inhibiting hh signaling in zebrafish has been shown also leads to the abnormal cardiomyocyte, retina and notochord development [136]. Accordingly, we collected embryos at the gastrulation stage and examined whether hh signaling was impaired by measuring the expression of *shh*-related genes. However, our RT-qPCR results revealed the unchanged *shha* (n=9), *patch1* (n=5) and *gli1* (n=6) expression in the KD1 embryos, compared to the WT (Figure 5.6A).

Alternatively, due to the dorsal embryonic expression of *adpgk*, we investigated whether there were changes of the dorsal organizer genes in adpgk deficiency. For instance, chordin regulates dorsal-ventral patterning in the early embryonic development [137]. Chordin and sox17 are required for the formation of Kupffer's vesicle and the determination of left-right asymmetry in zebrafish. Also, it has been shown that knockdown of sox 17 in zebrafish results in slightly shortened body axis, heart edema and cell death phenotypes [138]. However, we did not observe significant changes of the *chordin* and *sox17* embryonic patterning in adpgk deficiency from the *in situ* hybridization staining (Figure 5.6B).

Since several developmental signaling pathways orchestrate the body patterning and embryonic development [62], to further understand whether there was a dysregulation of the main developmental pathway in the KD1 embryos during the gastrulation, we used a "signal transduction PathwayFinder PCR array (Qiagen, Hilden, Germany)" for a broad screening. The array includes genes involving in the tgfβ, wnt, nf-κb, jak/stat, notch, hedgehog, ppar, oxidative stress, hypoxia and p53 signaling pathways (Table 5.3). Surprisingly, the KD1 embryos showed only few significant changes of the gene expression in the screened signaling pathways, compared to the WT. The volcano plot (Figure 5.6C) summarized the fold changes and p values of the screened genes. The identified promising target genes were *wnt6*, *carbonic anhydrase9 (ca9)*, *inhibitor of dna binding1 (id1)*, *NAD(P)H dehydrogenase, quinone 1 (nqo1)* and *bmp4* as well as cell death and cell cycle related genes. Overall, based on the mRNA screening, it seemed that the main developmental signaling pathways were not strongly affected in the KD1 embryos. Mechanisms other than the altered developmental signaling seemed to be the culprit for causing the phenotypes in adpgk deficienc

Table 5.3 List of genes in the "signal transduction PathwayFinder PCR array".

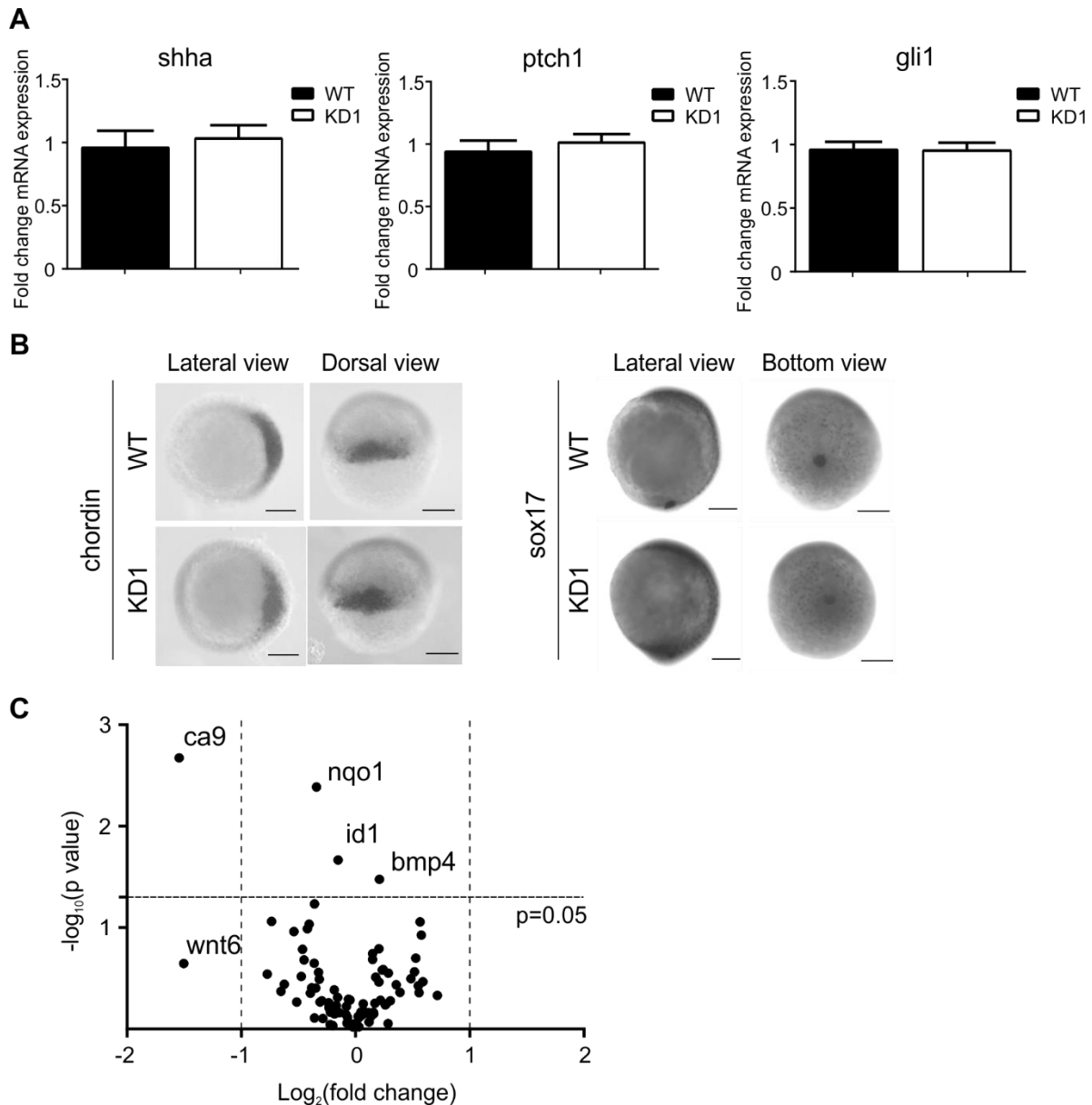| Pathways	Genes
TGFβ	atf4b1, atf4b2, emp1, herpud1, ifrd1, myca, mycb, nfixa, tnfsf10.
WNT	axin2, ccnd1, ccnd2a, dab2, fosl1a, ppardb, wisp1a, wisp1b, wnt2bb, wnt5a.
NFκB	bcl2l1, birc2, stat1a
JAK/STAT	bcl2l1, cebpd, gata3, irf1a, mcl1a, mcl1b, lrg1, socs3a, socs3b, stat1a
p53	baxa, bbc3, btg2, cdkn1a, egfra, fas, gadd45aa, gadd45ab, gadd45ba, pcna, rb1
Notch	her6, hey1, hey2, heyl, id1, jag1b, lfng, notch1b
Hedgehog	bcl2, bmp2b, bmp4, wnt6, ptch1, wnt1, wnt3a
PPAR	acsl3a, acsl3b, acsl4a, acsl5, cpt2, fabp1a, sorbs1, slc27a4
Oxidative Stress	fth1a, fth1b, gclc, gclm, hmox1a, nqo1, sqstm1, txnrd1, gsr
Hypoxia	arnt, ca9, csf1a, csf1b, epo, ldha, adm, serpine1, slc2a1a, slc2a1b, vegfab

Figure 5.6 Unchanged gene expressions of the developmental signaling pathways in adpgk deficiency. (A) Compared to the WT, the KD1 embryos showed unchanged expression of *shha*, *ptch1* and *gli1* (n ≥ 5). (B) *In situ* hybridization showed that adpgk knockdown did not affect the patterning of organizer genes, *chordin* (n=12 embryos) and *sox17* (n=15 embryos). (C) The volcano plot showed the correlation between the fold change (x-axis) and the p value (y-axis) of the gene expression from the signal transduction PathwayFinder PCR array. The array identified significant changes of ca9, nqo1 and bmp4, and a more than 2 fold-decreased *wnt6a* in the KD1 embryos (n=3). The n number shown in the *in situ* hybridization indicated the exact numbers of evaluated embryos. The RT-qPCR results were done from at least three independent batches of pooled embryos. Unpaired *t*-test was performed with p value less than 0.05 considered as statistically significant.

5.7 Increased apoptosis in adpgk knockdown embryos

The results from the signal transduction PathwayFinder PCR array showed, albeit high variation, changes of the apoptosis-related and the cell cycle-regulating molecules in adpgk deficiency. Since the embryonic development is a coordinated process between different cell behaviors such as the cell proliferation and cell death, we sought whether adpgk knockdown exhibited increased apoptosis, which led to the short body phenotype. Accordingly, we investigated the cell death of embryos at the 24 hpf by Acridine Orange and TUNEL staining.

Acridine orange is a nucleic acid-selective fluorescent dye. It stains DNA and presents a condensed green fluorescence in the dead cells. [139] Acridine Orange staining showed increased dead cells through the whole body of the 22 hpf KD1 embryos, while the WT had only few patches of the condensed green fluorescent staining indicative of apoptosis (Figure 5.7A).

TUNEL staining detects double-strand DNA breaks (green fluorescence), a hallmark of apoptosis. In accordance with the Acridine Orange staining, TUNEL assay showed increased numbers of apoptotic cells in both 22 hpf KD1 and KD2 embryos, compared to the WT. (Figure 5.7B) The irregular shape of the body part in the KD embryos coincided with the area of increased apoptotic cells, implying apoptosis resulted in the body phenotype.

To confirm the increased apoptosis, we collected embryos at the gastrulation stage and measured the expression of the apoptosis-related genes using RT-qPCR. In line with the increased apoptosis, albeit unchanged *bcl* expression, the KD1 embryos showed induced expression of the pro-apoptotic factor, *bbc3* ($p<0.05$, n ≥ 5) and reduced expression of the anti-apoptotic gene, *bcl2l* ($p<0.005$, n ≥ 5), compared to the WT. The reduced *bcl2l* expression could also be rescued when injecting synthetic zebrafish *adpgk* mRNA in the KD1 embryos ($p<0.05$, n ≥ 5, compared to the KD1) (Figure 5.7C).

Therefore, the results overall showed that adpgk deficiency induced apoptosis, which could possibly lead to the crippled body phenotype.
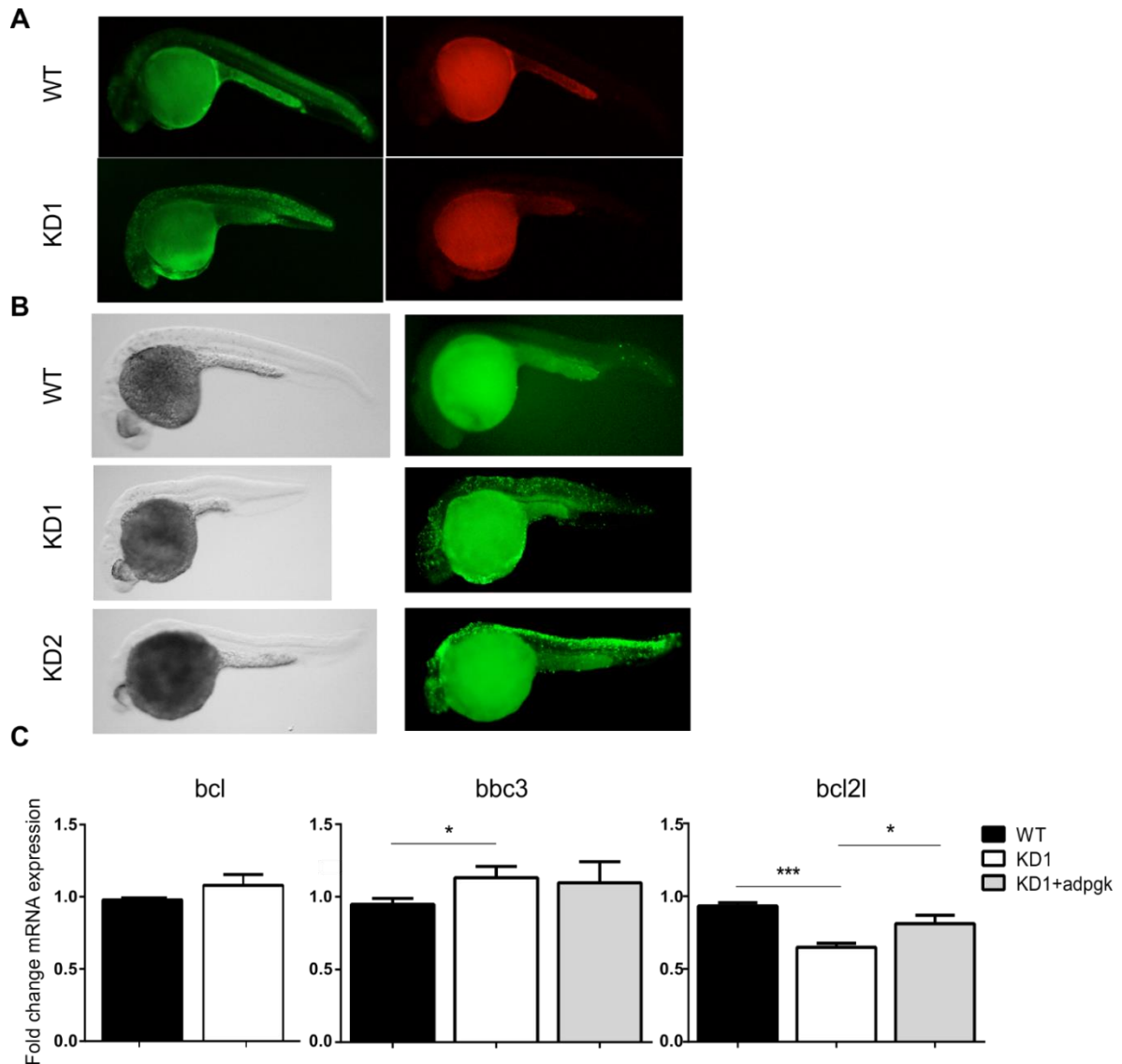
Fig. 5.7 Increased apoptosis in adpgk deficiency. (A) Compared to the WT, the KD1 embryos had more dead cells, indicated by the increase of the condensed green fluorescent in Acridine Orange staining. (B) The result from TUNEL assay showed increased apoptotic cells in the KD1 and KD2 embryos, compared to the WT. (C) The KD1 embryos had activated *bbc3* ($p<0.05$) and reduced *bcl2l* ($p<0.005$) expression, compared to the WT. The reduction of *bcl2l* expression could be rescued with *adpgk* mRNA ($p<0.05$, compared to KD1). The embryos were collected from at least 5 independent batches. Unpaired *t*-test was performed with p value less than 0.05 considered as statistically significant.

5.8 The activated cell cycle checkpoints in adpgk knockdown embryos

Cell death and cell proliferation are regulated by the cell cycle checkpoints. Cells with DNA damage or under certain stress activate cell cycle checkpoints. Generally, cells undergo quiescence or apoptosis when the damages are unrepairable [140].

Thus, to investigate whether adpgk deficiency triggered the activation of the cell cycle checkpoints and led to apoptosis, we screened the expression of cell cycle-related genes including *cyclin-dependent kinase inhibitor 1A* (*cdkn1a*; *p21*), *mycb*, *growth arrest and DNA-damage-inducible, alpha, a* (*gadd45aa*) and *rb1* in the embryos during the gastrulation stage using RT-qPCR.

Consistent with the increased apoptosis, the cell cycle checkpoints were activated in the KD1 embryos. The KD1 embryos had increased expression of the cell cycle checkpoint genes, *cdkn1a* ($p < 0.005$, $n \geq 5$) and *gadd45aa* ($p < 0.005$, $n \geq 5$), compared to the WT. In addition, the KD1 embryos also showed slightly increased *mycb* expression ($p = 0.06$, $n \geq 5$) but unchanged *rb1* expression, compared to the WT. Notably, the increased expression of *cdkn1a* could also be reduced when supplying synthetic zebrafish *adpgk* mRNA in the KD1 embryos ($p < 0.05$, $n \geq 5$, compared to the KD1) (Figure 5.8A), indicating the expression of *cdkn1a* was highly correlated to adpgk.

Since p53 up-regulation is one of the most common mechanisms triggering the activation of cdkn1a and further promoting cell cycle arrest and cell death [141], we thought the activation of p53 led to the cell cycle arrest and cell death in adpgk deficiency. According to the hypothesis, we knocked down *p53* expression by MO-p53 in the KD1 embryos and evaluated whether decreasing p53 expression could rescue the phenotype. Our results showed that 73 % (n=91) of the KD1 embryos had the short/dorsalized body phenotypes; however, the percentage increased to 92 % (n=72) when suppressing *p53* expression in the KD1 embryos (Figure 5.8B). Consistently, the exacerbation outcome was also observed in the KD2 embryos. Seventy-two percent (n=152) of the KD2 embryos had the short/dorsalized body phenotypes and the percentage increased to 89 % (n=84) when suppressing *p53* expression in the KD2 embryos

Overall, the insufficiency of p53 rescue experiments suggested that the cell cycle arrest and apoptosis in embryos with adpgk deficiency was through a p53-independent pathway.
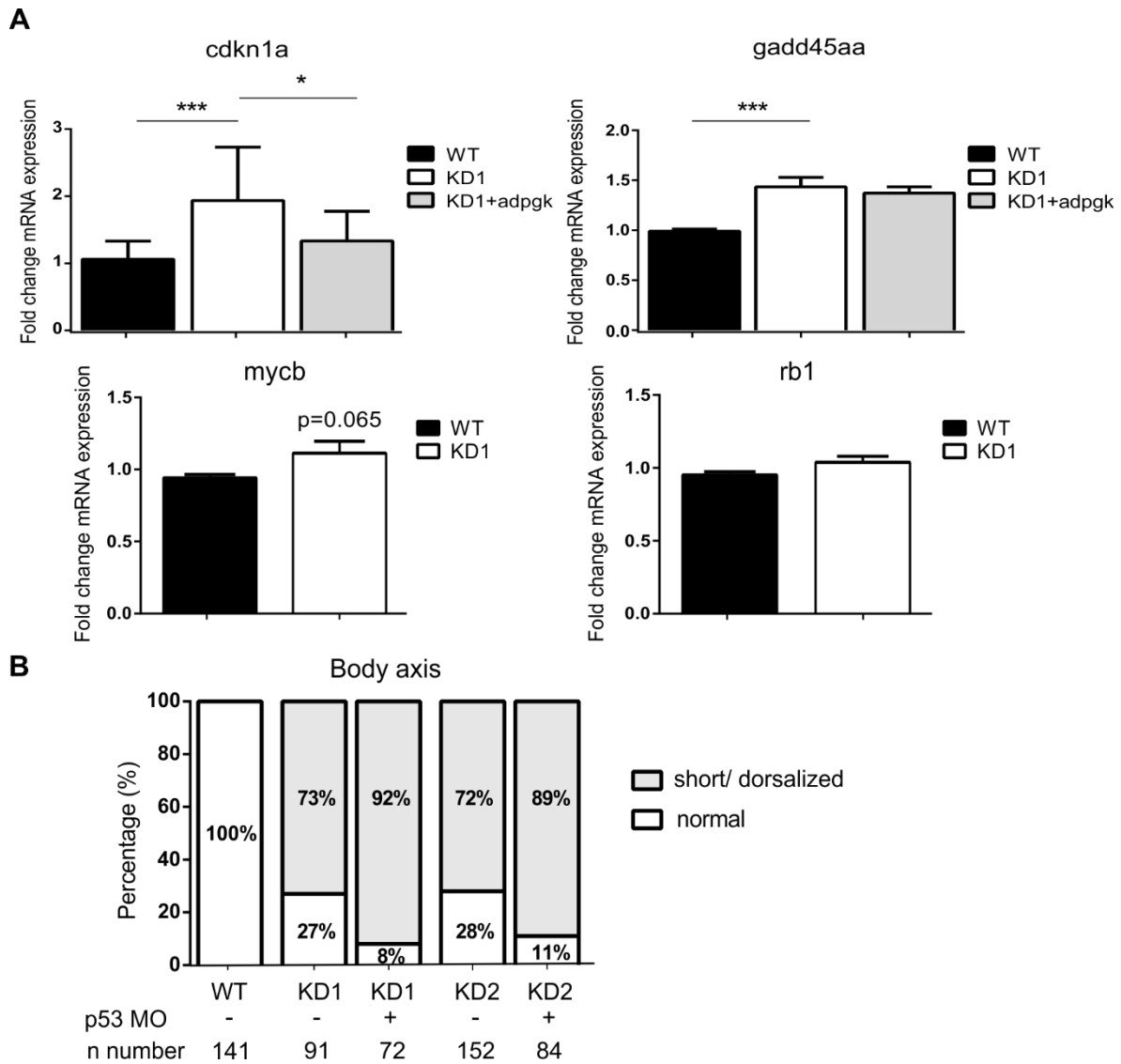
A

B

Figure 5.8 Activated cell cycle checkpoints in adpgk deficiency. (A) The RT-qPCR results revealed the increased expression of the cell cycle checkpoint genes, *cdkn1a* (p<0.005, n ≥ 5) and *gadd45aa* (p<0.005, n ≥ 5) in the KD1 embryos, compared to the WT. The increased *cdkn1a* could also be rescued in the KD1 embryos (p<0.05, compared to the KD1) The KD1 embryos also showed slightly increased *mycb* (p=0.065, n ≥ 5) and unchanged rb1. (B) Reducing *p53* in adpgk deficiency could not rescue the short/doralized body phenotype. Seventy-three percent (n=91) of the KD1 embryos showed short/dorsalized body, while knockdown *p53* in the KD1 embryos increased the percentage of embryos with the phenotypes increased to 92 % (n=72). Compared to 72 % (n=152) of the KD2 embryos showed short body axis, the percentage of embryos with the phenotypes increased to 89 % (n=84) when suppressing *p53* expression. The gene expressions were investigated using embryos collected from more than 5 independent batches. Unpaired *t*-test was performed with p value less than 0.05 considered as statistically significant.

60

5.9 The disturbed glucose homeostasis and pH balance in embryos with adpgk deficiency

Growing body of evidences have suggested that the cell cycle progression and cell death are controlled by the nutrient status, and the metabolic disturbance eventually leads to the cell death. [142, 143] Thereby, we hypothesized the activated cell cycle arrest and cell death were resulted from the altered glucose homeostasis in adpgk deficiency.

According to our speculation, we first measured the free glucose level of the embryos. Our results showed that both KD1 (0.387±0.0259 mmol/g, p<0.01, n=6) and KD2 embryos (0.306±0.0216 mmol/g, p<0.005, n=6) had significantly decreased free glucose, compared to the WT (0.533±0.0372 mmol/g) (Figure 5.9A). Intriguingly, the decreased glucose did not alter the energy status in the embryos. Compared to the WT, the KD1 embryos showed unchanged ATP, ADP and AMP (n=5) (Figure 5.9B). Thus, it seemed that the embryonic cells in adpgk deficiency had increased glucose usage for maintaining the energy level.

Since the increased glucose uptake and lactate production are the hallmarks of cells employ aerobic glycolysis (Warburg effect) to maintain the sufficient energy generation[7], we wondered whether adpgk knockdown benefited from the Warburg phenotype. Accordingly, we measured the gene expression of the glucose transporter and hexokinases including *solute carrier family 2 member 1 (slc2a1a)*, *hk1* and *hk4*, and the level of lactate and pyruvate. Indeed, we found the increased *hk1* expression (p<0.01, n≥5), despite of the unchanged *glucose transporter (slc2a1a)* and *hk4* expression in the embryos at the gastrulation stage (Figure 5.9C). However, adpgk deficiency exhibited reduced lactate-to-pyruvate ratio (lactate/pyruvate). The KD1 embryos showed a 1.59-fold decreased lactate/pyruvate (72.31 ± 14.120 in the WT vs. 45.59 ± 5.346 in the KD1, p=0.076, n=3) and also the KD2 embryos had a 1.81-fold decreased lactate/pyruvate (72.31 ± 14.120 in the WT vs. 40.00 ± 7.329 in the KD2, p=0.056, n=3) (Figure 5.9D). Thus, the result of decreased lactate/pyruvate suggested an altered glucose metabolism (anti-Warburg phenotype) in adpgk deficiency.

In addition to the energy generation, the level of lactate influences the acid and base status [144]. Interestingly, the results from the RT-qPCR array also suggested the change of *ca9* in the KD1 embryos. Ca9 maintains intracellular and extracellular pH and is increased in response to the accumulation of intracellular lactate [145]. Consistent with the decreased lactate, we confirmed that the KD1 embryos exhibited a significant decrease of *ca9* expression (p<0.005, compared to the WT, n≥5). The decreased expression of c*a9* could be rescued when supplying *adpgk* mRNA (p<0.005, compared to the KD1, n≥5) (Figure 5.9E), suggesting the high correlation between *ca9* and *adpgk* expression. In concert with the decreased

lactate/pyruvate, the decreased ca9 expression also indicated a perturbed acid-basic homeostasis in adpgk deficiency. Overall, the altered glucose homeostasis and pH balance could induce cell death in adpgk deficiency.
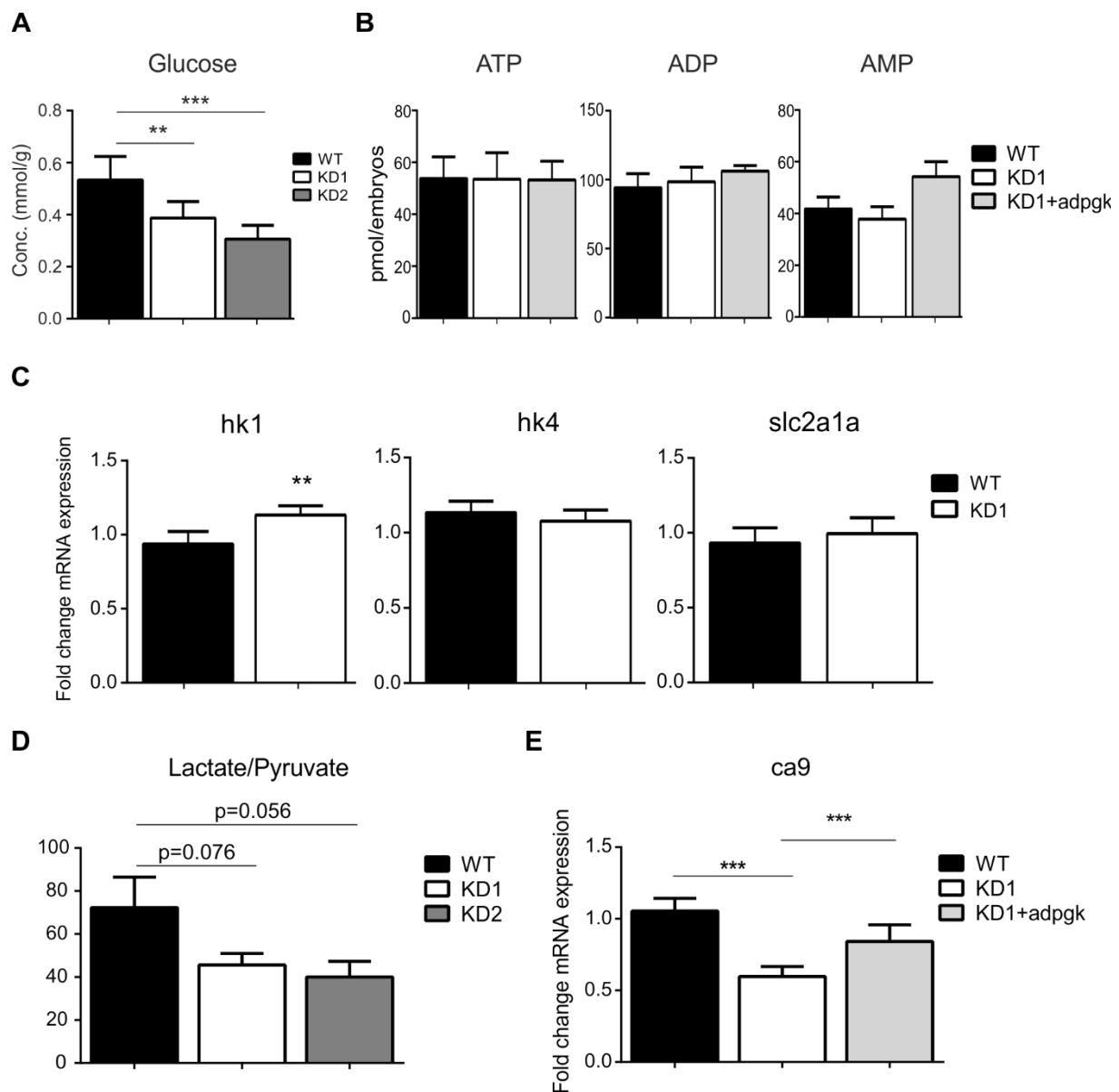
Figure 5.9 An altered glucose metabolism and pH balance in adpgk deficiency. (A) Both KD1 (0.387±0.0259, p<0.01, n=6) and KD2 (0.306±0.0216, p<0.005, n=6) embryos showed significantly decreased free glucose, compared to the WT (0.533±0.0372) (B) The level of ATP, ADP and AMP was not changed in the KD1 embryos. (C) The KD1 embryos showed increased expression of *hk1* (p<0.01, n≥5) but unchanged hk4 and slc2a1a, compared to the WT. (D) Decreased lactate to pyruvate ratio in adpgk deficiency. The KD1 embryos showed a 1.59-fold decreased lactate/pyruvate (72.31 ± 14.120 in the WT vs. 45.59 ± 5.346 in the KD1, p=0.076, n=3) and the KD2 embryos had a 1.81-fold decreased lactate/pyruvate (72.31 ± 14.120 in the WT vs. 40.00 ± 7.329 in the KD2, p=0.056, n=3). (E) *Ca9* expression was significantly decreased in the KD1 embryos (p<0.005, compared to the WT, n≥5) and the decreased *ca9* expression could be rescued when supplying *adpgk* mRNA (p<0.005, compared to KD1, n≥5). The metabolic measurements were carried out using embryos collected from at least 3 independent batches while the the gene expression were investigated using embryos collected from more than 5 independent batches. Unpaired *t*-test was performed with p value less than 0.05 considered as statistically significant.
The measurement of ATP, ADP and AMP was performed by the Metabolomics Core Facility of Heidelberg University.

5.10 Increased PPP in adpgk knockdown embryos

Due to the altered glucose homeostasis, we performed glucose flux studies to understand how glucose was metabolized in adpgk deficiency. We first aimed to establish a liquid chromatography tandem mass spectrometry (LC-MS/MS) method for measuring the main glucose intermediates in the embryos including G6P, FBP, GAP, PEP, PYR, and Ru5P. The detailed parameters of the MS/MS were listed in Table 5.4.

First, we established the standard curves of G6P, FBP, GAP, PEP, PYR and Ru5P from 0.1 µM to 10 µM with the linearity between 0.98 and 0.99. To test the reliability of the measurement, we next spiked the known concentration (1.6 µM, 4 µM and 8 µM) of G6P, FBP, GAP, PEP, PYR and Ru5P to the blank matrix and calculated the measured concentration (recovery rate). The recovery rate of G6P, FBP, GAP, PEP, PYR and Ru5P at 1.6 µM, 4 µM and 8 µM were from 80 % to 119 %, 94 % to 114 %, and 82 % to 104 %, respectively (Table 5.5). The overall recovery rates fell into the range between 80% and 120 %, indicating the good reliability of the measurement. In addition, we tested the precision of the method by measuring 10 samples that had the same concentration. The variation (precision CV %) of G6P, FBP, GAP, PEP, PYR and Ru5P measurement were 8.4 %, 7.5 %, 8.1 %, 7.4 %, 7.8 % and 6.2 %, respectively (Table 5.5). Therefore, based on the good recovery rate and precision, we successfully established the LC-MS/MS method for measuring glucose intermediates.

Next, we used the established LC-MS/MS method to study glycolytic flux in adpgk deficiency (Figure 5.10A). In accordance with the decreased free glucose, the MS/MS results showed that KD1 embryos had significantly increased G6P level (2.17 ± 0.098 µmol/g in WT vs. 2.92 ± 0.213 µmol/g in KD1, $p<0.01$), suggesting an increased glucose consumption. However, the level of FBP and PEP were unchanged. Interestingly, Ru5P, the product of PPP and GAP, the metabolite in both glycolysis and PPP were strongly increased. The KD1 embryos showed a 1.6-fold-increased Ru5P (0.11 ± 0.008 µmol/g in WT vs. 0.18 ± 0.008 µmol/g in KD1, $p<0.005$) and a 2-fold-increased GAP (0.22 ± 0.047 µmol/g in WT vs. 0.45 ± 0.083 µmol/g in KD1, $p<0.05$).

The increased Ru5P in KD1 embryos could also be reduced when rescuing with zebrafish *adpgk* mRNA (0.18 ± 0.008 µmol/g in KD1 vs. 0.13 ± 0.009 µmol/g in KD1+adpgk, $p<0.01$) (Fig. 5.10B). Overall, our glycolytic flux study indicated an increased glucose flux to PPP in adpgk deficiency.

Table 5.4 Tandem mass spectrometry parameters of the targeted glucose intermediates

Compounds	Parent ion (m/z)	Daughter ion (m/z)	Cone (Volts)	Coll energy (eV)
G6P	-258.70	-96.70	-51.00	-14.00
FBP	-338.90	-96.80	-117.00	-21.00
GAP	-168.90	-96.80	-38.00	-8.00
PEP	-166.70	-78.80	-36.00	-13.00
PYR	-86.80	-43.20	-60.00	-8.00
Ru5P	-228.90	-96.70	-46.00	-10.00
LAC-$^{13}C_3$	-89.90	-44.10	-68.00	-9.00

Table 5.5 Recovery rate and intra-run imprecision of the measurement

Compounds	Recovery (%) 1.6 µM	Recovery (%) 4 µM	Recovery (%) 8 µM	Imprecision (CV %)
G6P	100	114	104	8.4
FBP	80	105	82	7.5
GAP	119	107	103	8.1
PEP	116	97	99	7.4
PYR	86	94	82	7.8
Ru5P	99	114	102	6.2

Glucose-6-Phosphate (G6P), Fructose-1,6-Bisphosphate (FBP), Glyceraldehyde-3-Phosphate (GAP), Phosphoenylpyruvate (PEP), Ribulose-5-Phosphate (Ru5P), Phosphoenylpyruvate (PEP), Pyruvate (PYR)
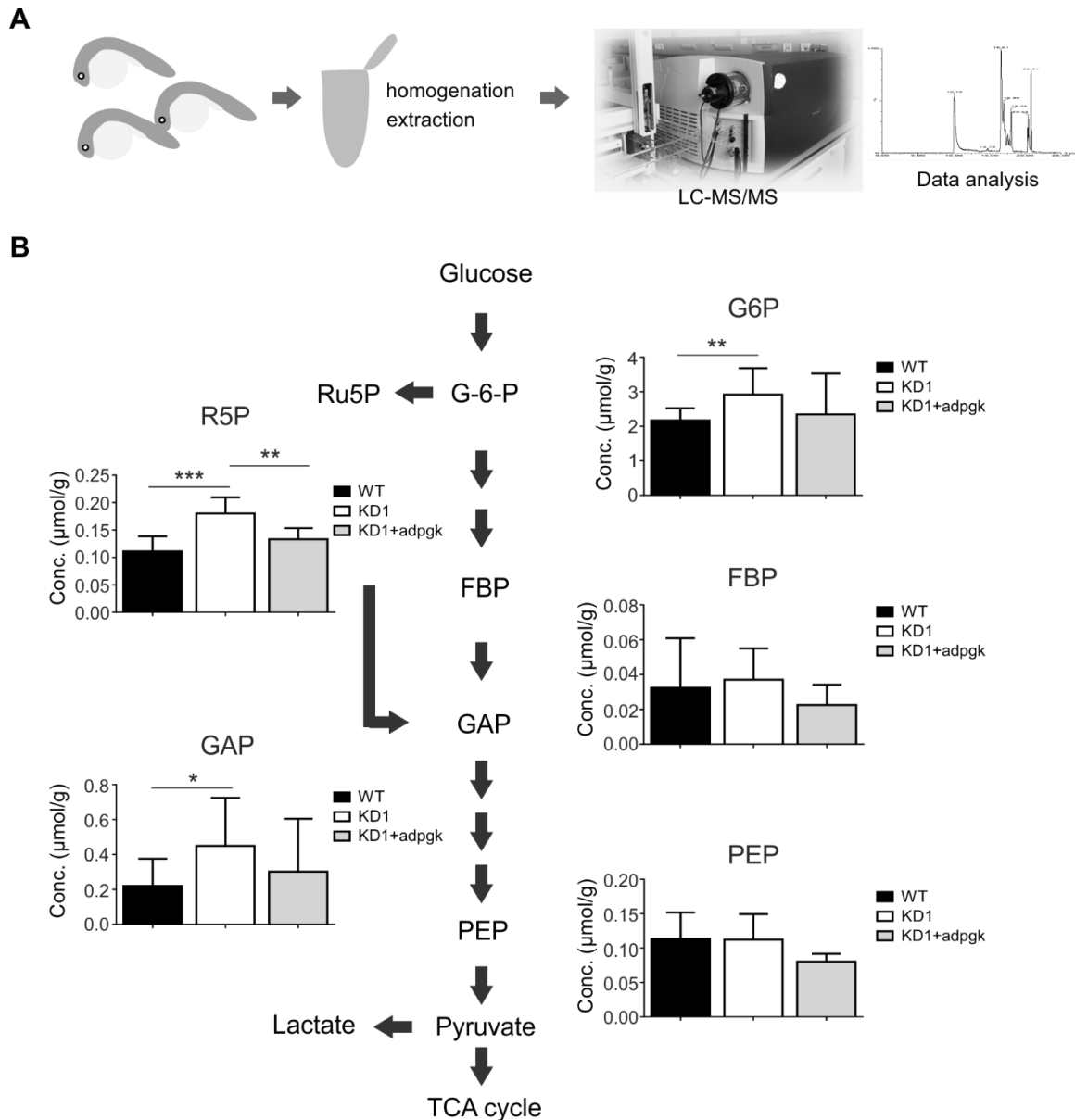
Figure 5.10 Increased glucose flux to PPP in adpgk deficiency. (A) Scheme of the glucose flux study. (B) The LC-MS/MS result showed a significant increase of G6P (2.17 ± 0.098 µmol/g in WT vs. 2.92 ± 0.213 µmol/g in KD1, p<0.01) but unchanged FBP and PEP level. KD1 embryos had activated PPP, indicated by increased Ru5P (0.11 ± 0.008 µmol/g in WT vs. 0.18 ± 0.008 µmol/g in KD1, p<0.005) and GAP (0.22 ± 0.047 µmol/g in WT vs. 0.45 ± 0.083 µmol/g in KD1, p<0.05). The increased Ru5P in KD1 embryos could be reduced when rescuing with zebrafish *adpgk* mRNA (0.18 ± 0.008 µmol/g in KD1 vs. 0.13 ± 0.009 µmol/g in KD1+adpgk, p<0.01). The measurement were done using embryos collected from more than 5 independent batches. Unpaired *t*-test was performed with p value less than 0.05 considered as statistically significant.

5.11 Altered defense system against ROS in adpgk knockdown embryos

Next, we sought why adpgk deficiency exhibited the increased glucose flux to PPP. Since the main function of the PPP is detoxify ROS [146], and we also observed the increased cell death in adpgk deficiency, we first speculated an altered ROS defense system in the adpgk KD embryos. Accordingly, we measured the level of NADPH, the downstream product of PPP participating in the conversion of GSSG to GSH for the detoxification of ROS. However, our results showed unchanged NADPH level in the KD1 embryos (Figure 5.11A) and additionally unchanged $NADH/NAD^+$, the indicator of nitrosative stress and GSSG/GSH, the indicator of ROS. It was worth noting that despite of the unchanged GSSG/GSH, the KD1 embryos rather showed a decrease of total glutathione (127.3 ± 3.033 pmol/embryos in the WT vs. 118.2 ± 2.520 pmol/embryos in the KD, $p < 0.05$, n=5) (Figure 13A).

In addition to glutathione, several enzymes and molecules possess anti-oxidant activities.[146, 147] Because the preliminary data from the "signal transduction PathwayFinder PCR array" revealed the possible changes of *thioredoxin reductase1 (txnrd1)* and *NAD(P)H:(quinone-acceptor) oxidoreductase (nqo1)* in adpgk deficiency, we then focused on investigating the effect of *adpgk* on the gene expression of these anti-oxidant enzymes. Our results showed that the KD1 embryos had significantly decreased *txnrd1* ($p < 0.005$, n ≥ 5) expression, compared to the WT. The decreased *txnrd1* expression in the KD1 embryos could be partially rescued with *adpgk* mRNA (p=0.062, compared to the KD1 embryos, n ≥ 5) (Figure 5.11B). In addition, the expression of *nqo1* was also decreased in the KD1 embryos (p<0.005, compared to the WT, n ≥ 5) and the decreased expression could be partially rescued when supplying zebrafish adpgk mRNA (p=0.067, compared to the KD1, n ≥ 5) (Figure 5.11B). Thereby, the results suggested the high correlation of the gene expression between adpgk and the anti-oxidant enzymes, *txnrd1* and *nqo1*. Furthermore, the decreased *txnrd1* and *nqo1* also indicated the dysregulation of the defense system against ROS in adpgk deficiency.
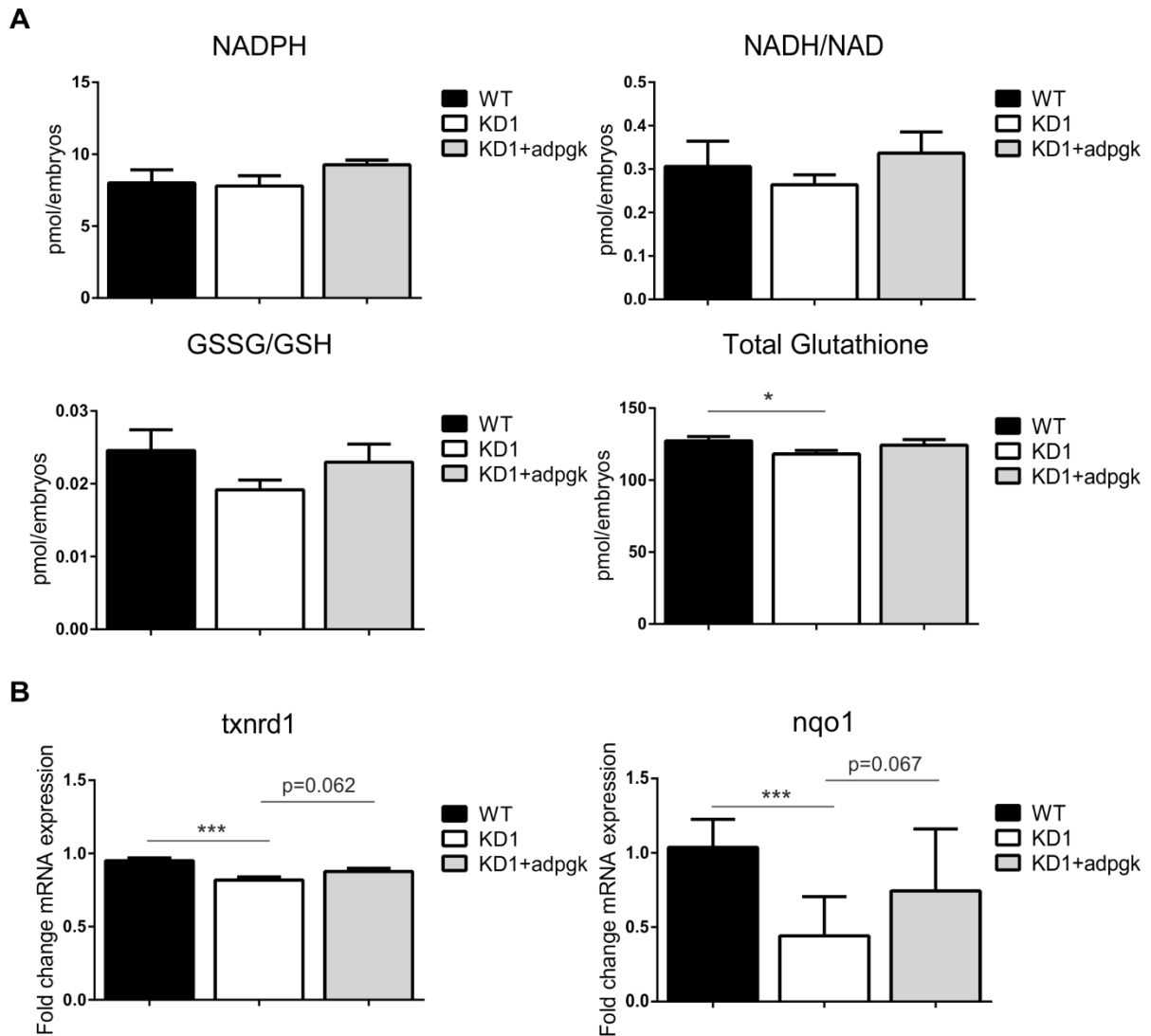
A

B

Figure 5.11 The dysregulation of the defense system against ROS in adpgk deficiency. (A) The KD1 embryos showed unchanged NADPH level, NADH/NAD and GSH/GSSG (n=5) but decreased total glutathione (127.3 ± 3.033 pmol/embryos in the WT vs. 118.2 ± 2.520 pmol/embryos in the KD, p<0.05, n=5). (B) The gene expression of the anti-oxidant enzymes, txnrd1 (p<0.005, n ≥ 5) and nqo1 (p<0.005, n ≥ 5) were decreased in the KD1 embryos, compared to the WT. Supplying *adpgk* mRNA could partially rescued the decreased expression of *txnrd1* (p=0.062, compared to the KD1, n ≥ 5) and *nqo1* (p=0.067, compared to the KD1, n ≥ 5).The embryos used for the measurements were collected from at least 5 independent batches. Unpaired *t*-test was performed with p value less than 0.05 considered as statistically significant.

The measurement of NADPH, NAD, NADH, and the glutathione was performed by the Metabolomics Core Facility of Heidelberg University.

5.12 Altered one-carbon metabolism and metabolic disturbance in embryos with adpgk deficiency

Glucose metabolism also provides precursors for the one-carbon metabolism and the synthesis of glycans. Thus, we wondered whether the altered glucose homeostasis in adpgk deficiency disturbed the one-carbon metabolism and/or hexosamine biosynthesis pathways. Accordingly, we first studied the levels of the amino acids and the metabolites involving in the one-carbon metabolism. Our metabolic study showed that compared to the WT, the KD1 embryos had 1.22-fold decreased threonine (17.62 ± 1.451 µmol/g in the WT vs. 14.37 ± 0.717 µmol/g in KD1, p=0.058, n=3), 1.35-fold decreased glycine (14.60 ± 0.313 µmol/g in WT vs. 10.78 ± 0.507 µmol/g in KD1, p<0.01, n=3) and 1.25-fold decreased methionine (13.68 ± 1.100 µmol/g in WT vs. 10.93 ± 0.185 µmol/g in KD1, p<0.05, n=3) (Figure 5.12A). Although the levels of SAM, SAH and MTA were not changed, SAM/SAH, the indicator of the methylation modification seemed to be increased (p=0.081, n=3) in the KD1 embryos. The increased SAM/SAH could be rescued with *adpgk* mRNA (p<0.01, compared to the KD1, n=3) (Figure 5.12B) Thereby, these results indicated an altered one-carbon metabolism in adpgk deficiency.

Furthermore, we investigated whether adpgk deficiency also caused the perturbation of other amino acid synthesis since amino acids are crucial for the embryonic development. The KD1 embryos showed decreased citrulline (0.99 ± 0.058 µmol/g in WT vs. 0.41 ± 0.238 µmol/g in KD1, p<0.05), histidine (8.84 ± 0.334 µmol/g in WT vs 7.27 ± 0.394µmol/g in KD1, p<0.05), phenylalanine (15.85 ± 0.528 µmol/g in WT vs 11.19 ± 0.414 µmol/g in KD1, p<0.01) and tyrosine (21.91 ± 0.732 µmol/g in WT vs. 16.24 ± 1.109 µmol/g in KD1, p<0.05), compared to the WT (Figure 5.12C). Interestingly, the metabolic phenotypes reflected the morphological phenotypes of the KD1 embryos. Phenylalanine is converted to tyrosine and both involve in melanin synthesis [148, 149]. The decreased phenylalanine and tyrosine coincided with the reduced pigmentation at the eye region of the KD1 embryos. The decreased glycine also correlated to the decrease of total glutathione synthesis in the KD1 embryos. Overall, adpgk deficiency showed a disturbed amino acid biosynthesis, which possibly affected the resource supply for methylation modification and the overall nutrients requirement for the embryonic development.
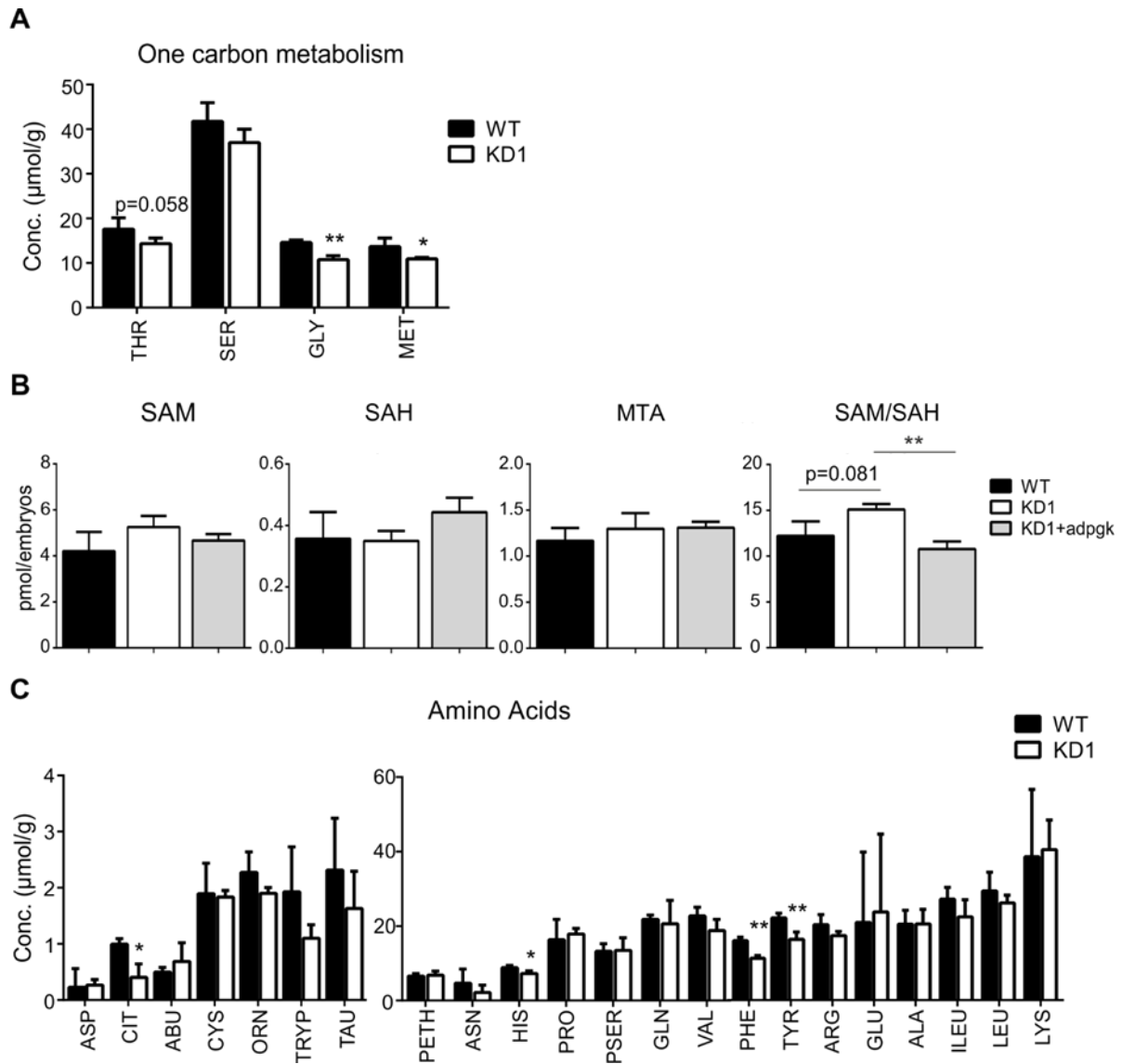
Figure 5.12 The disturbed metabolic network in adpgk deficiency. (A) Altered one-carbon metabolism in adpgk deficiency. The KD1 embryos showed 1.22-fold decreased threonine (p=0.058, n=3), 1.35-fold decreased glycine (p<0.01, n=3) and 1.25-fold decreased methionine (p<0.05, n=3), compared to the WT. (B) Despite of the unchanged SAM, SAH and MTA, SAM/SAH seemed to be increased (p=0.081, n=3) in the KD1 embryos and the increased SAM/SAH could be rescued with *adpgk* mRNA (p<0.01, compared to the KD1, n=3) (C) The KD1 embryos showed decreased citrulline (0.99 ± 0.058 in WT vs. 0.41 ± 0.238 in KD1, p<0.05, n=3), histidine (8.84 ± 0.334 in WT vs 7.27 ± 0.394 in KD1, p<0.05, n=3), phenylalanine (15.85 ± 0.528 in WT vs 11.19 ± 0.414 in KD1, p<0.01, n=3) and tyrosine (21.91 ± 0.732 in WT vs. 16.24 ± 1.109 in KD1, p<0.05, n=3). The measurement was performed from the pooled embryos collected from three independent batches. The p value less than 0.05 was considered as statistically significant.

The measurement of SAM, SAH and MTA was performed by the Metabolomics Core Facility of Heidelberg University.

5.13 Perturbation of glycan synthesis in adpgk knockdown embryos

Since adpgk is localized in the ER where the glycosylation occurs, we next investigated whether the disturbed glucose metabolism also altered glycan synthesis in adpgk deficiency.

To understand the activity of hexosamine biosynthesis pathway, we extracted the proteins from 50 embryos and examined the level of GFAT, the rate limiting enzyme. Our preliminary result showed that KD1 and KD2 embryos exhibited reduced GFAT, compared to CO (Figure 5.13A). It seemed that knockdown of adpgk downregulated hexosamine biosynthesis pathway.

To investigate the effect of adpgk on protein glycosylation, we next examined the levels of O-GlcNACylation and glycans by western blots and lectin blots, respectively. From the O-GlcNAc blot, the KD1 and KD2 embryos both showed a slight decrease of O-GlcNAc at the proteins size between 26 kDa to 55 kDa, compared to the CO (Figure 5.13B). The result suggested that in adpgk knockdown embryos, the O-GlcNACylation on the specific proteins were altered.

Lectins are the carbohydrates-binding proteins. Concanavalin A (ConA) binds to the α-linked mannose residues, Sambucus Nigra Lectin (SNA) binds to the sialic acid with α-2,6 attachment to the terminal galactose, and Wheat Germ Agglutinin (WGA) binds to the terminal *N*-acetylglucosamine or chitobiose [150]. The results from the ConA, SNA and WGA lectin blots revealed the different lectin patterns in the KD1 and KD2 embryos (as marked in the box), compared to the CO embryos (Figure 5.13C-E). Therefore, these preliminary O-GlcNAc and lectins results implied the disturbance of glycan synthesis and the alteration of protein glycosylation in adpgk deficiency.

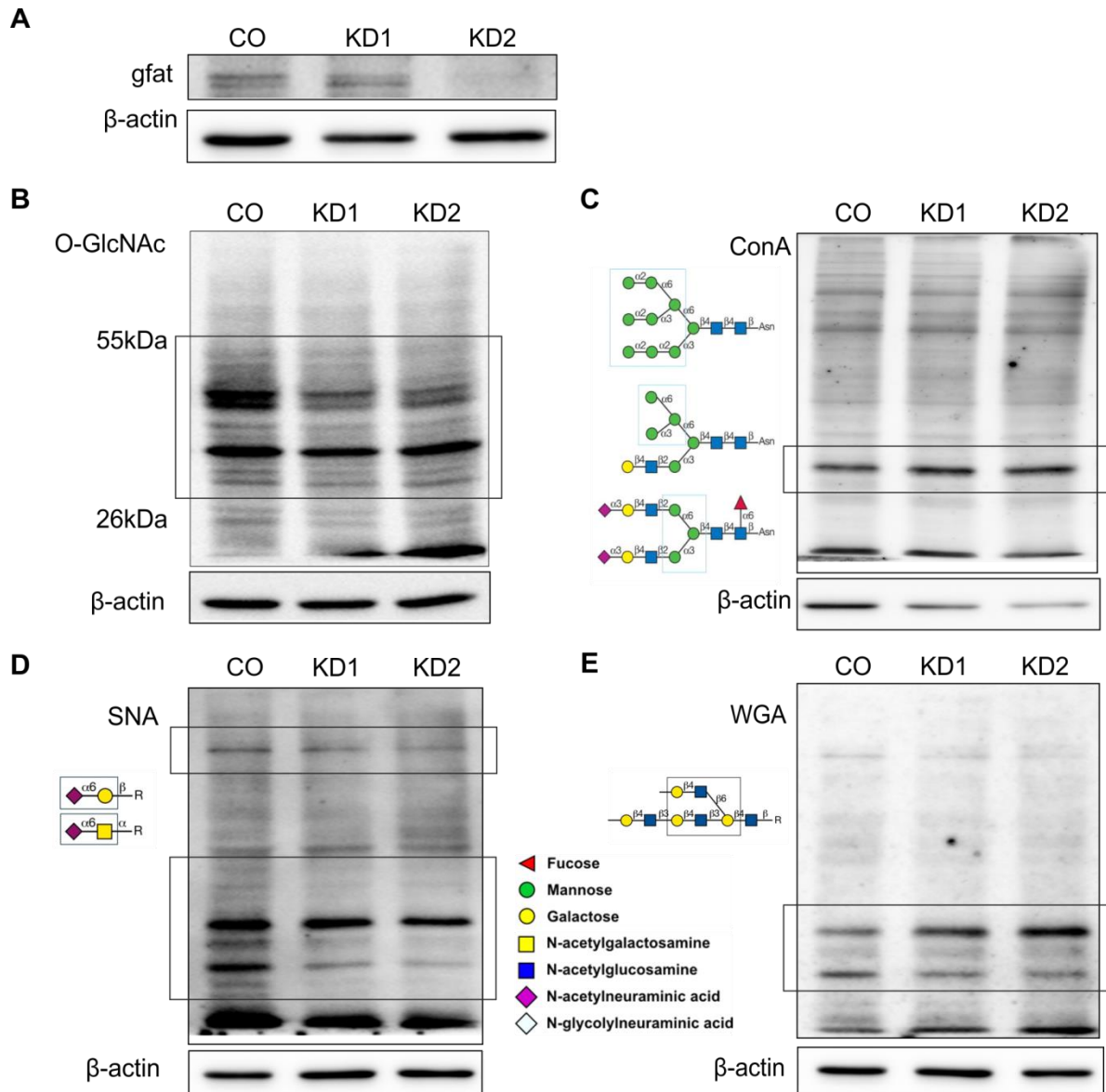**Figure 5.13** Disturbed protein glycosylation in adpgk deficiency. (A) Decreased GFAT level in the KD1 and KD2 embryos, compared to CO. (B) The KD1 and KD2 embryos showed decreased O-GlcNAc patterns at the proteins size between 26 kDa to 55 kDa, compared to the CO. (C-E) The ConA, SNA, and WGA lectin blots showed discrete glycan patterns (highlighted in the box) between the adpgk knockdown and CO.

5.14 Altered N-glycosylation in adpgk knockdown embryos

To further specifically identify the effects of adpgk deficiency on the protein glycosylation, we performed glycomics study focusing on N-glycans in the cooperation with the National Institute for Bioprocessing Research and Training (NIBRT), Ireland. The scheme of the glycomics study was indicated in the Figure 5.14A. The extracts of the released glycans from a pooled of 200 embryos were first separated according to the degree of charge by weak anion exchange HPLC. Subsequently, the fractions containing different charged glycans were collected and digested with a serial of glycosidase enzymes and further separated by the LC-FLR-QTOF-MS for the identification of glycan structures.

Our glycomics analysis showed the significant decrease of high mannose glycan in the KD1 embryos, compared to the WT (Figure 5.14B). The glycans of $GlcNAc_2$ attached with high mannose are the precursors of all the N-glycans. Accordingly, the decreased high mannose glycan structures suggested a general decrease of N-glycan biosynthesis in adpgk deficiency. The detailed information of high mannose-type glycans regarding the charge, structures and fold changes were summarized in Table 5.6. Interestingly, several complex- and hybrid-type glycans were also decreased in the KD1 embryos (Table 5.7). In particular, $HexNAc_4Hex_7Fuc_2NeuGc_2$ was decreased with a 5.85 fold change, and $GlcNAc_3Hex_6$ ($GlcNAc_2Man_5GlcNAcGal$) was decreased with a 1.6 fold change (as marked in the boxes) in the KD1 embryos, compared to the WT (Figure 5.14C). Overall, adpgk deficiency showed an altered glycan synthesis. It is worth noting that, glycosylation determines the proper function of several proteins involving in the developmental signaling pathways and the cell cycle [17, 151]. Therefore, the disturbed glycosylation could lead to the catastrophe of the signaling pathways, which we could not see from the genomics level, and eventually resulted in the malformation of embryonic development in adpgk deficiency.
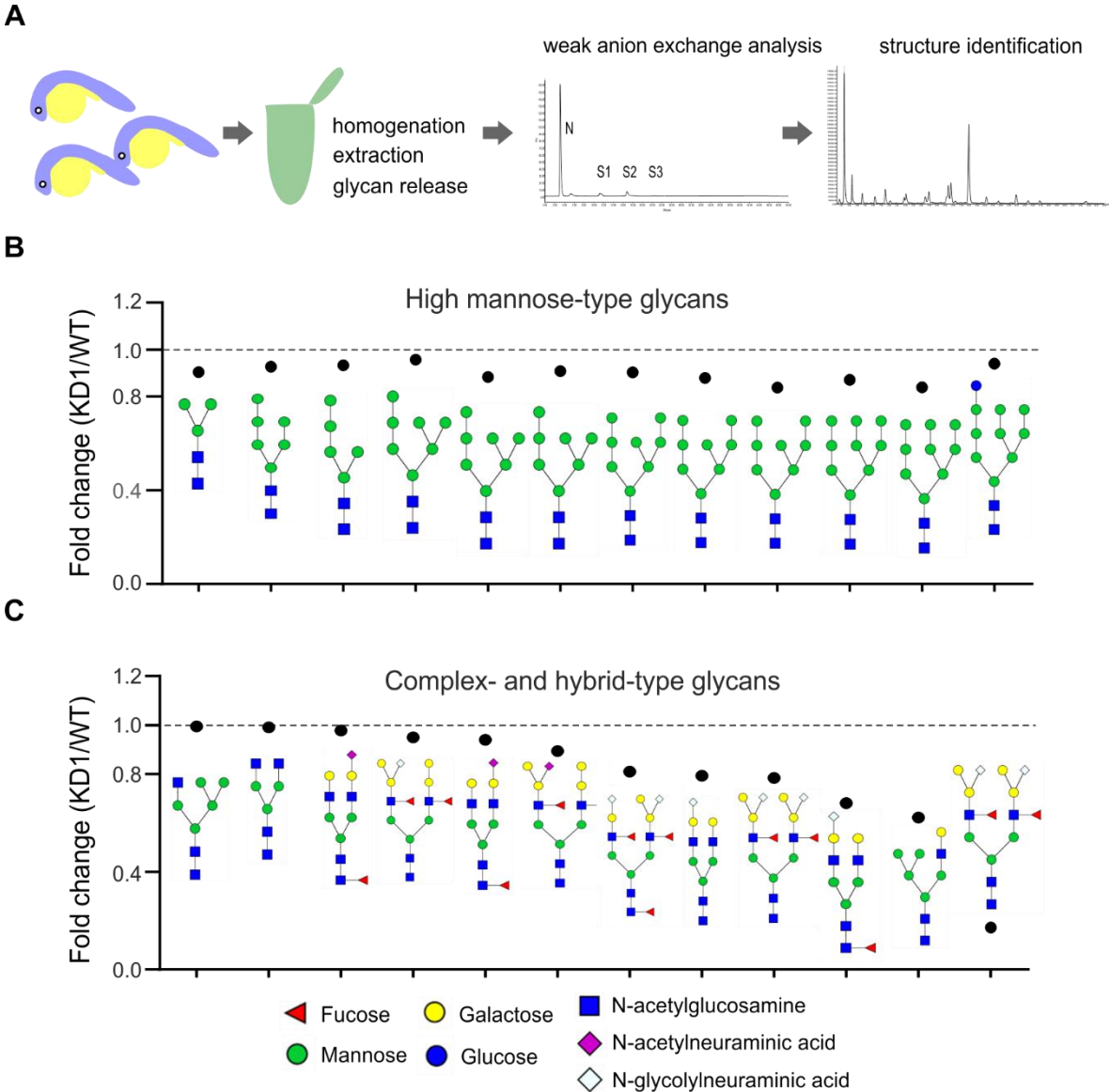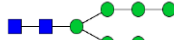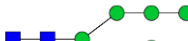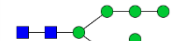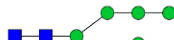
Figure 5.14 The dysregulation of N-glycosylation in adpgk deficiency. (A) Scheme of the glycomics study. (B) KD1 embryos showed decreased high mannose glycans with different charge. (C) The complex- and hybrid-type glycans were also decreased in the KD1 embryos. The glycan measurements and data analysis were done by Dr. Stefan Mittermayr and Dr. Sara Carillo at the NIBRT.

Table 5.6 Summary of the high mannose-type N-glycans

m/z	Charge	Retention time (min)	Anova (p)	Max Fold Change	Highest Mean	Lowest Mean	Maximum Abundance	Name	Name
1029.386	1	4.713583	0.027056	0.903208	WT	KD	232.6738	GlcNAc$_2$Man$_3$	
1353.491	1	10.09452	0.043886	0.926869	WT	KD	8888.481	GlcNAc$_2$Man$_5$	
757.2658	2	13.22837	0.019844	0.932585	WT	KD	10309	GlcNAc$_2$Man$_6$	
838.2919	2	16.0497	0.145742	0.956814	WT	KD	6440.646	GlcNAc$_2$Man$_7$	
838.2927	2	16.5481	0.009447	0.882303	WT	KD	12409.9	GlcNAc$_2$Man$_7$	
1839.645	1	19.17535	0.016774	0.90777	WT	KD	1154.68	GlcNAc$_2$Man$_8$	
919.3165	2	19.19225	0.009371	0.902867	WT	KD	20865.64	GlcNAc$_2$Man$_7$	
919.3156	2	19.5554	0.003392	0.878514	WT	KD	17976.99	GlcNAc$_2$Man$_8$	

1839.645	1	19.5554	0.015413	0.837473	WT	KD	1330.272	GlcNAc$_2$Man$_8$	
2001.694	1	21.92905	0.001509	0.870389	WT	KD	4362.468	GlcNAc$_2$Man$_9$	
1000.846	2	21.92905	0.037585	0.83812	WT	KD	27657.2	GlcNAc$_2$Man$_9$	
1081.368	2	24.20127	0.069483	0.939776	WT	KD	6323.053	GlcNAc$_3$Hex$_9$	

◄ Fucose   ● Glucose

● Mannose   ☐ N-acetylgalactosamine   ◆ N-acetylneuraminic acid

○ Galactose   ■ N-acetylglucosamine   ◇ N-glycolylneuraminic acid
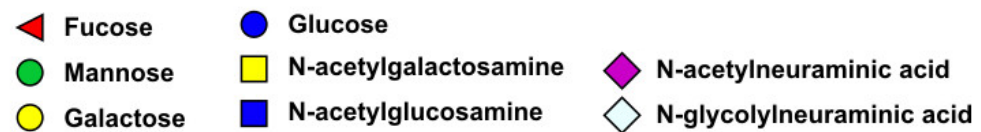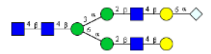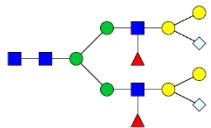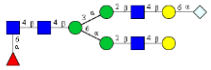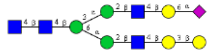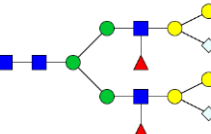
Table 5.7 Summary of the complex- and hybris-type N-glycans

m/z	Charge	Retention time (min)	Anova (p)	Max Fold Change	Highest Mean	Lowest Mean	Maximum Abundance	Name	Structure
777.7807	2	11.86833	0.889237	0.994286	WT	KD	348.9237	GlcNAc$_3$Hex$_5$	
717.2674	2	7.898033	0.889017	0.990437	KD	WT	125.4934	GlcNAc$_4$Hex3	
1097.892	2	19.09082	0.56172	0.97768	WT	KD	726.7034	GlcNAc$_4$Hex$_5$Fuc$_1$NeuAc	
1340.975	2	27.44535	0.791328	0.949306	KD	WT	102.461	GlcNAc$_4$Hex$_7$Fuc$_2$NeuGc	
1097.889	2	18.67695	0.483568	0.939807	KD	WT	133.3381	GlcNAc$_4$Hex$_5$Fuc$_1$NeuAc$_1$	
1332.969	2	25.8149	0.03413	0.893234	WT	KD	1724.327	GlcNAc$_4$Hex$_7$Fuc$_2$NeuAc	
1486.514	2	29.49777	0.001214	0.809614	WT	KD	2478.518	GlcNAc$_4$Hex$_6$Fuc$_3$NeuGc$_2$	

1032.859	2	19.5723	0.04534	0.792709	WT	KD	387.7771	$GlcNAc_4Hex_5NeuGc_1$	
1494.514	2	31.00988	0.000605	0.78321	WT	KD	1728.907	$GlcNAc_4Hex_7Fuc_2NeuGc_2$	
1105.892	2	20.98297	0.105802	0.680286	WT	KD	76.76036	$GlcNAc_4Hex_5Fuc_1NeuGc_1$	
								$GlcNAc_4Hex_6NeuAc$	
858.8025	2	15.0867	0.08931	0.621453	WT	KD	80.59007	$GlcNAc_3Hex_6$	
996.3373	3	30.99298	0.002938	0.171048	WT	KD	36.40406	$HexNAc_4Hex_7Fuc_2NeuGc_2$	

◄ Fucose   ● Glucose

● Mannose   ■ N-acetylgalactosamine   ◆ N-acetylneuraminic acid

○ Galactose   ■ N-acetylglucosamine   ◇ N-glycolylneuraminic acid
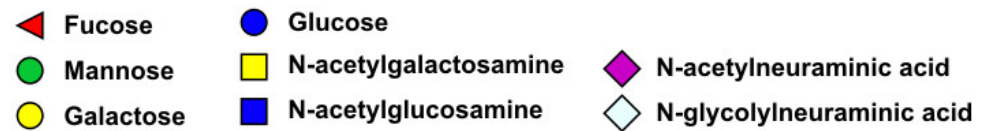
6. DISCUSSION

6.1 Adpgk fine tunes the glucose metabolism during embryonic development

Our study is the first study characterizing the function of adpgk on the zebrafish embryonic development. Zebrafish embryos showed the highest *adpgk* expression at one cell stage; however, the expression started decreasing and remained at low levels afterwards. Unlike *adpgk*, the expression of *hk1* was low during the very early embryonic development but hk1 became the dominant hexokinase after the mid-blastrula stage. Consistent with our study, Rocha, F et al. have also reported the higher *hk1* expression in the late zebrafish developmental stages [152]. Based on the low expression of adpgk, it seems that adpgk is not an important hexokinase post the maternal to zygotic transition. Despite adpgk not being the dominant hexokinase during the embryonic development. Knockdown of adpgk could significantly induce *hk1* expression, suggesting the important role of adpgk in fine-tuning the glucose metabolism.

The compensatory induction of hk1 strongly increased the glucose consumption, indicated by decreased free glucose and increased G6P. The adaptive glucose metabolism in adpgk deficiency showed increased glucose flux to the PPP but disturbed one-carbon metabolism and hexosamine biosynthesis pathways. The dysregulated N-glycans synthesis is proposed to further cause the malfunctions of proteins in developmental signaling pathways which led to the observed deformed convergent extension in adpgk deficient zebrafish embryos.

In concert with the metabolic disturbance, adpgk knockdown embryonic cells endure an acid-base imbalance and altered defense system against ROS. Furthermore, the metabolic stress induced the activation of cell cycle checkpoints [153] and apoptosis. Overall, the malfunction of the developmental signaling pathways and the increase of cell death eventually led to the crippled body patterning in adpgk deficient zebrafish.

6.2 Adpgk knockdown disturbs glucose homeostasis and activates the PPP

Adpgk knockdown embryos showed increased glucose consumption and glycolytic flux to the PPP, indicated by the decreased free glucose and increased G6P, Ru5P and GAP levels. High proliferative cells undergo aerobic glycolysis (Warburg phenotype) and activate PPP to provide precursors for the nucleotides synthesis [8]. However, the embryos with adpgk deficiency did not show increased lactate, the hallmark of aerobic glycolysis. Instead of performing aerobic glycolysis, the decreased lactate/pyruvate in adpgk knockdown embryos implied that the

embryonic cells employed the glucose metabolism through the TCA cycle for energy generation.

According to our glycolytic flux study, knockdown of adpgk did not significantly alter the main glucose metabolism (glycolysis) and the energy generation but the PPP, one-carbon metabolism and hexosamine biosynthesis pathway. During early embryonic development, amino acids and fatty acids are the main energy resources and glucose is rather used in a biosynthetic role [152, 154]. Accordingly, the effect of adpgk on glycolysis and energy generation would not be prominent. The activated PPP can be observed in high proliferative cells due to the increased nucleotides synthesis [8]. However, the adpgk knockdown embryos were under cell cycle arrest and apoptosis. In addition, our preliminary result of the EdU staining indicated a rather decreased cell proliferation in ADPGK knockout Jurkat cells (data not shown). Besides, the activated PPP could also be a stress-response protecting cells from the ROS-induced damages. It has been shown that when cells are under a small level of stress, the activation of TIGAR (TP53-inducible glycolysis and apoptosis regulator) by p53 induces glucose-6-phsophate dehydrogenase (G6PD), the first enzyme in the PPP and deviates the glucose flux from glycolysis to the PPP to increase the production of antioxidants [155]. However, the activated PPP did not increase GSH/GSSG (antioxidants) in the adpgk knockdown embryos and cell death was increased. Thereby, it seemed that the activated PPP did not benefit the cells by either increasing the protection against ROS or supporting the cell proliferation.

6.3 Adpgk knockdown decreases hexosamine biosynthesis and dysregulates glycoproteins of the developmental signaling pathways

In addition to the increased G6P, Ru5P and GAP, the hexosamine biosynthesis pathway was dysregulated in the adpgk knockdown embryos. UDP-GlcNAc provides the building blocks for glycan synthesis and acts as a nutrient sensor by controlling the glycosylation of proteins involved in regulating glucose homeostasis [156, 157]. For instance, the decreased level of UDP-GlcNAc reduces the multiplicities of N-glycans. The glycans with low degree of branching, in turn, stabilize glycoproteins at the cell surface for increasing hexosamine concentration [158]. It has been shown that the levels of UDP-GlcNAc and Golgi *N*-acetylglucosaminyltransferases regulate the expression and function of glucagon receptor [157] and glucose transporters [159, 160]. Therefore, in accompany with the decreased complex-type N-glycans in adpgk knockdown embryos, the increased G6P could also be a compensatory effect of cells attempting to increase hexosamine biosynthesis.

Many proteins involving in the developmental signaling pathways are glycoproteins [151]. During convergent extension and epithelial-mesenchymal transition in the embryonic development, the orchestration of different cell behaviors such as cell adhesion rearrangement, cytoskeletal reorganization and cellular polarity remodeling determine the embryonic body patterning [161-163].

Adpgk knockdown embryos showed defective convergent extension during gastrulation and dysregulated Rac1/2/3 protein. Surprisingly, even though the developmental signaling pathways such as wnt, hh, notch, and bmp cross talk to one another [164-166], our results from the RT-qPCR screening did not reveal any significant changes of the main developmental signaling pathways in adpgk deficiency. Since wnt [167, 168], tgf-β receptor [169], notch receptor [170-172] and hh ligands [173] are glycoproteins bearing N-glycans, O-GlcNAc and/or O-glycans [151, 174] and adpgk knockdown embryos showed altered glycan patterning, we postulated that adpgk knockdown affects the posttranslational modification rather than the gene expression of the molecules involving in the developmental signaling pathways. The effect of adpgk on protein levels could also explain the insufficiency of *dsh* mRNA in rescuing the short body phenotype.

Furthermore, the defect in developmental signaling pathway resulted in the disorganization of cell movement during convergent extension in the embryos with adpgk deficiency. The coordination of small GTPase Rac1/RacA and E-cadherin mediates the traction forces between cells and determines the cell motility [175]. It has been shown that E- and N-cadherin regulate the collective cell movement [176, 177] and knockdown of E-cadherin reduces the cell-cell adhesion and influences convergent extension during zebrafish gastrulation [178, 179]. Interestingly, Richter, S. et al. has indicated the decreased *cadherins* expression in ADPGK knockout H460 cells [55], which suggests the possible defect of cadherin in the embryos with adpgk deficiency and supports the disorganized cell movement observed in our study.

6.4 Disturbed one-carbon metabolism in embryos with adpgk deficiency

The targeted metabolic screening identified the decreased glycine, methionine and threonine, suggesting a disturbed one-carbon metabolism in the embryos with adpgk deficiency. One-carbon metabolism generates the components essential for the synthesis of proteins, lipids and nucleotides, and the methylation modification [15, 180, 181]. Growing body of evidences have shown that the consumption of glycine and the mitochondrial expression of glycine biosynthetic enzymes as well as the activity of one carbon metabolism determine cancer cell

proliferation [13, 182, 183]. Therefore, the disturbed one-carbon metabolism in adpgk knockdown embryos indicates reduced cell proliferation.

In addition, the growth of mouse embryonic stem cells shows a critical dependency on threonine [184]. Threonine or methionine deprivation reduces histone methylation and promotes cell death [184, 185]. Methionine deprivation down-regulates methylation, indicated by decreased SAM/SAH in vitro. Intriguingly, adpgk knockdown embryos showed decreased methionine but increased SAM/SHC, which seemed to be inconsistent that with the previous studies [186]. It could be possible that the consumption of methionine was higher, suggesting the increased methylation modification in adpgk deficiency [186]. Or it could be possible that the recycling of SAH to SAM was impaired due to the decreased threonine and glycine in regenerating SAM from SAH. Overall, the imbalanced production or consumption of threonine and methionine could lead to the dysregulation of methylation modification in adpgk deficiency, indicting the effect of adpgk on post translational modification.

6.5 The imbalanced pH environment disturbs the cell behavior

The results from the signal transduction PathwayFinder PCR array showed a significant decrease of *ca9* expression in adpgk deficiency. The reduced *ca9* expression could be rescued when co-injecting *adpgk* mRNA to adpgk deficient embryos, implying that the expression of *ca9* and *adpgk* were highly correlated. Ca9 (EC 4.2.1.1) is a zinc metalloenzyme catalyzing the reversible hydration of carbon dioxide to bicarbonate and hydrogen ion. In response to the increased lactate production in cancer cells, ca9 is increased to facilitate the excretion of the intracellular lactate and CO_2 [7, 8, 187], thereby, creating a "reversed" pH gradient with increased intracellular pH (pH_i) and decreased extracellular pH (PH_e). Studies have shown that high pH_i inhibits apoptosis and induces glycolysis for cancer cell survival/proliferation while low pH_e facilitates the damage of extracellular matrix and cell junction for cancer cell invasion [145, 188].

Accordingly, the strongly decreased *ca9* expression in adpgk deficiency could imply a decreased pH_i. The value of pH_i less than 7.2 is a conserved characteristic of cells that undergo apoptosis [189, 190]. It addition, low pH_i limits the activity of CDK1-cyclin B through the inhibitory phosphorylation of CDK1 and decreased expression of cyclin B [191]. Interestingly, in accordance with the decreased *ca9* expression, the cdkn1a was activated in adpgk deficiency, which restricted the activity of CDK1-cyclin B and induced cell cycle arrest. Therefore, it seemed that adpgk knockdown embryos exhibited a pH environment prone for cell cycle arrest and cell death.

Moreover, pH status is important for cell migration. The expression of ca9 creates the correct pH cues with low pH_e and high pH_i at the moving cell front, and high pH_e and low pH_i at the cell rear [192-194]. In addition, Ca9 can also mediate the cell disassociation by regulating the binding of E-cadherin to β-catenin [192, 195]. It has been shown that suppressing Ca9 in HT1080 fibrosarcoma cells down-regulates the expression of small GTPase protein, MMP2, MMP9 and collegen IV [196, 197]. In accordance with the decreased *ca9* expression, the level of Rac1/2/3 was significantly reduced, again suggesting the dysregulation of the cell adhesion/migration molecules in adpgk knockdown embryos.

6.6 Knockdown of adpgk alters the defense system against ROS

Knockdown of adpgk decreased the gene expression of anti-oxidant enzymes, *nqo1* and *txnrd1* and led to increased cell cycle arrest. Consistently, it has been reported that knockdown of nqo1 induces cdkn1a and reduces cyclin D1, which activates cell cycle arrest, and limits cell proliferation and migration in cholangiocarcinoma cells [198]. Besides, nqo1 participates in the first step (complex I) of OXPHOS. The decreased nqo1 suggested the possibility of impaired mitochondrial respiratory chain in adpgk deficiency. Previous study has shown that ADPGK knockout H460 cells exhibits compromised mitochondrial biogenesis, indicated by increased *PPARGC1A* (PGC-1α) and decreased OXPHOS complex I and II [55]; thus, leading to the depletion of mitochondrial membrane potential.

Moreover, the metabolic changes reflected the alteration of defense system against ROS in adpgk deficiency. Glycine is the precursor of glutathione [199] and has been recognized as one of the main antioxidant molecule protecting cells against oxidative stress [200-202]. In accordance with the decreased glycine, the level of total glutathione was reduced in adpgk knockdown embryos. In addition to glycine, taurine scavenges ROS, alleviates lipid peroxidation and reduces apoptotic cells [203-205]. Taurine also acts as mitochondrial matrix buffer and the depletion of taurine is directly correlated to mitochondrial dysfunction [206]. Owing to the measurement of taurine in pooled embryos and keeping in mind the biological variations, a 1.4 fold decrease of taurine, could actually be meaningful in adpgk knockdown embryos. Overall, the increased glucose flux to PPP and the decreased anti-oxidant enzymes and molecules suggested a compromised defense system against ROS which could further alter the mitochondrial dysfunction and induce cell death in adpgk knockdown embryos. However, the level of oxidative stress in adpgk deficiency requires further studies for confirmation.

6.7 Adpgk deficiency induced apoptosis with an unknown mechanism

The body phenotype correlated with the observed increased apoptosis in adpgk deficient embryos. In line with the increased apoptotic cells, indicated by Acridine Orange and TUNEL staining, adpgk knockdown showed increased pro-apoptotic factor, *bbc3* and decreased anti-apoptotic molecule, *bcl2l*. Studies have shown that akt2 modulates glucose availability and the downstream cell death pathways during zebrafish development [207-209]. It affects glucose uptake by regulating the expression of glucose transporters and induces glycolysis by stimulating the activity of hexokinase [208, 209]. In addition, akt is an antiapoptotic factor promoting cell survival by phosphorylating bad, a proapoptotic factor and further preventing the apoptosis by inhibiting the translocation of bax to mitochondria [207]. Our RT-qPCR results revealed, albeit the disturbed glucose homeostasis and increased apoptosis, unchanged *akt* and *bad* (data not shown) in the KD1 embryos, compared to the WT; indicating that adpgk deficiency did not trigger akt-mediated cell death.

Moreover, p53 is the most common cell cycle and apoptosis regulator. When p53 is activated, it directly binds to the anti-apoptotic proteins (bcl-2 and bcl2l) and activates pro-apoptotic factors (bax and bak). The activation of bax and bak alters the permeabilization of mitochondrial outer membrane and further triggers apoptosis [210, 211]. Although our studies showed increased apoptosis in adpgk knockdown embryos, reducing *p53* expression in adpgk deficient embryos could not rescue the phenotype. Instead, it increased the severity of phenotype and lethality.

It seems that p53 is not activated or its expression remains unchanged or decreased in the embryos with adpgk deficiency. Interestingly, nqo1, in addition to its antioxidant activity, has been identified as a p53 stabilizer that can directly protect it from degradation [212]. The result of decreased *nqo1* expression in the adpgk knockdown embryos supports the speculation of an unstable or decreased p53. Accordingly, it could be possible that knockdown of adpgk triggered a p53-independent apoptosis pathway.

On the other hand, it could also be possible that adpgk knockdown embryos did show activated p53 and the activated p53 is protective for the cells. P53 induces cell cycle arrest by directly binding to the cell cycle checkpoint molecules such as cdkn1a and gadd45aa [213], allowing cells to repair the damage. The activation of cdkn1a can protect cells against apoptosis [214]. In this case, supposing that the suppression of *p53* by morpholino also reduced *cdkn1a* expression in adpgk knockdown embryos, the exacerbation outcome observed could be explained. Therefore, the activated cell cycle checkpoints in the embryos with adpgk deficiency could be a compensatory effect of cells attempting to repair the damages and/or the metabolic stress [142]. However, the role of cdkn1a in apoptosis has been conflicting. Depends on the

stimuli, cdkn1a can inhibit or promote apoptosis [214, 215]. It remains puzzling whether cdkn1a acts as an anti-apoptotic or pro-apoptotic factor in adpgk knockdown embryos.

Besides p53, cdkn1a can be regulated by the signals generating from growth factors and GTPase Rho-mediated Ras. Epidermal growth factor or interferon-γ activates cdkn1a by triggering the targeting of stat1 to cdkn1a [216]. On the other hand, the activation of cdkn1a can be suppressed by GTPase Rho-mediated Ras induction [217]. Given the decreased GTPase protein, rac1/2/3 in adpgk deficiency, we attempted to investigate whether ras and/or stat1 were involved in activating cdkn1a. However, the expression of *ras* and *stat1* remained unchanged in the KD1 embryos (data not shown). Therefore, mechanism of the cdkn1a activation and its role in apoptosis merit further investigation.

6.8 Disturbed N-glycan synthesis affects the embryonic development

Glycosylation is important in determining the proper protein functions. There are several studies regarding the gene regulation of glycosylation; however, the understanding and research of glycan structures in zebrafish are scarce [151].

We extracted glycans from 200 zebrafish embryos at 22 hpf and performed glycomics study. The results showed a general decrease of high mannose type-glycans in adpgk knockdown embryos; however, the fold change was not very prominent. It is known that the yolk contains high amounts of nutrients such as phospholipoglycoproteins for supporting embryonic development [218, 219]. The high amount glycoproteins present in the yolk [220] can mask the actual change of glycans in the embryos; thus, the effect of adpgk knockdown on decreasing glycan synthesis were actually underestimated in our study.

Our glycomic analysis identified several complex- and hybrid-type glycans in the zebrafish embryos at 22 hpf. Consistent with our findings, previous studies also have reported the same complex- and hybrid-type glycans expressed in the zebrafish embryos [219, 221] and found the high expression of the atypical complex-glycans during the embryonic segmentation stage [221]. It has been indicated that the structures and patterns of glycans are very diverse and stage-specific during the embryogenesis [151].

Adpgk knockdown embryos showed a 1.6 fold decrease of glycans bearing β1,4-linkage of galactose to GlcNAc ($GlcNAc_2Man_5GlcNAcGal$). This type of β1,4-linkage is formed by β1,4-galactosyltransferase (beta4GalT). Interestingly, beta4GalT knockdown zebrafish embryos show aberrant convergent extension, which is consistent with our study [222].

DISCUSSION

In addition to N-glycosylation, the O-GlcNAc blot revealed the changes of protein O-GlcNAcylation in adpgk knockdown embryos. O-GlcNAc transferase (OGT) and O-GlcNAcase (OGA) catalyzes the attachment and removal of O-GlcNac on proteins, respectively [32]. Overexpression of OGT or OGT in zebrafish embryos showed cytoskeletal disorganization, short body axis, small brain and increased cell death [223], which are similar to the adpgk knockdown embryos. Moreover, O-GlcNAcylation is highly correlated with phosphorylation [224]. Wang, Z. et al. has reported that inhibiting a single kinase, GSK3β, can increase the O-GlcNAcylation of cytoskeletal and heat shock proteins, and decrease the O-GlcNAcylation of transcription factors and RNA-binding proteins [225]. Thus, knockdown of adpgk could directly link to the altered protein O-GlcNAcylation. Due to the extensive crosstalk between O-GlcNAcylation and phosphorylation, the altered O-GlcNAcylation in adpgk knockdown embryos possibly disturbs the protein phosphorylation, which affects the protein function in very diverse ways.

Overall, we revealed the altered glycosylation in adpgk knockdown embryos. The dysregulated protein and lipid glycosylation are the features of congenital disorders of glycosylation (CDG) [226]. CDG is resulted from the malfunctioning of enzymes or proteins involved in regulating glycan synthesis, Golgi architecture, vesicular trafficking and pH [227]. Patients with CDG show wide range of symptoms including neurological defects, muscular dystrophy, cardiomyopathy, retinal degeneration, anemia, and enteropathy as well as growth retardation [226, 228]. Knockdown of adpgk also showed various phenotypes including deformed eyes, short body axis, dysregulated somitogenesis and deformed cardiovascular system in the zebrafish embryos. Therefore, adpgk deficiency could be linked to a novel type of CDG.

7. CONCLUSION

We successfully established the morpholino-mediated loss-of-function zebrafish model and observed the phenotypes of defective convergent extension movement and short/dorsalized body axis. Knockdown of adpgk disturbed glucose metabolism with activated pentose phosphate pathway, exhibiting a reduction in one-carbon metabolism and hexosamine biosynthesis pathway. The dysregulated N-glycans synthesis caused the malfunctioning of proteins in the developmental signaling pathways which led to deformed embryonic body patterning in zebrafish. Overall, adpgk acts as a key regulator of glucose metabolism during the early stages of embryonic development in zebrafish.

8. REFERENCES

1.   Middleton, R.J., Hexokinases and glucokinases. Biochem Soc Trans, 1990. 18(2): p. 180-3.

2.   Kornberg, H., Krebs and his trinity of cycles. Nat Rev Mol Cell Biol, 2000. 1(3): p. 225-228.

3.   Krebs, H.A., The citric acid cycle: A reply to the criticisms of F. L. Breusch and of J. Thomas. Biochemical Journal, 1940. 34(3): p. 460-463.

4.   Hay, N., Reprogramming glucose metabolism in cancer: can it be exploited for cancer therapy? Nat Rev Cancer, 2016. 16(10): p. 635-649.

5.   Warburg, O., On the Origin of Cancer Cells. Science, 1956. 123(3191): p. 309-314.

6.   Otto, A.M., Warburg effect(s)—a biographical sketch of Otto Warburg and his impacts on tumor metabolism. Cancer & Metabolism, 2016. 4: p. 5.

7.   Vander Heiden, M.G., L.C. Cantley, and C.B. Thompson, Understanding the Warburg effect: the metabolic requirements of cell proliferation. Science, 2009. 324(5930): p. 1029-33.

8.   Liberti, M.V. and J.W. Locasale, The Warburg Effect: How Does it Benefit Cancer Cells? Trends Biochem Sci, 2016. 41(3): p. 211-8.

9.   Horecker, B.L., The pentose phosphate pathway. J Biol Chem, 2002. 277(50): p. 47965-71.

10.   Patra, K.C. and N. Hay, The pentose phosphate pathway and cancer. Trends Biochem Sci, 2014. 39(8): p. 347-54.

11.   Zhao, Y., et al., Mechanisms and Methods in Glucose Metabolism and Cell Death. Methods in enzymology, 2008. 442: p. 439-457.

12.   Yang, M. and K.H. Vousden, Serine and one-carbon metabolism in cancer. Nat Rev Cancer, 2016. 16(10): p. 650-662.

13.   Amelio, I., et al., Serine and glycine metabolism in cancer. Trends Biochem Sci, 2014. 39(4): p. 191-8.

14.   Selhub, J., Folate, vitamin B12 and vitamin B6 and one carbon metabolism. J Nutr Health Aging, 2002. 6(1): p. 39-42.

15.   Deberardinis, R.J., et al., Brick by brick: metabolism and tumor cell growth. Curr Opin Genet Dev, 2008. 18(1): p. 54-61.

16.   Hart, G.W., M.P. Housley, and C. Slawson, Cycling of O-linked [beta]-N-acetylglucosamine on nucleocytoplasmic proteins. Nature, 2007. 446(7139): p. 1017-1022.

17.   Hart, G.W., et al., Cross talk between O-GlcNAcylation and phosphorylation: roles in signaling, transcription, and chronic disease. Annu Rev Biochem, 2011. 80: p. 825-58.

18.   Varshney, S. and P. Stanley, EOGT and O-GlcNAc on secreted and membrane proteins. Biochem Soc Trans, 2017. 45(2): p. 401-408.

19.   Ruan, H.-B., et al., O-GlcNAc Transferase/Host Cell Factor C1 Complex Regulates Gluconeogenesis by Modulating PGC-1α Stability. Cell Metabolism. 16(2): p. 226-237.

20.   Whisenhunt, T.R., et al., Disrupting the enzyme complex regulating O-GlcNAcylation blocks signaling and development. Glycobiology, 2006. 16(6): p. 551-63.

21.   Kelly, W.G., M.E. Dahmus, and G.W. Hart, RNA polymerase II is a glycoprotein. Modification of the COOH-terminal domain by O-GlcNAc. J Biol Chem, 1993. 268(14): p. 10416-24.

22.   Lewis, B.A., A.L. Burlingame, and S.A. Myers, Human RNA Polymerase II Promoter Recruitment in Vitro Is Regulated by O-Linked N-Acetylglucosaminyltransferase (OGT). J Biol Chem, 2016. 291(27): p. 14056-61.

23.   Ramakrishnan, P., et al., Activation of the transcriptional function of the NF-kappaB protein c-Rel by O-GlcNAc glycosylation. Sci Signal, 2013. 6(290): p. ra75.

24.   Li, M.-D., et al., O-GlcNAc Transferase Is Involved in Glucocorticoid Receptor-mediated Transrepression. The Journal of biological chemistry, 2012. 287(16): p. 12904-12912.

25.   Yang, X., et al., O-linkage of N-acetylglucosamine to Sp1 activation domain inhibits its transcriptional capability. Proc Natl Acad Sci U S A, 2001. 98(12): p. 6611-6.

26.   Han, I. and J.E. Kudlow, Reduced O glycosylation of Sp1 is associated with increased proteasome susceptibility. Mol Cell Biol, 1997. 17(5): p. 2550-8.

27.   Daou, S., et al., Crosstalk between O-GlcNAcylation and proteolytic cleavage regulates the host cell factor-1 maturation pathway. Proc Natl Acad Sci U S A, 2011. 108(7): p. 2747-52.

28.   Chu, C.S., et al., O-GlcNAcylation regulates EZH2 protein stability and function. Proc Natl Acad Sci U S A, 2014. 111(4): p. 1355-60.

29.   Singh, J.P., et al., O-GlcNAc signaling in cancer metabolism and epigenetics. Cancer Lett, 2015. 356(2 Pt A): p. 244-50.

30.   Hart, G.W., Minireview Series on the Thirtieth Anniversary of Research on O-GlcNAcylation of Nuclear and Cytoplasmic Proteins: Nutrient Regulation of Cellular Metabolism and Physiology by O-GlcNAcylation. The Journal of Biological Chemistry, 2014. 289(50): p. 34422-34423.

31.   Hanover, J.A., M.W. Krause, and D.C. Love, Bittersweet memories: linking metabolism to epigenetics through O-GlcNAcylation. Nat Rev Mol Cell Biol, 2012. 13(5): p. 312-21.

32.   Yang, X. and K. Qian, Protein O-GlcNAcylation: emerging mechanisms and functions. Nat Rev Mol Cell Biol, 2017. 18(7): p. 452-465.

33.   Wang, Z., M. Gucek, and G.W. Hart, Cross-talk between GlcNAcylation and phosphorylation: site-specific phosphorylation dynamics in response to globally elevated O-GlcNAc. Proc Natl Acad Sci U S A, 2008. 105(37): p. 13793-8.

34.   Comer, F.I. and G.W. Hart, Reciprocity between O-GlcNAc and O-phosphate on the carboxyl terminal domain of RNA polymerase II. Biochemistry, 2001. 40(26): p. 7845-52.

35.   Chou, T.Y., G.W. Hart, and C.V. Dang, c-Myc is glycosylated at threonine 58, a known phosphorylation site and a mutational hot spot in lymphomas. J Biol Chem, 1995. 270(32): p. 18961-5.

36.   Ball, L.E., M.N. Berkaw, and M.G. Buse, Identification of the major site of O-linked beta-N-acetylglucosamine modification in the C terminus of insulin receptor substrate-1. Mol Cell Proteomics, 2006. 5(2): p. 313-23.

37.   Aebi, M., et al., N-glycan structures: recognition and processing in the ER. Trends Biochem Sci, 2010. 35(2): p. 74-82.

38.   Apweiler, R., H. Hermjakob, and N. Sharon, On the frequency of protein glycosylation, as deduced from analysis of the SWISS-PROT database. Biochim Biophys Acta, 1999. 1473(1): p. 4-8.

39.   Aebi, M., N-linked protein glycosylation in the ER. Biochimica et Biophysica Acta (BBA) - Molecular Cell Research, 2013. 1833(11): p. 2430-2437.

40.   Helenius, A. and M. Aebi, Roles of N-linked glycans in the endoplasmic reticulum. Annu Rev Biochem, 2004. 73: p. 1019-49.

41.   Thiel, C. and C. Korner, Mouse models for congenital disorders of glycosylation. J Inherit Metab Dis, 2011. 34(4): p. 879-89.

42.   Schwarz, F. and M. Aebi, Mechanisms and principles of N-linked protein glycosylation. Curr Opin Struct Biol, 2011. 21(5): p. 576-82.

43.   Kozlov, G., et al., Crystal structure of the bb' domains of the protein disulfide isomerase ERp57. Structure, 2006. 14(8): p. 1331-9.

44.   Frickel, E.M., et al., TROSY-NMR reveals interaction between ERp57 and the tip of the calreticulin P-domain. Proc Natl Acad Sci U S A, 2002. 99(4): p. 1954-9.

45.   Wada, I., et al., Promotion of transferrin folding by cyclic interactions with calnexin and calreticulin. Embo j, 1997. 16(17): p. 5420-32.

46.   Vasconcelos-dos-Santos, A., et al., Biosynthetic Machinery Involved in Aberrant Glycosylation: Promising Targets for Developing of Drugs Against Cancer. Frontiers in Oncology, 2015. 5(138).

47.   Kengen, S.W., et al., Evidence for the operation of a novel Embden-Meyerhof pathway that involves ADP-dependent kinases during sugar fermentation by Pyrococcus furiosus. J Biol Chem, 1994. 269(26): p. 17537-41.

48.   Richter, J.P., et al., The Structural and Functional Characterization of Mammalian ADP-dependent Glucokinase. J Biol Chem, 2016. 291(8): p. 3694-704.

49.   Ronimus, R.S. and H.W. Morgan, Cloning and biochemical characterization of a novel mouse ADP-dependent glucokinase. Biochem Biophys Res Commun, 2004. 315(3): p. 652-8.

50.   Kamiński, Marcin M., et al., T cell Activation Is Driven by an ADP-Dependent Glucokinase Linking Enhanced Glycolysis with Mitochondrial Reactive Oxygen Species Generation. Cell Reports, 2012. 2(5): p. 1300-1315.

51.   Ramaswamy, S., et al., Multiclass cancer diagnosis using tumor gene expression signatures. Proc Natl Acad Sci U S A, 2001. 98(26): p. 15149-54.

52.   Richter, S., et al., Expression and role in glycolysis of human ADP-dependent glucokinase. Mol Cell Biochem, 2012. 364(1-2): p. 131-45.

53.   Kamiński, M.M., et al., Mitochondrial Reactive Oxygen Species Control T Cell Activation by Regulating IL-2 and IL-4 Expression: Mechanism of Ciprofloxacin-Mediated Immunosuppression. The Journal of Immunology, 2010. 184(9): p. 4827-4841.

54.   Kaminski, M., et al., Novel role for mitochondria: protein kinase Ctheta-dependent oxidative signaling organelles in activation-induced T-cell death. Mol Cell Biol, 2007. 27(10): p. 3625-39.

55.   Richter, S., et al., Zinc finger nuclease mediated knockout of ADP-dependent glucokinase in cancer cell lines: effects on cell survival and mitochondrial oxidative metabolism. PLoS One, 2013. 8(6): p. e65267.

56.   Bradbury, J., Small fish, big science. PLoS Biol, 2004. 2(5): p. E148.

57.   Kalueff, A.V., A.M. Stewart, and R. Gerlai, Zebrafish as an emerging model for studying complex brain disorders. Trends Pharmacol Sci, 2014. 35(2): p. 63-75.

58.   Spence, R., et al., The behaviour and ecology of the zebrafish, Danio rerio. Biol Rev Camb Philos Soc, 2008. 83(1): p. 13-34.

59.   Kimmel, C.B., et al., Stages of embryonic development of the zebrafish. Developmental Dynamics, 1995. 203(3): p. 253-310.

60.   Collins, J.E., et al., Incorporating RNA-seq data into the zebrafish Ensembl genebuild. Genome Res, 2012. 22(10): p. 2067-78.

61.   Howe, K., et al., The zebrafish reference genome sequence and its relationship to the human genome. Nature, 2013. 496(7446): p. 498-503.

62.   Schier, A.F. and W.S. Talbot, Molecular genetics of axis formation in zebrafish. Annu Rev Genet, 2005. 39: p. 561-613.

63.   Tada, M. and C.P. Heisenberg, Convergent extension: using collective cell migration and cell intercalation to shape embryos. Development, 2012. 139(21): p. 3897-904.

64.   Essner, J.J., et al., Kupffer's vesicle is a ciliated organ of asymmetry in the zebrafish embryo that initiates left-right development of the brain, heart and gut. Development, 2005. 132(6): p. 1247-60.

65.   Angers, S. and R.T. Moon, Proximal events in Wnt signal transduction. Nat Rev Mol Cell Biol, 2009. 10(7): p. 468-77.

66.   Logan, C.Y. and R. Nusse, The Wnt signaling pathway in development and disease. Annu Rev Cell Dev Biol, 2004. 20: p. 781-810.

67.   De Robertis, E.M., et al., The establishment of Spemann's organizer and patterning of the vertebrate embryo. Nat Rev Genet, 2000. 1(3): p. 171-81.

68.   Schier, A.F. and M.M. Shen, Nodal signalling in vertebrate development. Nature, 2000. 403(6768): p. 385-9.

69.   Kondo, M., Bone morphogenetic proteins in the early development of zebrafish. Febs j, 2007. 274(12): p. 2960-7.

70.   Kimelman, D., Mesoderm induction: from caps to chips. Nat Rev Genet, 2006. 7(5): p. 360-372.

71.   Dick, A., et al., Essential role of Bmp7 (snailhouse) and its prodomain in dorsoventral patterning of the zebrafish embryo. Development, 2000. 127(2): p. 343-54.

72.   Yamashita, S., et al., Stat3 Controls Cell Movements during Zebrafish Gastrulation. Dev Cell, 2002. 2(3): p. 363-75.

73.   Yamashita, S., et al., Zinc transporter LIVI controls epithelial-mesenchymal transition in zebrafish gastrula organizer. Nature, 2004. 429(6989): p. 298-302.

74.   Montero, J.A., et al., Phosphoinositide 3-kinase is required for process outgrowth and cell polarization of gastrulating mesendodermal cells. Curr Biol, 2003. 13(15): p. 1279-89.

75.   Komiya, Y. and R. Habas, Wnt signal transduction pathways. Organogenesis, 2008. 4(2): p. 68-75.

76.   Kilian, B., et al., The role of Ppt/Wnt5 in regulating cell shape and movement during zebrafish gastrulation. Mech Dev, 2003. 120(4): p. 467-76.

77.   Heisenberg, C.P., et al., Silberblick/Wnt11 mediates convergent extension movements during zebrafish gastrulation. Nature, 2000. 405(6782): p. 76-81.

78.   Sumanas, S., et al., Zebrafish frizzled-2 morphant displays defects in body axis elongation. Genesis, 2001. 30(3): p. 114-8.

79. Topczewski, J., et al., The zebrafish glypican knypek controls cell polarity during gastrulation movements of convergent extension. Dev Cell, 2001. 1(2): p. 251-64.

80. Myers, D.C., D.S. Sepich, and L. Solnica-Krezel, Bmp Activity Gradient Regulates Convergent Extension during Zebrafish Gastrulation. Developmental Biology, 2002. 243(1): p. 81-98.

81. Matsui, T. and Y. Bessho, Left-right asymmetry in zebrafish. Cell Mol Life Sci, 2012. 69(18): p. 3069-77.

82. Oishi, I., et al., Regulation of primary cilia formation and left-right patterning in zebrafish by a noncanonical Wnt signaling mediator, duboraya. Nat Genet, 2006. 38(11): p. 1316-22.

83. Hamada, H., et al., Establishment of vertebrate left-right asymmetry. Nat Rev Genet, 2002. 3(2): p. 103-13.

84. Kane, D.A. and C.B. Kimmel, The zebrafish midblastula transition. Development, 1993. 119(2): p. 447-56.

85. Dalle Nogare, D.E., P.T. Pauerstein, and M.E. Lane, G2 acquisition by transcription-independent mechanism at the zebrafish midblastula transition. Developmental Biology, 2009. 326(1): p. 131-142.

86. Ikegami, R., et al., Effect of inhibitors of DNA replication on early zebrafish embryos: evidence for coordinate activation of multiple intrinsic cell-cycle checkpoints at the mid-blastula transition. Zygote, 1997. 5(2): p. 153-75.

87. Ikegami, R., P. Hunter, and T.D. Yager, Developmental activation of the capability to undergo checkpoint-induced apoptosis in the early zebrafish embryo. Dev Biol, 1999. 209(2): p. 409-33.

88. Ikegami, R., et al., Activation of the metaphase checkpoint and an apoptosis programme in the early zebrafish embryo, by treatment with the spindle-destabilising agent nocodazole. Zygote, 1997. 5(4): p. 329-50.

89. Verduzco, D. and J.F. Amatruda, Analysis of Cell Proliferation, Senescence and Cell Death in Zebrafish Embryos. Methods in cell biology, 2011. 101: p. 10.1016/B978-0-12-387036-0.00002-5.

90. Sherr, C.J. and J.M. Roberts, Living with or without cyclins and cyclin-dependent kinases. Genes Dev, 2004. 18(22): p. 2699-711.

91. Malumbres, M. and M. Barbacid, Cell cycle, CDKs and cancer: a changing paradigm. Nat Rev Cancer, 2009. 9(3): p. 153-66.

92. Otto, T. and P. Sicinski, Cell cycle proteins as promising targets in cancer therapy. Nat Rev Cancer, 2017. 17(2): p. 93-115.

93. Malumbres, M. and M. Barbacid, To cycle or not to cycle: a critical decision in cancer. Nat Rev Cancer, 2001. 1(3): p. 222-31.

94.   Bertoli, C., J.M. Skotheim, and R.A. de Bruin, Control of cell cycle transcription during G1 and S phases. Nat Rev Mol Cell Biol, 2013. 14(8): p. 518-28.

95.   Giono, L.E. and J.J. Manfredi, The p53 tumor suppressor participates in multiple cell cycle checkpoints. J Cell Physiol, 2006. 209(1): p. 13-20.

96.   Aguilar, V. and L. Fajas, Cycling through metabolism. EMBO Molecular Medicine, 2010. 2(9): p. 338-348.

97.   Elmore, S., Apoptosis: a review of programmed cell death. Toxicol Pathol, 2007. 35(4): p. 495-516.

98.   Inohara, N. and G. Nunez, Genes with homology to mammalian apoptosis regulators identified in zebrafish. Cell Death Differ, 2000. 7(5): p. 509-10.

99.   Kratz, E., et al., Functional characterization of the Bcl-2 gene family in the zebrafish. Cell Death Differ, 2006. 13(10): p. 1631-40.

100.   Cole, L.K. and L.S. Ross, Apoptosis in the developing zebrafish embryo. Dev Biol, 2001. 240(1): p. 123-42.

101.   Meier, P., A. Finch, and G. Evan, Apoptosis in development. Nature, 2000. 407(6805): p. 796-801.

102.   Ichim, G. and S.W. Tait, A fate worse than death: apoptosis as an oncogenic process. Nat Rev Cancer, 2016. 16(8): p. 539-48.

103.   Martin, S.J., et al., Early redistribution of plasma membrane phosphatidylserine is a general feature of apoptosis regardless of the initiating stimulus: inhibition by overexpression of Bcl-2 and Abl. J Exp Med, 1995. 182(5): p. 1545-56.

104.   Green, D.R. and J.C. Reed, Mitochondria and apoptosis. Science, 1998. 281(5381): p. 1309-12.

105.   Hardwick, J.M. and R.J. Youle, SnapShot: BCL-2 proteins. Cell, 2009. 138(2): p. 404, 404.e1.

106.   Ashkenazi, A. and V.M. Dixit, Death receptors: signaling and modulation. Science, 1998. 281(5381): p. 1305-8.

107.   Wajant, H., The Fas signaling pathway: more than a paradigm. Science, 2002. 296(5573): p. 1635-6.

108.   Kischkel, F.C., et al., Cytotoxicity-dependent APO-1 (Fas/CD95)-associated proteins form a death-inducing signaling complex (DISC) with the receptor. Embo j, 1995. 14(22): p. 5579-88.

109.   Ashkenazi, A. and G. Salvesen, Regulated cell death: signaling and mechanisms. Annu Rev Cell Dev Biol, 2014. 30: p. 337-56.

110.   Bill, B.R., et al., A primer for morpholino use in zebrafish. Zebrafish, 2009. 6(1): p. 69-77.

111. Morcos, P.A., Achieving targeted and quantifiable alteration of mRNA splicing with Morpholino oligos. Biochem Biophys Res Commun, 2007. 358(2): p. 521-7.

112. Hsu, P.D., E.S. Lander, and F. Zhang, Development and applications of CRISPR-Cas9 for genome engineering. Cell, 2014. 157(6): p. 1262-78.

113. Gasiunas, G., et al., Cas9-crRNA ribonucleoprotein complex mediates specific DNA cleavage for adaptive immunity in bacteria. Proc Natl Acad Sci U S A, 2012. 109(39): p. E2579-86.

114. Sander, J.D. and J.K. Joung, CRISPR-Cas systems for editing, regulating and targeting genomes. Nat Biotech, 2014. 32(4): p. 347-355.

115. Doudna, J.A. and E. Charpentier, Genome editing. The new frontier of genome engineering with CRISPR-Cas9. Science, 2014. 346(6213): p. 1258096.

116. Qi, L.S., et al., Repurposing CRISPR as an RNA-guided platform for sequence-specific control of gene expression. Cell, 2013. 152(5): p. 1173-83.

117. Swiech, L., et al., In vivo interrogation of gene function in the mammalian brain using CRISPR-Cas9. Nat Biotechnol, 2015. 33(1): p. 102-6.

118. Yin, H., et al., Genome editing with Cas9 in adult mice corrects a disease mutation and phenotype. Nat Biotechnol, 2014. 32(6): p. 551-3.

119. Peng, R., G. Lin, and J. Li, Potential pitfalls of CRISPR/Cas9-mediated genome editing. Febs j, 2016. 283(7): p. 1218-31.

120. Burstenbinder, K., et al., The role of methionine recycling for ethylene synthesis in Arabidopsis. Plant J, 2007. 49(2): p. 238-49.

121. Rossi, A., et al., Genetic compensation induced by deleterious mutations but not gene knockdowns. Nature, 2015. 524(7564): p. 230-233.

122. Bill B. R., P.A.M., Clark K. J., et al., A Primer for Morpholino Use in Zebrafish. Zebrafish, 2009. 6(1).

123. Gonzalez-Alvarez, R., et al., The hexokinase gene family in the zebrafish: structure, expression, functional and phylogenetic analysis. Comp Biochem Physiol B Biochem Mol Biol, 2009. 152(2): p. 189-95.

124. Makita, R., et al., Zebrafish wnt11: pattern and regulation of the expression by the yolk cell and No tail activity. Mech Dev, 1998. 71(1-2): p. 165-76.

125. Kalev-Zylinska, M.L., et al., Runx1 is required for zebrafish blood and vessel development and expression of a human RUNX1-CBF2T1 transgene advances a model for studies of leukemogenesis. Development, 2002. 129(8): p. 2015-30.

126. Kok, F.O., et al., Reverse genetic screening reveals poor correlation between morpholino-induced and mutant phenotypes in zebrafish. Dev Cell, 2015. 32(1): p. 97-108.

127. Eisen, J.S. and J.C. Smith, Controlling morpholino experiments: don't stop making antisense. Development, 2008. 135(10): p. 1735-43.

128. Xiong, K.M., R.E. Peterson, and W. Heideman, Aryl hydrocarbon receptor-mediated down-regulation of sox9b causes jaw malformation in zebrafish embryos. Mol Pharmacol, 2008. 74(6): p. 1544-53.

129. Bedell, V.M., S.E. Westcot, and S.C. Ekker, Lessons from morpholino-based screening in zebrafish. Brief Funct Genomics, 2011. 10(4): p. 181-8.

130. Timme-Laragy, A.R., S.I. Karchner, and M.E. Hahn, Gene knockdown by morpholino-modified oligonucleotides in the zebrafish (Danio rerio) model: applications for developmental toxicology. Methods Mol Biol, 2012. 889: p. 51-71.

131. Matsui, T., et al., Noncanonical Wnt signaling regulates midline convergence of organ primordia during zebrafish development. Genes Dev, 2005. 19(1): p. 164-75.

132. Solnica-Krezel, L. and M.S. Cooper, Cellular and genetic mechanisms of convergence and extension. Results Probl Cell Differ, 2002. 40: p. 136-65.

133. Tahinci, E. and K. Symes, Distinct functions of Rho and Rac are required for convergent extension during Xenopus gastrulation. Developmental Biology, 2003. 259(2): p. 318-335.

134. Sokol, S.Y., Analysis of Dishevelled signalling pathways during Xenopus development. Curr Biol, 1996. 6(11): p. 1456-67.

135. Rimkus, T.K., et al., Targeting the Sonic Hedgehog Signaling Pathway: Review of Smoothened and GLI Inhibitors. Cancers (Basel), 2016. 8(2).

136. Thomas, N.A., et al., Hedgehog signaling plays a cell-autonomous role in maximizing cardiac developmental potential. Development, 2008. 135(22): p. 3789-99.

137. Schulte-Merker, S., et al., The zebrafish organizer requires chordino. Nature, 1997. 387(6636): p. 862-3.

138. Aamar, E. and I.B. Dawid, Sox17 and Chordin are required for formation of Kupffer's vesicle and Left-Right asymmetry determination in zebrafish. Developmental dynamics : an official publication of the American Association of Anatomists, 2010. 239(11): p. 2980-2988.

139. Ribble, D., et al., A simple technique for quantifying apoptosis in 96-well plates. BMC Biotechnol, 2005. 5: p. 12.

140. Pucci, B., M. Kasten, and A. Giordano, Cell Cycle and Apoptosis. Neoplasia (New York, N.Y.), 2000. 2(4): p. 291-299.

141. Levine, A.J., p53, the cellular gatekeeper for growth and division. Cell, 1997. 88(3): p. 323-31.

142. Bohnsack, B.L. and K.K. Hirschi, Nutrient regulation of cell cycle progression. Annu Rev Nutr, 2004. 24: p. 433-53.

143. Green, D.R., L. Galluzzi, and G. Kroemer, Cell biology. Metabolic control of cell death. Science, 2014. 345(6203): p. 1250256.

144. Kemp, G., Lactate accumulation, proton buffering, and pH change in ischemically exercising muscle. American Journal of Physiology - Regulatory, Integrative and Comparative Physiology, 2005. 289(3): p. R895.

145. Swietach, P., et al., The Role of Carbonic Anhydrase 9 in Regulating Extracellular and Intracellular pH in Three-dimensional Tumor Cell Growths. Journal of Biological Chemistry, 2009. 284(30): p. 20299-20310.

146. Ma, Q., Role of Nrf2 in Oxidative Stress and Toxicity. Annual Review of Pharmacology and Toxicology, 2013. 53(1): p. 401-426.

147. Nebert, D.W., et al., NAD(P)H:quinone oxidoreductase (NQO1) polymorphism, exposure to benzene, and predisposition to disease: A HuGE review. Genet Med, 2002. 4(2): p. 62-70.

148. Parichy, D.M., et al., An orthologue of the kit-related gene fms is required for development of neural crest-derived xanthophores and a subpopulation of adult melanocytes in the zebrafish, Danio rerio. Development, 2000. 127(14): p. 3031-44.

149. Wood, J.M., et al., A specific tetrahydrobiopterin binding domain on tyrosinase controls melanogenesis. Biochem Biophys Res Commun, 1995. 206(2): p. 480-5.

150. Cummings, R.D., Use of lectins in analysis of glycoconjugates. Methods Enzymol, 1994. 230: p. 66-86.

151. Flanagan-Steet, H.R. and R. Steet, "Casting" light on the role of glycosylation during embryonic development: insights from zebrafish. Glycoconj J, 2013. 30(1): p. 33-40.

152. Rocha, F., et al., Glucose overload in yolk has little effect on the long-term modulation of carbohydrate metabolic genes in zebrafish (Danio rerio). J Exp Biol, 2014. 217(Pt 7): p. 1139-49.

153. Gorospe, M., X. Wang, and N.J. Holbrook, Functional role of p21 during the cellular response to stress. Gene Expr, 1999. 7(4-6): p. 377-85.

154. Gardner, D.K., T.B. Pool, and M. Lane, Embryo nutrition and energy metabolism and its relationship to embryo growth, differentiation, and viability. Semin Reprod Med, 2000. 18(2): p. 205-18.

155. Bensaad, K., et al., TIGAR, a p53-inducible regulator of glycolysis and apoptosis. Cell, 2006. 126(1): p. 107-20.

156. Ruan, H.-B., et al., Cracking the O-GlcNAc Code in Metabolism. Trends in endocrinology and metabolism: TEM, 2013. 24(6): p. 301-309.

157. Johswich, A., et al., N-Glycan Remodeling on Glucagon Receptor Is an Effector of Nutrient Sensing by the Hexosamine Biosynthesis Pathway. The Journal of Biological Chemistry, 2014. 289(23): p. 15927-15941.

158.   Lau, K.S., et al., Complex N-glycan number and degree of branching cooperate to regulate cell proliferation and differentiation. Cell, 2007. 129(1): p. 123-34.

159.   Ohtsubo, K., et al., Dietary and genetic control of glucose transporter 2 glycosylation promotes insulin secretion in suppressing diabetes. Cell, 2005. 123(7): p. 1307-21.

160.   Haga, Y., K. Ishii, and T. Suzuki, N-glycosylation is critical for the stability and intracellular trafficking of glucose transporter GLUT4. J Biol Chem, 2011. 286(36): p. 31320-7.

161.   Kalluri, R. and R.A. Weinberg, The basics of epithelial-mesenchymal transition. J Clin Invest, 2009. 119(6): p. 1420-8.

162.   Lamouille, S., J. Xu, and R. Derynck, Molecular mechanisms of epithelial-mesenchymal transition. Nat Rev Mol Cell Biol, 2014. 15(3): p. 178-96.

163.   Taparra, K., P.T. Tran, and N.E. Zachara, Hijacking the Hexosamine Biosynthetic Pathway to Promote EMT-Mediated Neoplastic Phenotypes. Front Oncol, 2016. 6: p. 85.

164.   Nusse, R., Wnts and Hedgehogs: lipid-modified proteins and similarities in signaling mechanisms at the cell surface. Development, 2003. 130(22): p. 5297-305.

165.   Hayward, P., T. Kalmar, and A.M. Arias, Wnt/Notch signalling and information processing during development. Development, 2008. 135(3): p. 411-24.

166.   Guo, X. and X.F. Wang, Signaling cross-talk between TGF-beta/BMP and other pathways. Cell Res, 2009. 19(1): p. 71-88.

167.   Sengupta, P.K., M.P. Bouchie, and M.A. Kukuruzinska, N-glycosylation gene DPAGT1 is a target of the Wnt/beta-catenin signaling pathway. J Biol Chem, 2010. 285(41): p. 31164-73.

168.   Willert, K. and R. Nusse, Wnt proteins. Cold Spring Harb Perspect Biol, 2012. 4(9): p. a007864.

169.   Kim, Y.W., et al., TGF-beta sensitivity is determined by N-linked glycosylation of the type II TGF-beta receptor. Biochem J, 2012. 445(3): p. 403-11.

170.   Moloney, D.J., et al., Mammalian Notch1 is modified with two unusual forms of O-linked glycosylation found on epidermal growth factor-like modules. J Biol Chem, 2000. 275(13): p. 9604-11.

171.   Matsuura, A., et al., O-linked N-acetylglucosamine is present on the extracellular domain of notch receptors. J Biol Chem, 2008. 283(51): p. 35486-95.

172.   Rana, N.A., et al., O-glucose trisaccharide is present at high but variable stoichiometry at multiple sites on mouse Notch1. J Biol Chem, 2011. 286(36): p. 31623-37.

173.   Marada, S., et al., Functional Divergence in the Role of N-Linked Glycosylation in Smoothened Signaling. PLoS Genet, 2015. 11(8): p. e1005473.

174. MacDonald, B.T., K. Tamai, and X. He, Wnt/beta-catenin signaling: components, mechanisms, and diseases. Dev Cell, 2009. 17(1): p. 9-26.

175. Kardash, E., et al., A role for Rho GTPases and cell-cell adhesion in single-cell motility in vivo. Nat Cell Biol, 2010. 12(1): p. 47-53; sup pp 1-11.

176. Warga, R.M. and D.A. Kane, A role for N-cadherin in mesodermal morphogenesis during gastrulation. Dev Biol, 2007. 310(2): p. 211-25.

177. Arboleda-Estudillo, Y., et al., Movement directionality in collective migration of germ layer progenitors. Curr Biol, 2010. 20(2): p. 161-9.

178. Sepich, D.S., et al., Initiation of convergence and extension movements of lateral mesoderm during zebrafish gastrulation. Dev Dyn, 2005. 234(2): p. 279-92.

179. Han, M.K., et al., alphaE-catenin-dependent mechanotransduction is essential for proper convergent extension in zebrafish. Biol Open, 2016. 5(10): p. 1461-1472.

180. Piskac-Collier, A.L., et al., Variants in folate pathway genes as modulators of genetic instability and lung cancer risk. Genes Chromosomes Cancer, 2011. 50(1): p. 1-12.

181. Teperino, R., K. Schoonjans, and J. Auwerx, Histone methyl transferases and demethylases; can they link metabolism and transcription? Cell Metab, 2010. 12(4): p. 321-7.

182. Tedeschi, P.M., et al., Contribution of serine, folate and glycine metabolism to the ATP, NADPH and purine requirements of cancer cells. Cell Death Dis, 2013. 4: p. e877.

183. Jain, M., et al., Metabolite profiling identifies a key role for glycine in rapid cancer cell proliferation. Science, 2012. 336(6084): p. 1040-4.

184. Wang, J., et al., Dependence of mouse embryonic stem cells on threonine catabolism. Science, 2009. 325(5939): p. 435-9.

185. Shiraki, N., et al., Methionine Metabolism Regulates Maintenance and Differentiation of Human Pluripotent Stem Cells. Cell Metabolism. 19(5): p. 780-794.

186. Shyh-Chang, N., et al., Influence of Threonine Metabolism on S-Adenosylmethionine and Histone Methylation. Science, 2013. 339(6116): p. 222-226.

187. Porporato, P.E., et al., Anticancer targets in the glycolytic metabolism of tumors: a comprehensive review. Front Pharmacol, 2011. 2: p. 49.

188. Webb, B.A., et al., Dysregulated pH: a perfect storm for cancer progression. Nat Rev Cancer, 2011. 11(9): p. 671-677.

189. Lagadic-Gossmann, D., L. Huc, and V. Lecureur, Alterations of intracellular pH homeostasis in apoptosis: origins and roles. Cell Death Differ, 2004. 11(9): p. 953-61.

190. Matsuyama, S., et al., Changes in intramitochondrial and cytosolic pH: early events that modulate caspase activation during apoptosis. Nat Cell Biol, 2000. 2(6): p. 318-325.

191.   Putney, L.K. and D.L. Barber, Na-H Exchange-dependent Increase in Intracellular pH Times G2/M Entry and Transition. Journal of Biological Chemistry, 2003. 278(45): p. 44645-44649.

192.   Svastova, E., et al., Carbonic Anhydrase IX Interacts with Bicarbonate Transporters in Lamellipodia and Increases Cell Migration via Its Catalytic Domain. Journal of Biological Chemistry, 2012. 287(5): p. 3392-3402.

193.   Stock, C. and A. Schwab, Protons make tumor cells move like clockwork. Pflugers Arch, 2009. 458(5): p. 981-92.

194.   Martin, C., et al., Intracellular pH gradients in migrating cells. Am J Physiol Cell Physiol, 2011. 300(3): p. C490-5.

195.   Svastova, E., et al., Carbonic anhydrase IX reduces E-cadherin-mediated adhesion of MDCK cells via interaction with beta-catenin. Exp Cell Res, 2003. 290(2): p. 332-45.

196.   Radvak, P., et al., Suppression of carbonic anhydrase IX leads to aberrant focal adhesion and decreased invasion of tumor cells. Oncol Rep, 2013. 29(3): p. 1147-53.

197.   Sedlakova, O., et al., Carbonic anhydrase IX, a hypoxia-induced catalytic component of the pH regulating machinery in tumors. Frontiers in Physiology, 2013. 4: p. 400.

198.   Butsri, S., et al., Downregulation of NAD(P)H:quinone oxidoreductase 1 inhibits proliferation, cell cycle and migration of cholangiocarcinoma cells. Oncol Lett, 2017. 13(6): p. 4540-4548.

199.   Sies, H., Glutathione and its role in cellular functions. Free Radic Biol Med, 1999. 27(9-10): p. 916-21.

200.   Pompella, A., et al., The changing faces of glutathione, a cellular protagonist. Biochem Pharmacol, 2003. 66(8): p. 1499-503.

201.   Weinberg, J.M., A. Bienholz, and M.A. Venkatachalam, The role of glycine in regulated cell death. Cell Mol Life Sci, 2016. 73(11-12): p. 2285-308.

202.   di Salvo, M.L., et al., Glycine consumption and mitochondrial serine hydroxymethyltransferase in cancer cells: the heme connection. Med Hypotheses, 2013. 80(5): p. 633-6.

203.   Wang, G.G., et al., Taurine attenuates oxidative stress and alleviates cardiac failure in type I diabetic rats. Croat Med J, 2013. 54(2): p. 171-9.

204.   Higuchi, M., et al., Taurine plays an important role in the protection of spermatogonia from oxidative stress. Amino Acids, 2012. 43(6): p. 2359-69.

205.   Zhang, Z., et al., Taurine supplementation reduces oxidative stress and protects the liver in an iron-overload murine model. Mol Med Rep, 2014. 10(5): p. 2255-62.

206.   Hansen, S.H., et al., A role for taurine in mitochondrial function. J Biomed Sci, 2010. 17 Suppl 1: p. S23.

207. Jensen, P.J., L.B. Gunter, and M.O. Carayannopoulos, Akt2 Modulates Glucose Availability and Downstream Apoptotic Pathways during Development. The Journal of Biological Chemistry, 2010. 285(23): p. 17673-17680.

208. Hill, M.M., et al., A role for protein kinase Bbeta/Akt2 in insulin-stimulated GLUT4 translocation in adipocytes. Mol Cell Biol, 1999. 19(11): p. 7771-81.

209. Gottlob, K., et al., Inhibition of early apoptotic events by Akt/PKB is dependent on the first committed step of glycolysis and mitochondrial hexokinase. Genes Dev, 2001. 15(11): p. 1406-18.

210. Fridman, J.S. and S.W. Lowe, Control of apoptosis by p53. Oncogene, 2003. 22(56): p. 9030-40.

211. Chipuk, J.E. and D.R. Green, Dissecting p53-dependent apoptosis. Cell Death Differ, 2006. 13(6): p. 994-1002.

212. Asher, G., et al., NQO1 stabilizes p53 through a distinct pathway. Proc Natl Acad Sci U S A, 2002. 99(5): p. 3099-104.

213. Vousden, K.H., Outcomes of p53 activation - spoilt for choice. Journal of Cell Science, 2006. 119(24): p. 5015-5020.

214. Abbas, T. and A. Dutta, p21 in cancer: intricate networks and multiple activities. Nature reviews. Cancer, 2009. 9(6): p. 400-414.

215. Gartel, A.L., The conflicting roles of the cdk inhibitor p21(CIP1/WAF1) in apoptosis. Leuk Res, 2005. 29(11): p. 1237-8.

216. Gartel, A.L. and A.L. Tyner, Transcriptional regulation of the p21((WAF1/CIP1)) gene. Exp Cell Res, 1999. 246(2): p. 280-9.

217. Olson, M.F., H.F. Paterson, and C.J. Marshall, Signals from Ras and Rho GTPases interact to regulate expression of p21Waf1/Cip1. Nature, 1998. 394(6690): p. 295-9.

218. Denslow, N.D., et al., Vitellogenin as a Biomarker of Exposure for Estrogen or Estrogen Mimics. Ecotoxicology, 1999. 8(5): p. 385-398.

219. Hanzawa, K., N. Suzuki, and S. Natsuka, Structures and developmental alterations of N-glycans of zebrafish embryos. Glycobiology, 2017. 27(3): p. 228-245.

220. Link, V., A. Shevchenko, and C.P. Heisenberg, Proteomics of early zebrafish embryos. BMC Dev Biol, 2006. 6: p. 1.

221. Guerardel, Y., et al., Glycomic survey mapping of zebrafish identifies unique sialylation pattern. Glycobiology, 2006. 16(3): p. 244-57.

222. Machingo, Q.J., A. Fritz, and B.D. Shur, A beta1,4-galactosyltransferase is required for convergent extension movements in zebrafish. Dev Biol, 2006. 297(2): p. 471-82.

223. Webster, D.M., et al., O-GlcNAc modifications regulate cell survival and epiboly during zebrafish development. BMC Developmental Biology, 2009. 9(1): p. 28.

224. Zeidan, Q. and G.W. Hart, The intersections between O-GlcNAcylation and phosphorylation: implications for multiple signaling pathways. J Cell Sci, 2010. 123(Pt 1): p. 13-22.

225. Wang, Z., A. Pandey, and G.W. Hart, Dynamic Interplay between O-Linked N-Acetylglucosaminylation and Glycogen Synthase Kinase-3-dependent Phosphorylation. Molecular & Cellular Proteomics, 2007. 6(8): p. 1365-1379.

226. Freeze, H.H., Genetic defects in the human glycome. Nat Rev Genet, 2006. 7(7): p. 537-51.

227. Grunewald, S., G. Matthijs, and J. Jaeken, Congenital Disorders of Glycosylation: A Review. Pediatr Res, 2002. 52(5): p. 618-624.

228. Grunewald, S., The clinical spectrum of phosphomannomutase 2 deficiency (CDG-Ia). Biochim Biophys Acta, 2009. 1792(9): p. 827-34.